

Roope Rinne

Particle Characterisation Using Image Analysis Tools

Improving and developing methods for polyolefin catalysts

Helsinki Metropolia University of Applied Sciences

Bachelor of Science

Chemical Engineering

Thesis

23 March 2015

Author	Roope Rinne
Title	Particle Characterisation Using Image Analysis Tools, Improving and Developing Methods for Polyolefin Catalysts
Number of Pages	90 pages
Date	23 March 2015
Degree	Bachelor of Engineering
Degree Programme	Chemical Engineering
Specialisation option	Process Design
Instructors	David Quin, Senior Scientist Veli-Matti Taavitsainen, Principal Lecturer
<p>This thesis discusses particle characterisation using image analysis tools, and it had two objectives: the improvement of the currently-used method and the development of two new methods. The thesis was done for Borealis, which is a leading manufacturer of polyolefins and fertilizers.</p> <p>The mathematical background of standard particle size analysis is based on certain practices and conventions, which may not be straight-forward without a proper introduction. The theoretical examination presented in this thesis is, therefore, an essential part of the work.</p> <p>For quick screening of multitudes of test catalysts, a high-throughput method was requested. The method development required finding a serviceable compromise between measurement accuracy and speed. For the other method to be developed, the acquisition of a sufficiently large collection of high-resolution images was to be implemented as a method. The use of optical microscopy can reveal the otherwise hidden internal morphology of transparent particles.</p> <p>Method improvement and development are based on clear understanding of the instrument's capabilities and limitations. The discussion on several features of the method and the instrument will be useful for everyone working with the instrument or the results obtained thereby. It can also be used as a reference in future method development.</p>	
Keywords	Particle size measurement, image analysis, method development, particle size data analysis, Malvern Morphologi G3

Tekijä	Roope Rinne
Otsikko	Partikkelien karakterisointi kuva-analysaattorilla, menetelmien kehitys ja parannus polyolefiinikatalyyteille
Sivumäärä Aika	90 sivua 23. maaliskuuta 2015
Tutkinto	Insinööri (AMK)
Koulutusohjelma	Kemiantekniikka
Suuntautumisvaihtoehto	Prosessien suunnittelu ja käyttö
Ohjaajat	David Quin, Senior Scientist Veli-Matti Taavitsainen, Yliopettaja
<p>Tässä työssä tutkittiin partikkelien karakterisointia kuva-analysaattorilla, ja sen tarkoitus oli kahtalainen: jo käytössä olevien menetelmien arviointi ja parannus sekä kahden uuden menetelmän kehitys. Työ tehtiin Borealiksella, joka on johtava polyolefiinien ja lannoitteiden valmistaja Euroopassa.</p> <p>Virallisten standardien mukainen partikkelikokodatan käsittely perustuu tiettyihin käytänteisiin, joiden omaksuminen vaatii paneutumista, ja sen tähden työn alussa esitetty teoreettinen tarkastelu oli olennainen osa työtä.</p> <p>Uudet menetelmät perustuivat kahdelle erityyppiselle tarpeelle. Nopean menetelmän on tarkoitus mahdollistaa nopea ja luetettava määrittäminen tavanomaisille laboratorionäytteille. Toisella, yksityiskohtaisten kuvien menetelmällä sen sijaan oli tarkoitus kerätä suuri joukko tarkkoja kuvia eräistä läpinäkyvistä katalyyteistä. Näitä kuvia käytettäneen myöhemmin hyväksi partikkelien sisäisen morfologian tutkimisessa.</p> <p>Menetelmäkehitys perustuu laitteiston perusteelliseen tuntemukseen. Menetelmiä ja laitteistoa koskeva kriittinen tarkastelu sisältää hyödyllistä tietoa kaikille menetelmän ja sillä saatujen tulosten kanssa työskenteleville, mitä paitsi sitä voi käyttää pohjana tulevalle menetelmäkehitykselle.</p>	
Avainsanat	Partikkelikoon mittaaminen, kuva-analyysi, menetelmäkehitys, partikkelikokodatan analysointi, Malvern Morphologi G3

Table of contents

Used Acronyms and Symbols	1
1 Introduction	3
Part I. Theoretical Background	4
2 Terminology for catalysts and methods	4
3 Particle Size Analysis	5
3.1 Analysis methods	5
3.2 Characterisation of particles	6
3.2.1 Equivalent diameter	6
3.3 Particle distributions	7
3.3.1 Moments of distribution	8
3.3.2 Mean diameters, percentiles and the mode	10
3.3.3 Standard deviation	12
3.4 Graphical presentation	13
3.4.1 Histogram	13
3.4.2 Frequency and volume curves	16
4 Image Analysis using <i>Morphologi G3</i>	18
4.1 <i>Malvern Morphologi G3</i>	18
4.2 Sample preparation	19
4.3 Image acquisition	21
4.3.1 General	21
4.3.2 Frame overlap	23
4.3.3 Z-stacking	23
4.3.4 Merged-objective measurement	24
4.3.5 Measurement phases	24
4.4 Image segmentation	25
4.4.1 Segmentation by threshold	25
4.4.2 Segmentation by watershed	27
4.5 Particle image measurements	27
4.5.1 Pixel size and measurement resolution	27
4.5.2 Image size and shape descriptors	28
4.6 Post-measurement	30
4.6.1 Particle image exclusion	30
4.6.2 Results reporting	32

Part II. Examination of the currently-used method	33
5 Sample preparation and measurement	33
5.1 Sample concentration	33
5.2 Focusing	35
5.3 Watershed segmentation experiment	36
5.3.1 Background	36
5.3.2 The experiment	37
5.3.3 Results and conclusions	38
5.4 Fines detection experiment	38
5.4.1 Background and experiment	38
5.4.2 Results and discussion	39
6 Data handling	42
6.1 Particle classification	42
6.1.1 Spherical	42
6.1.2 Particle aggregates	42
6.1.3 Incomplete images	42
6.1.4 Bubbles	42
6.2 Histogram construction	44
6.2.1 Linear and logarithmical bin size	44
6.2.2 Number-based resolution	44
6.2.3 Large particles	47
6.3 Documentation of results	50
6.3.1 The mode	50
6.3.2 The span	51
6.3.3 The mean diameters and the percentiles	52
7 ISO and BS standards-based assessment	53
7.1 Estimation of statistical error	53
7.1.1 Theoretical background	53
7.1.2 Assessment and conclusions	54
7.2 Estimation of minimum sample size	56
7.2.1 Theoretical background	56
7.2.2 Assessment and conclusions	57
7.3 Homogeneity of frame counts	61
7.3.1 Standard's recommendations	61
7.3.2 Assessment and conclusions	61

Part III. Development of two new methods	64
8 The High-throughput Method	64
8.1 Method development	64
8.1.1 Measurement parameters	64
8.1.2 Threshold optimisation	64
8.1.3 Classification	66
8.2 Comparison with the currently-used method	66
8.2.1 Comparison using standard microscopy slides	67
8.2.2 Comparison using concave microscope slides	68
8.2.3 Sample dispersion on the concave slide	69
8.3 Discussion and conclusions	70
9 The Detailed Method	72
9.1 Background	72
9.2 Method development	73
9.2.1 Designs for the detailed measurement	73
9.2.2 Sample carrier	73
9.2.3 Acquisition of high-resolution imagery	74
9.3 Comparison of size distributions	78
9.4 Discussion and conclusions	79
10 Conclusions	81
11 Summary	82
12 References	83

Used Acronyms and Symbols

Acronyms

BSI	<i>British Standards Institution</i>
CE	<i>Circular Equivalent</i>
DIN	<i>Deutsches Institut für Normung</i>
DOF	<i>Depth of Field</i>
ISO	<i>International Organization for Standardization</i>
M-R	<i>Moment-Ratio</i>
NA	<i>Numerical Aperture</i>
PE	<i>Polyethylene</i>
PP	<i>Polypropylene</i>
PSD	<i>Particle Size Distribution</i>
SOP	<i>Standard Operating Procedure</i>
SS	<i>Single-Site catalyst</i>
ZN	<i>Ziegler-Natta catalyst</i>

Mathematical symbols

$\bar{D}_{p,q}$	Mean particle diameter according to M-R notation (general formula)
i	Number of the size bin
k	Power of x
$\lg(x)$	Base 10 logarithm of x
$\ln(x)$	Natural logarithm of x
$\log(x)$	Logarithm of x , can be either $\lg(x)$ or $\ln(x)$
$M_{k,r}$	k -th raw moment of a $q_r(x)$ -distribution
M'_k	k -th sample moment
$m_{k,r}$	k -th central moment of a $q_r(x)$ -distribution
N	Sample size
N^*	Required sample size
n_i	Frequency of the i -th size bin
P	Confidence level
$Q_r(x)$	Cumulative distribution
$q_r(x)$	Probability density distribution
$\bar{q}_{r,i}$	The height of the i -th column in a histogram
$q_r^*(\xi)$	Transformed probability distribution, $\xi = f(x)$
$\bar{q}_{r,i}^*$	The height of the i -th column in a transformed histogram
r	Quantity type of a distribution $r = 0$, for number $r = 1$, for length $r = 2$, for surface $r = 3$, for volume
$S(x)$	Standard sampling error of random variable x

s_r	Standard deviation of type r distribution
u	A parameter
x	Independent variable; especially particle diameter
x_{\min}	Smallest particle diameter in a given sample
x_{\max}	Largest particle diameter in a given sample
x_r	Image resolution
$x_{10,r}$	10 th percentile of a $q_r(x)$ -distribution
$x_{50,r}$	50 th percentile of a $q_r(x)$ -distribution
$x_{90,r}$	90 th percentile of a $q_r(x)$ -distribution
x_{i-1}	Lower size of the i -th size bin
x_i	Upper size of the i -th size bin
\bar{x}_i	Midpoint of the i -th size bin
$\bar{x}_{k,r}$	Mean particle diameter according to DIN/ISO notation (general formula)
δ	Admissible error
$\Delta Q_{r,i}$	Increment of the cumulative distribution within the i -th size bin
Δx_i	$x_i - x_{i-1}$, width of the i -th size bin
ξ	$\xi(x)$, transformed coordinate
σ_g	Geometric standard deviation
$\Phi(x)$	Cumulative distribution function of normal distribution
ω	A parameter

1 Introduction

The purpose of this thesis was to evaluate and further develop methods for particle size distribution analysis based on an image analyser. The work was done for Borealis and conducted in collaboration with Helsinki Metropolia University of Applied Sciences.

Borealis is a producer of *polyethylene* (PE) and *polypropylene* (PP), collectively referred to as *polyolefins*, and also fertilisers. It is an international organisation headquartered in Vienna, Austria, and manufacturing operations in several countries in Europe, including the production plant and innovation centre in Porvoo, Finland. Borealis is owned by the International Petroleum Investment Company of United Arab Emirates and OMV of Austria.

This thesis is divided into three parts. The parts can be read independently although it is assumed in the latter two parts that the reader is familiar with the basic concepts in particle size analysis. The first part *Theoretical Background* serves as an introduction to particle size analysis, and it has three chapters. Chapter 2 *Terminology for catalysts and methods* defines essential terms relating to this thesis. Chapter 3 *Particle Size Analysis* is a literature review of the mathematical and statistical theory of particle size analysis with an emphasis on ISO standards. Chapter 4 *Image Analysis using Morphologi G3* introduces the instrument and its functions; image analysis in general, however, is not covered in this thesis work, and only the methodology that is applicable to *Morphologi G3* is discussed in the chapter.

The second part *Examination of the currently-used method* is a detailed examination and discussion of the currently-used method (see the next chapter for the terminology regarding methods). Chapter 5 *Sample preparation and measurement* discusses issues related to sample preparation and measurement, and Chapter 6 *Data handling* issues related to the treatment of the obtained data. Chapter 7 *ISO and BS standards-based assessment* presents a statistical assessment of the method based on the standards BS 3406-4:1993 and ISO 13322-1:2004(E).

The third part *Development of two new methods* presents the development of two new methods: the high-throughput method, the purpose of which is to enable the reliable screening of ZN catalysts (Chapter 8 *The High-throughput Method*), and the so-called *detailed method*, the purpose of which is to be used for obtaining high-quality imagery of SS catalysts (Chapter 9 *The Detailed Method*). The learnings obtained from the previous part were utilised in the method development.

Part I. Theoretical Background

2 Terminology for catalysts and methods

Particle size is one of the most important characteristics of a polymer product, and it is a well-known feature of polyolefin polymerisation that the size and shape characteristics of the *catalyst* are preserved during polymerisation – this is referred to as the *replication effect* – and thus the shape and size distribution of the polymer is directly related to the corresponding catalyst distribution. Particle size measurement is therefore an essential part of catalyst characterisation.

Two kinds of commercially used catalysts are used in polyolefin production: the traditional *Ziegler-Natta* (ZN) catalyst and the *Single-Site* (SS) metallocene catalysts. Both are available in *prepolymerised* and *non-prepolymerised* form – although only the SS is measured in both forms.

The method that is currently in use is different for the three types of catalysts owing to their different chemical and optical properties, and can, therefore, be divided in three:

$$\text{Currently-used method} \begin{cases} \text{for ZN} \\ \text{for prepolymerised SS} \\ \text{for non-prepolymerised SS} \end{cases}$$

In this thesis, the term *currently-used method* is used when the type of catalyst is of no interest; however, the catalyst will be specified whenever necessary, for example *currently-used ZN method*.

The two new methods that are to be developed are as follows:

High-throughput method for ZN

$$\text{Detailed method} \begin{cases} \text{for prepolymerised SS} \\ \text{for non-prepolymerised SS} \end{cases}$$

The term detailed method is used to refer to both versions of the method; if the type of catalyst makes a difference, it will be specified.

3 Particle Size Analysis

Clear understanding of the properties of particles is essential in most chemical engineering processes. In polyolefin production, the ideal catalyst is uniform in size and shape because polymer particle properties are derived directly from the corresponding catalyst particle properties. Nevertheless, in reality particles appear in a range of sizes and shapes. The purpose of particle size analysis is to characterise the particle size distribution of particulate matter.

3.1 Analysis methods

Sieving has for a long time been the standard way of performing particle size analysis. The sample is put through a tower of multiple sieves arranged in descending order of grid size. At each sieve, a fraction of the matter is retained, and these fractions are then plotted as a function of the grid size. Sieving is simple and cheap, but it has a poor resolution, and, therefore, it is mainly suitable for screening purposes.

Laser diffraction – more appropriately called *Low Angle Laser Light Scattering* (LALLS) – is one of the most commonly used techniques for particle size analysis. It is a calculated measurement, whose primary value is scattered light intensity and diffraction pattern, which are assumed to be directly proportional to particle size. Laser diffraction has a particularly wide size range; however, it works best only if particles are spherical. (Rawle (no date))

In image analysis, images are obtained from the sample, and these images are then analysed by a computer program. *Computer vision* is applied to recognise the particles in the images and then to measure their physical properties, such as size and shape characteristics. Owing to the recent developments in computer technology, image analysis methods have become increasingly accurate and automated. Image analysis methods are available for both optical and electron microscopes. Furthermore, image analysis can be used for dynamic screening.

3.2 Characterisation of particles

3.2.1 Equivalent diameter

Characterising a three-dimensional particle with one number is not a straight-forward task. To take particle shape into account, the concept of *equivalent diameter* has been adopted. (Leschonski 1984) It is defined in the British standard BS 2955:1993 as '[t]he diameter of a sphere which behaves like the observed particle relative to or deduced from a chosen property'.

The physical particle properties that can be chosen as the basis for defining the equivalent diameter are various. They can be one-dimensional properties, such as linear dimensions, two-dimensional, such as surface area or projected area, and three-dimensional, such as volume and mass. Other physical properties, such as settling rate in a viscous fluid or response to an electrical field may also be chosen. (Leschonski 1984) Some possible equivalent diameters are presented in Table 1. The choice of equivalent diameter depends on the application in which the particles are present. In many instances it is not possible to calculate the equivalent diameter theoretically, but it has to be measured instead.

Table 1 Equivalent diameters (BS 2955:1993)

Equivalent perimeter diameter	Diameter of a circle whose perimeter is equal to that of the particle
Equivalent projected area diameter	Diameter of a circle whose area is equal to the projected area of the particle
Equivalent surface diameter	Diameter of a sphere whose surface is equal to the surface of the particle
Stokes's diameter	Diameter of a sphere whose settling velocity is equal to that of the particle

Since an image analyser captures two-dimensional images of three-dimensional particles, the most natural choice of equivalent diameter is the projected area diameter. The British standard BS 3406-4:1993 introduces the term *equivalent circle diameter* (CE) to be used when the projection is an image. (The mathematical definition will be given in Equation (22)).

3.3 Particle distributions

There are two ways in which particle size distributions can be presented. The *cumulative distribution* $Q_r(x)$ represents the relative quantity of particles equal to or smaller than x . Cumulative distribution is usually normalised so that $Q_r(x_{min}) = 0$ and $Q_r(x_{max}) = 1$. The *probability density distribution* $q_r(x)$ is related to the $Q_r(x)$ according to Equation (1). (Leschonski 1984)

$$q_r(x) = \frac{dQ_r(x)}{dx} \Leftrightarrow Q_r(x) = \int_{x_{min}}^x q_r(x) dx \quad (1)$$

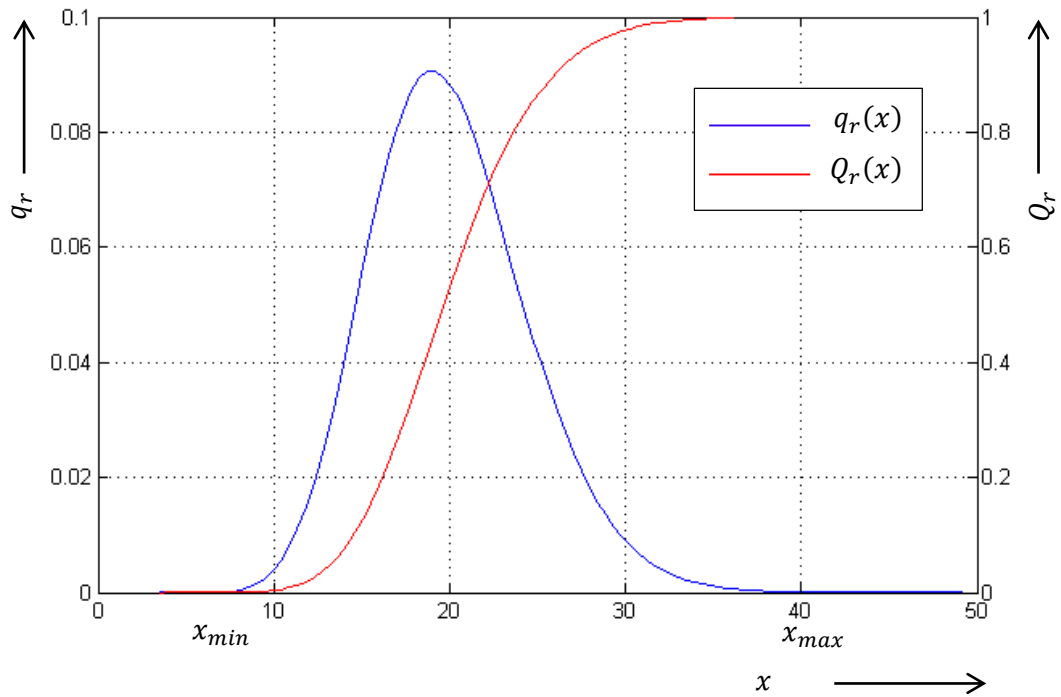


Figure 1 Graphical presentation of density and cumulative distributions

In statistics, distributions are usually based on how frequently each particle size is observed. However, many physical phenomena do not depend on the *number* of particles present, but on some other properties of the particles, such as surface area, volume or mass (Figure 2). For this reason, particle size distributions can be defined for different *types of quantities*, represented as the subscript r , as shown in Table 2. (Leschonski 1984)

Table 2 Different types of quantity for q_r and Q_r

Subscript r	Type of quantity
0	Number (frequency)
1	Diameter
2	Area
3	Volume

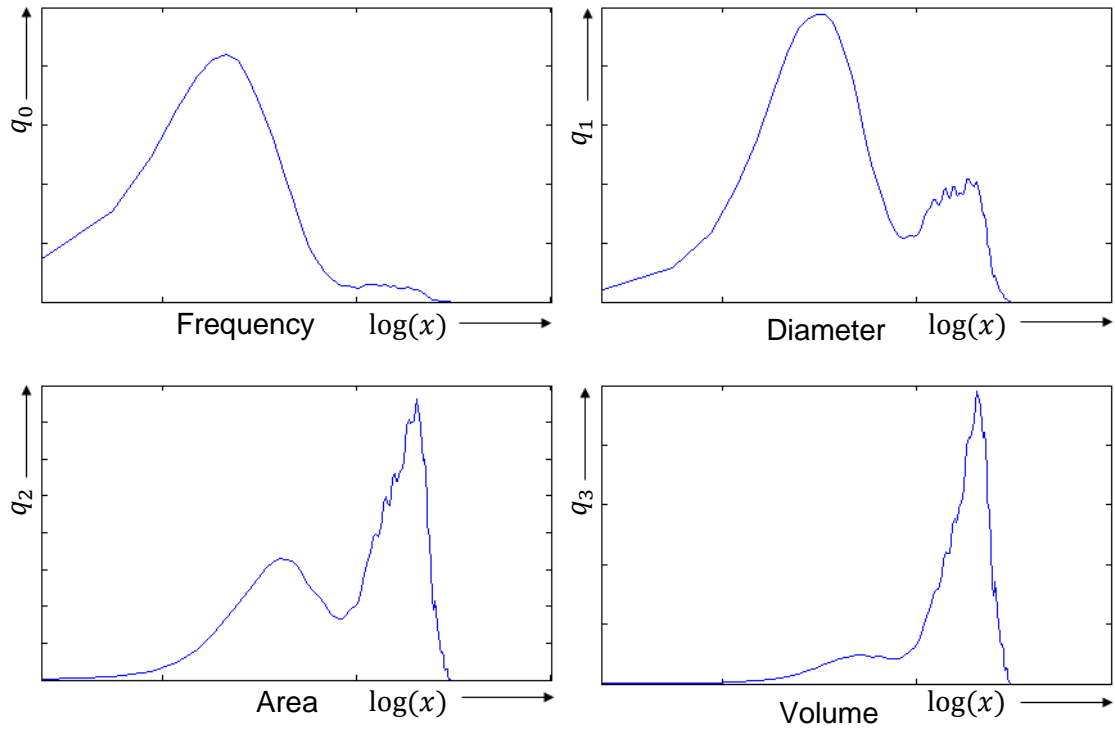


Figure 2 Graphical representation of the types of distributions presented in Table 2, based on the same particle size data

3.3.1 Moments of distribution

Distribution characteristics can be defined according to *moments of distribution*. The mathematical definition for the k -th *raw moment* of density distribution $q_r(x)$ of the random variable X is given by the equation

$$M_{k,r} = \int_{x_{\min}}^{x_{\max}} x^k q_r(x) dx. \quad (2)$$

The first subscript k represents the order of the moment and the second subscript r the type of quantity. (ISO 9276-2:1998(E))

Similarly the k -th *central moment* about the mean \bar{x} is defined in the equation below. (Alderliesten 1990a)

$$m_{k,r} = \int_{x_{\min}}^{x_{\max}} (x - \bar{x})^k q_r(x) dx \quad (3)$$

The raw moment of order k is the *expected value* of X^k , and the central moment is the expected value of $(X - \bar{x})^k$. The expected value of a random variable is the mean of possible values weighted according to their probabilities. (Dodge 2008, pp. 190–191, 358–359)

For the calculation of $M_{k,r}$, Equation (2) may in many instances be found impractical because it requires that $q_r(x)$ be known. Numerical integration techniques can be used to compute the integral over a series of measured data points, but it is often the case that data are given in size bins. It is therefore more convenient to discretise the equation. In a histogram, $q_r(x)$ is constant within a size interval $\Delta x_i = x_i - x_{i-1}$, and the Equation (2) can be rewritten as

$$M_{k,r} = \sum_{i=1}^N \bar{q}_{r,i} \int_{x_{i-1}}^{x_i} x^k dx,$$

which leads into the equation

$$\begin{aligned} M_{k,r} &= \frac{1}{k+1} \sum_{i=1}^N \bar{q}_{r,i} (x_i^{k+1} - x_{i-1}^{k+1}) \\ &= \frac{1}{k+1} \sum_{i=1}^N \Delta Q_{r,i} \left(\frac{x_i^{k+1} - x_{i-1}^{k+1}}{x_i - x_{i-1}} \right) \end{aligned} \quad \text{for } k \neq -1 \quad (4)$$

where $\bar{q}_{r,i}$ and $\Delta Q_{r,i}$ are the constant values of $q_r(x)$ and $Q_r(x)$ within the i -th size interval. It is possible to derive a corresponding equation with $k = -1$, and this would correspond to the so-called *harmonic mean*. This is, however, beyond the scope of this thesis. See the standard ISO 9276-2:1998(E) for more information.

3.3.2 Mean diameters, percentiles and the mode

The concept of *mean diameter* is defined by the British standard BS 2955:1993 as the '[s]ize of a hypothetical particle such that a population of particles having that size has, for the purpose involved, properties which are equal to those of a population of particles with different sizes and having that size as a mean size'.

Although the concept is easily defined, there are two different mathematical notations: ISO/DIN and *Moment-Ratio* (M-R) systems. (Alderliesten 2011) The German standard DIN 66141 and the ISO standard 9274-2 are based on the ISO/DIN system, hence the name, whereas many applications as well as the British standard BS 2955:1993 apply the Moment-Ratio system.

Both systems were extensively studied by *Maarten Alderliesten* in his articles (1990a) (1990b). His conclusion was that the statistical nature of the ISO/DIN system hampers its usability in practical applications, whereas the physical nature of the *M-R* system is more suitable in those cases. Here, the statistical nature of the former refers to the fact that it is calculated from a fitted size distribution, whilst the latter is calculated directly from measurement data, compare Equations (5) and (7). (Alderliesten 2011)

According to the DIN system the mean diameter $\bar{x}_{k,r}$ is based on Equation (5):

$$\bar{x}_{k,r} = \sqrt[k]{M_{k,r}} \quad (5)$$

Here, the subscripts k and r are the same as for the moment $M_{k,r}$. (ISO 9276-2:1998(E))

Mean sizes of the form $\bar{x}_{k,0}$ are called *arithmetic average particle diameters*, and mean sizes of the form $\bar{x}_{1,r}$ is called *weighted average particle diameters*. (ISO 9276-2:1998(E))

In most instances, particle size data are given either as number-based ($r = 0$) or volume-based ($r = 3$). Then Equation (5) can be rewritten as Equation (6) below. (ISO 9276-2:1998(E))

$$\bar{x}_{k,r} = \sqrt[k]{\frac{M_{k+r,0}}{M_{r,0}}} = \sqrt[k]{\frac{M_{k+r-3,3}}{M_{r-3,3}}} \quad (6)$$

According to the moment-ratio system the mean diameter $\bar{D}_{p,q}$ is defined by the equation

$$\bar{D}_{p,q} = \left(\frac{M'_p}{M'_q} \right)^{\frac{1}{p-q}}. \quad (7)$$

The prime in M'_k implies that, instead of the real moment, an estimator, called the *sample moment*, is used. The sample moment is defined by the formula

$$M'_k = N^{-1} \sum_i n_i \bar{x}_i^k, \quad (8)$$

where \bar{x}_i is the midpoint of the i -th size bin, and n_i is the bin frequency, and $N = \sum_i n_i$. (Alderliesten 1990a)

By combining Equations (7) and (8) one arrives at the following equation:

$$\bar{D}_{p,q} = \left(\frac{\sum_i n_i \bar{x}_i^p}{\sum_i n_i \bar{x}_i^q} \right)^{\frac{1}{p-q}}, \quad \text{for } p \neq q. \quad (9)$$

As shown by Alderliesten (1990a), for $p = q$, $\bar{D}_{p,q}$ can be obtained from

$$\bar{D}_{p,q} = \exp \left(\frac{\sum_i n_i \bar{x}_i^p \ln(\bar{x}_i)}{\sum_i n_i \bar{x}_i^p} \right), \quad \text{for } p = q. \quad (10)$$

If $p = q = 0$, $\bar{D}_{0,0}$ is called the *geometric mean*, and it is identical to the more common definition found in literature: $\bar{D}_{0,0} = \sqrt[N]{\prod_i \bar{x}_i}$. If $p = q > 0$, $\bar{D}_{p,q}$ is called the *weighted geometric mean*. (Alderliesten 1990a)

The two notations are related to one another by the equation below. (Alderliesten 1990a)

$$\bar{x}_{k,r} = \bar{D}_{p,q}, \quad \text{for } p = k + r, k \neq 0, r = q \quad (11)$$

Names for some of the most commonly used mean diameters are presented in Table 3.

Table 3 Recommended nomenclature for mean diameters

DIN/ISO	M-R	Recommended name (BS 2955:1993)
$\bar{x}_{1,0}$	$\bar{D}_{1,0}$	Arithmetic mean diameter
$\bar{x}_{2,0}$	$\bar{D}_{2,0}$	Mean surface diameter
$\bar{x}_{3,0}$	$\bar{D}_{3,0}$	Mean volume diameter
$\bar{x}_{1,1}$	$\bar{D}_{2,1}$	Diameter-weighted mean diameter
$\bar{x}_{1,2}$	$\bar{D}_{3,2}$	Surface-weighted mean diameter
—	$\bar{D}_{3,3}$	Volume-weighted geometric mean diameter
$\bar{x}_{1,3}$	$\bar{D}_{4,3}$	Volume-weighted mean diameter (Alderliesten 1990a)

One should be careful with the nomenclature of mean diameters because terms such as *volume mean* and *volume distribution mean* are ambiguous. The volume-weighted mean $\bar{D}_{4,3}$ is not the mean of the volumes of particles; instead, it is the mean of the particle diameters measured or weighted according to their volumes, hence the term *volume-weighted mean*. (Alderliesten 1990b)

The n -th percentile $x_{n,r}$ of a distribution is defined so that $Q_r(x_{n,r}) = n/100$, where n is a percentage, and it tells how much of the distribution lies below the given value. The most commonly used percentiles are the 10th, 50th and 90th percentiles – although others are also widely used. The 50th percentile is also referred to as the *median*. (Dodge 2008, pp. 419-421)

The *mode* is the most frequently observed value. Given a density distribution $q_r(x)$, the mode is the maximum of the distribution, and if the data are given as a histogram, the mode is the bin midpoint \bar{x}_i of the highest column. (Dodge 2008, pp. 351-353)

3.3.3 Standard deviation

The spread of a distribution $q_r(x)$ is characterised by the standard deviation s_r and its square s_r^2 , the variance. In the standard ISO 9276-2:2001, variance is defined as the second central moment of a distribution, $m_{2,r}$, and it can be calculated using Equation (3). In DIN/ISO notation this can also be presented by the equation below. (ISO 9276-2:1998(E))

$$s_r = \sqrt{M_{2,r} - M_{1,3}^2} \quad (12)$$

Using the Moment-Ratio system, the standard deviation can be calculated from Equation (13). (Alderliesten 1990a) This equation may be easier to compute because it can be calculated by applying the sample moment, presented in Equation (8). It is also the equation recommended by Alderliesten (1990a).

$$s_r = \sqrt{\bar{D}_{r+2,r}^2 - \bar{D}_{r+1,r}^2} \quad (13)$$

Another frequently used quantity is the *geometric standard deviation*, obtained from the equation

$$s_g = \exp \left(\sqrt{\frac{\sum_i n_i (\ln(\bar{x}_i / \bar{D}_{0,0}))^2}{N - 1}} \right). \quad (14)$$

It is useful when dealing with log-normal distributions because log-normal distributions have the property that $s = \ln(s_g)$. (Alderliesten 1990a)

3.4 Graphical presentation

Particle analysis data are most conveniently communicated in graphs. The graphs can be either direct measurement data visualisations or estimations of population probability density functions.

3.4.1 Histogram

The histogram is the most common representation. The data are divided into size bins, and each size bin is represented by one column, the area of each of which represents

the relative quantity of the corresponding size bin. Size bins need not be of the same width; in fact, it is a common practice to use a logarithmic series to determine the limits of the size bins (BS 3406-4:1993).

If $\Delta x_i = x_i - x_{i-1}$ is the width of the i -th size bin, then the corresponding increment of the $Q_r(x)$ -distribution $\Delta Q_{r,i} = Q_r(x_i) - Q_r(x_{i-1})$ represents the relative quantity of that size bin. Thus the histogram is obtained using the equation

$$\bar{q}_{r,i} = \bar{q}_r(x_{i-1}, x_i) = \frac{\Delta Q_{r,i}}{\Delta x_i}, \quad (15)$$

where $\bar{q}_{r,i}$ represents the height of the rectangular column. This is demonstrated in Figure 3. (ISO 9276-1:1998(E))

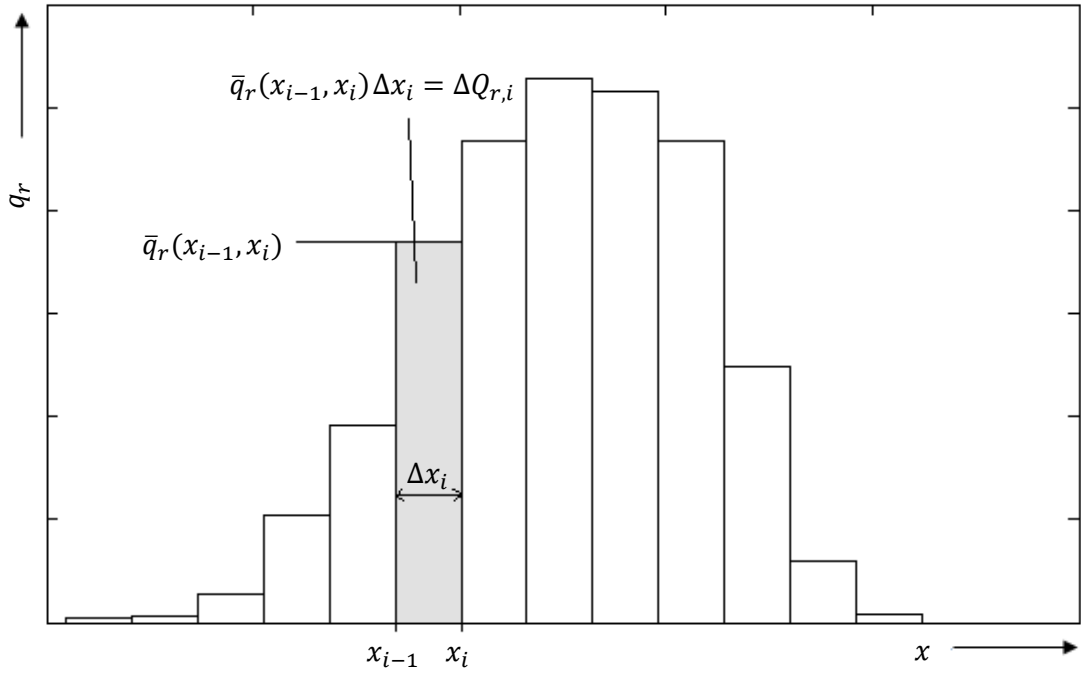


Figure 3 Histogram representation of the density distribution $q_r(x)$

The weighted quantity $\Delta Q_{r,i}$ can be calculated from frequency data using the following equation

$$\Delta Q_{r,i} = \frac{n_i \bar{x}_i^r}{\sum_i n_i \bar{x}_i^r}, \quad (16)$$

where r represents the type of quantity as specified in Table 2, n_i the frequency and \bar{x} the midpoint of the i -th size bin. (BS 3406-4:1993)

The standard ISO 9276-1:1998 recommends that, should the abscissa be changed, the total *visual* area should still remain constant irrespective of any changes of the abscissa. This requirement leads into the transformed distribution $q_r^*(\xi)$, for which $\xi = f(x)$, and the following equation holds:

$$\bar{q}_r^*(\xi_{i-1}, \xi_i) \Delta \xi_i = \bar{q}_r(x_{i-1}, x_i) \Delta x_i \quad (17)$$

Using a logarithmic abscissa, $\xi = \log(x)$, and thus the height of the column is obtained from

$$\bar{q}_{r,i}^* = \frac{\bar{q}_{r,i} \Delta x_i}{\log(x_i) - \log(x_{i-1})} = \frac{\Delta Q_{r,i}}{\log\left(\frac{x_i}{x_{i-1}}\right)}, \quad (18)$$

and it can be shown that the transformation between continuous density functions can be performed by

$$q_r^*(\xi) = x q_r(x). \quad (19)$$

Nevertheless, the cumulative distributions remain unchanged by any transformation:

$$Q_r^*(\xi) = Q_r(x) \quad (20)$$

It is important to realise that the logarithmically transformed distribution is essentially different from the traditional distribution. Figure 4 visualises the difference.

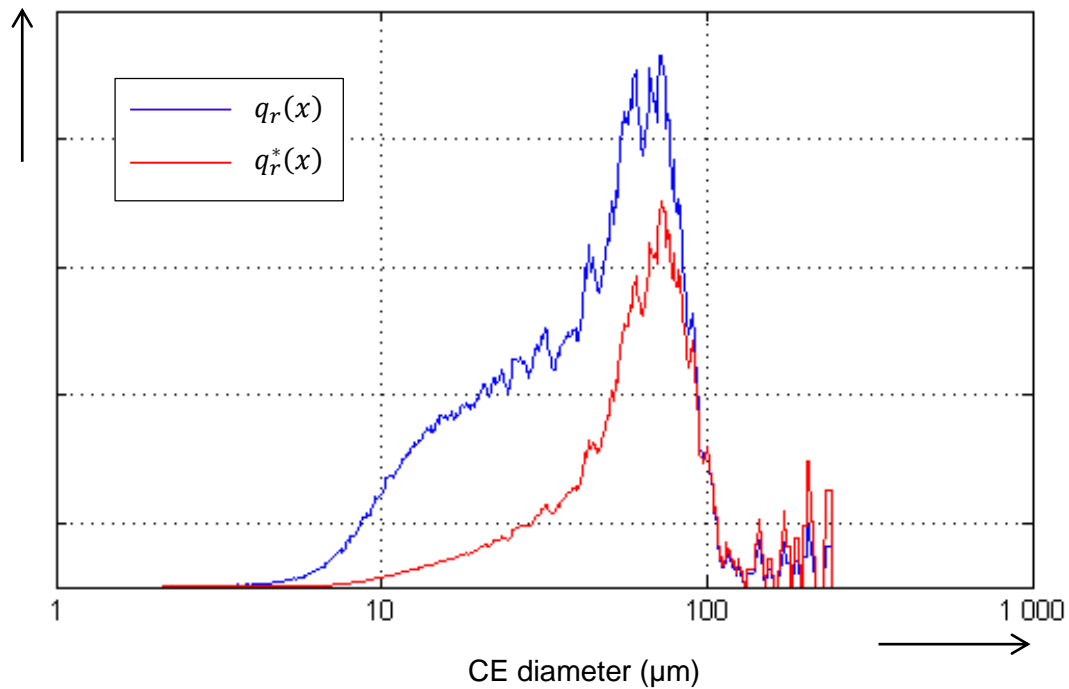


Figure 4 Comparison of the $q_r(x)$ - and $q_r^*(x)$ -distributions, both plotted on a logarithmic abscissa

3.4.2 Frequency and volume curves

The midpoints \bar{x}_i on top of each column in a histogram can be connected to form a segmented line. This line representation is called the *frequency polygon*. As the number of size bins approaches infinity and the width of the bins approach zero, the curve becomes an increasingly accurate estimation of the underlying probability density function – provided a sufficient enough sample population. The limiting case at a large number of small bins is called the *frequency curve*. (Dodge 2008, pp. 208-212)

Although not explicitly stated in any reference, polygons and curves based on histograms that represent observations weighted according to diameter, area or volume could be called *diameter*, *area* and *volume curves* respectively.

It is obvious that in order to accomplish a good frequency curve, the sample population has to be large. With insufficient populations, the curve can be smoothed by taking the running average of a certain number of adjacent points. (Malvern Instruments 2013, p. 9-26) This is especially convenient for plots of the volume distribution, since the effect of large outliers become amplified. This is demonstrated in Figure 5.

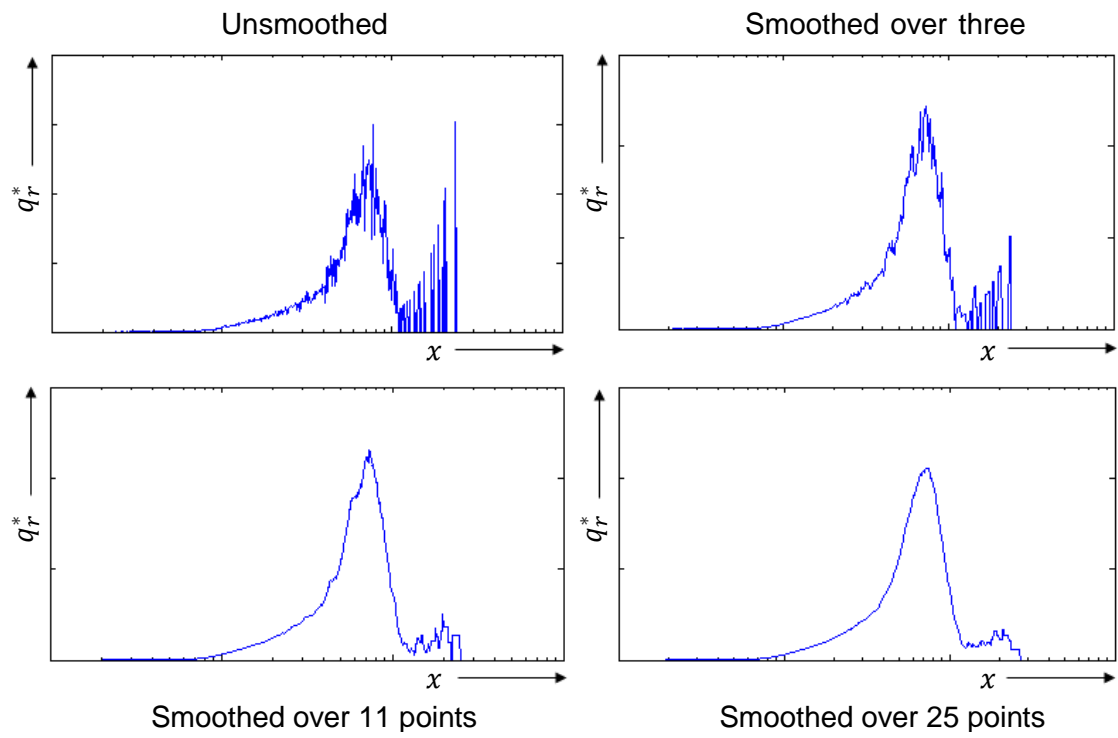


Figure 5 The effect of smoothing on the frequency curve by taking the running average

4 Image Analysis using *Morphologi G3*

4.1 *Malvern Morphologi G3*

Image analysis in general is the process of extracting information from images. One commercially-available image analysis system is the *Morphologi G3*, manufactured by *Malvern Instruments*, a British company specialising in analytical instruments (Figure 6). It is designed especially for characterising particle size and shape. The system comprises the instrument itself and the computer software that is used to control the instrument and to handle the results.

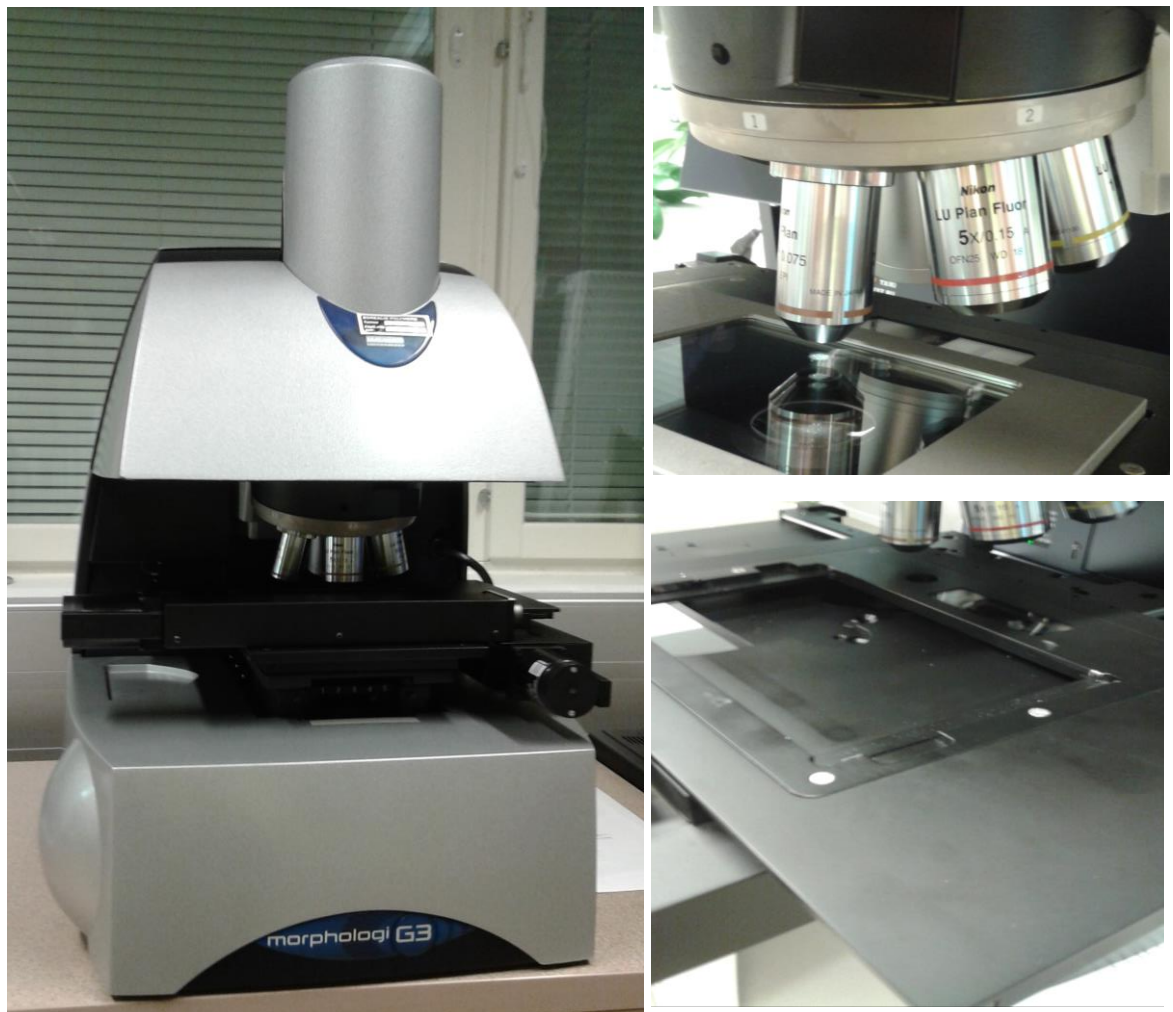


Figure 6 The instrument (left); close-up of the optics (top right); close-up of the movable stage

All photographed particles can be viewed and examined individually in the software. The software has also built-in features that calculate and present statistics (Figure 7). The software is also used to create *SOP*-files (*standard operating procedures*), which contain predetermined parameters for different kinds of measurements. Each method and catalyst type warrants its own *SOP*-file.

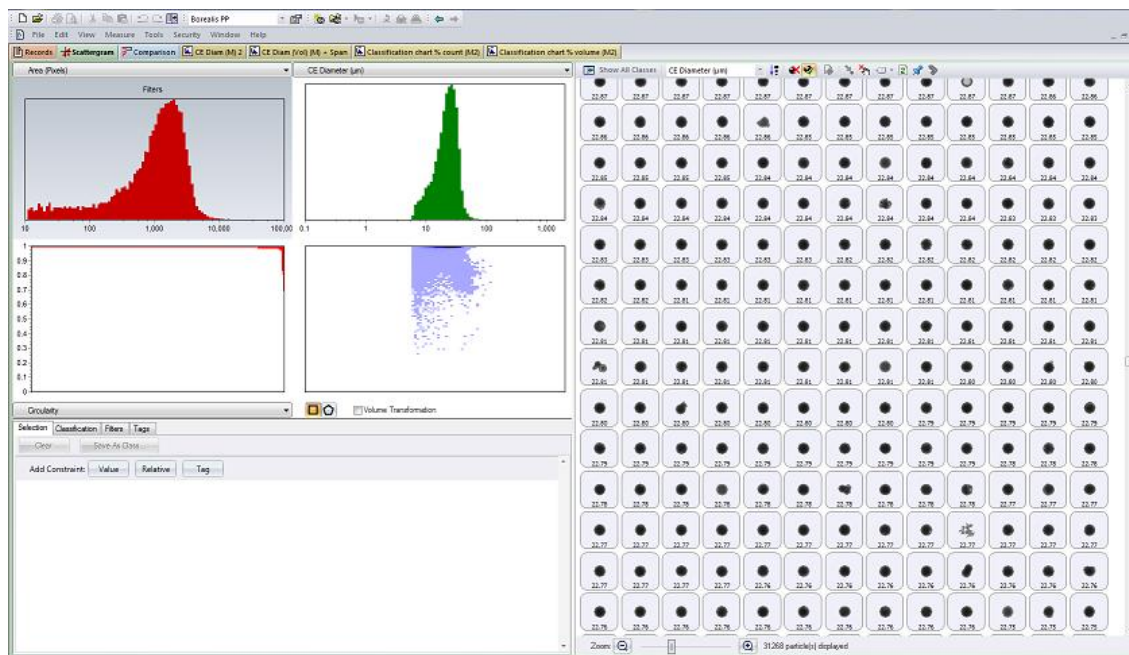


Figure 7 *Morphologi* software showing all captured images on the right, and statistics on the left

4.2 Sample preparation

Catalyst samples are received either as dry samples in septa bottles or as oil slurries in bigger bottles. A sample concentration of approximately 0.4% by weight of catalyst is prepared, either by adding the required amount of oil to a dry sample or by further diluting a slurry sample. The sample is then mixed using a rotator mixer in order to homogenise the sample. The use of shakers should be avoided if possible because they would cause air bubbles to form.

Two kinds of sample carrier plates are used; the *wet cell* is composed of two sheets of glass, which are separated by a spacer and hold the sample suspension in between the sheets of glass, and the *microscope slide holder* holds up to four standard microscope slides, see Figure 8.

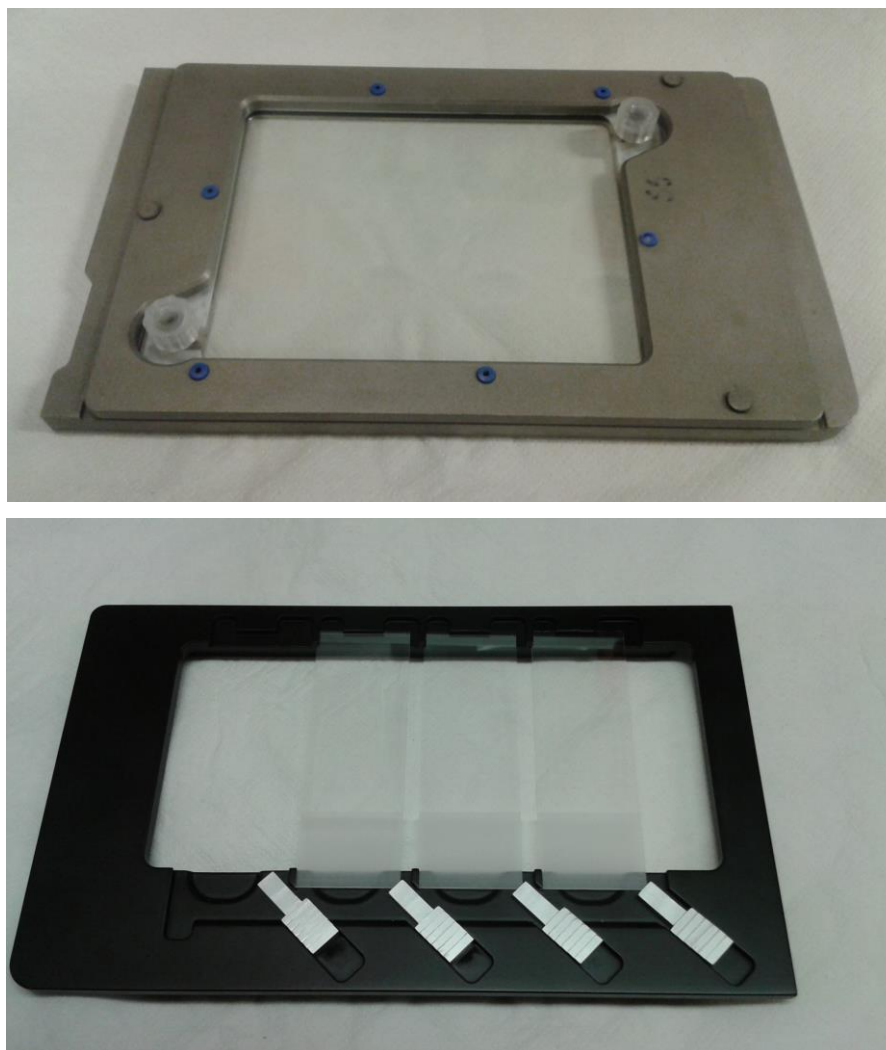


Figure 8 The wet cell and the microscope slide holder

After being thoroughly mixed, a subsample of approximately 3.5 ml is taken from the septa bottle and injected into the wet cell. The injection should be carried out smoothly by pushing the plunger steadily; otherwise particles will segregate. The wet cell is sealed by screwing on two caps. If the microscope slides are being used instead, the subsample is smaller and deposited onto a microscope slide. The sample plate is then placed onto the stage, and left for 20–30 minutes to allow particles to settle.

The whole sampling process is presented in the flowchart Figure 9. Only sample divisions 2, 3, and 4 are controlled in the laboratory, and can be considered as part of the method.

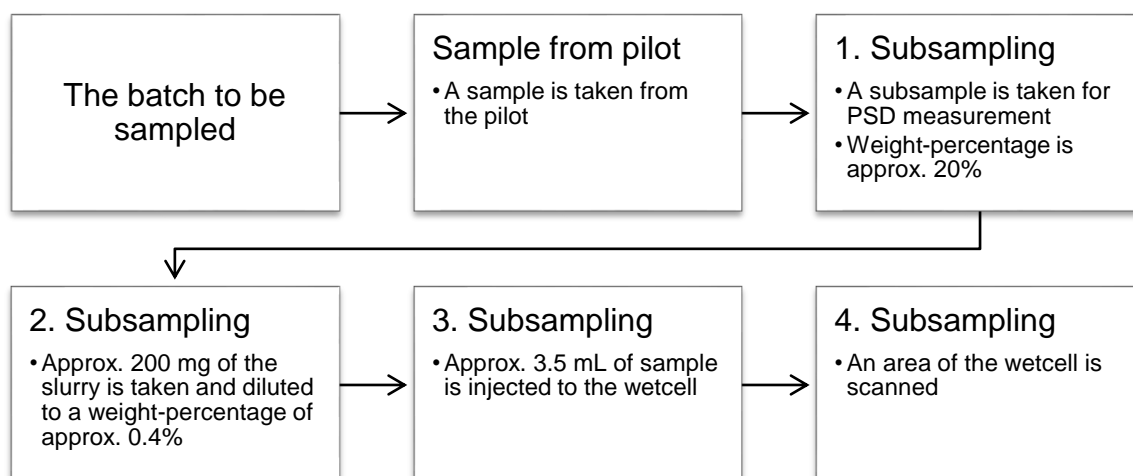


Figure 9 The sampling process for slurry samples from the pilot

4.3 Image acquisition

4.3.1 General

For image acquisition, *Morphologi G3* has five objectives. Each objective has its specific *Depth of Field (DOF)*, which is the depth at which particles appear sharp, and a certain range of recommended particle sizes. The range is based on pixel size, see Chapter 4.5.1 for more information. These specifications are presented in Table 4.

Table 4 Ranges and DOFs of the objectives (Malvern Instruments 2013)

Optics	DOF	Range
2.5x	97.78 μm	13 μm –1,000 μm
5x	24.44 μm	6.5 μm –420 μm
10x	6.11 μm	3.5 μm –210 μm
20x	3.44 μm	1.8 μm –100 μm
50x	1.82 μm	0.5 μm –40 μm

There are three illumination options: *diascopic* (bottom light), *episcopic* (top light) *bright field* and *episcopic dark field*, see Figure 10. Bottom light is recommended by default and has therefore been selected for all currently used *SOPs*; top light had been tested and found unsuitable in the development of the original methods.

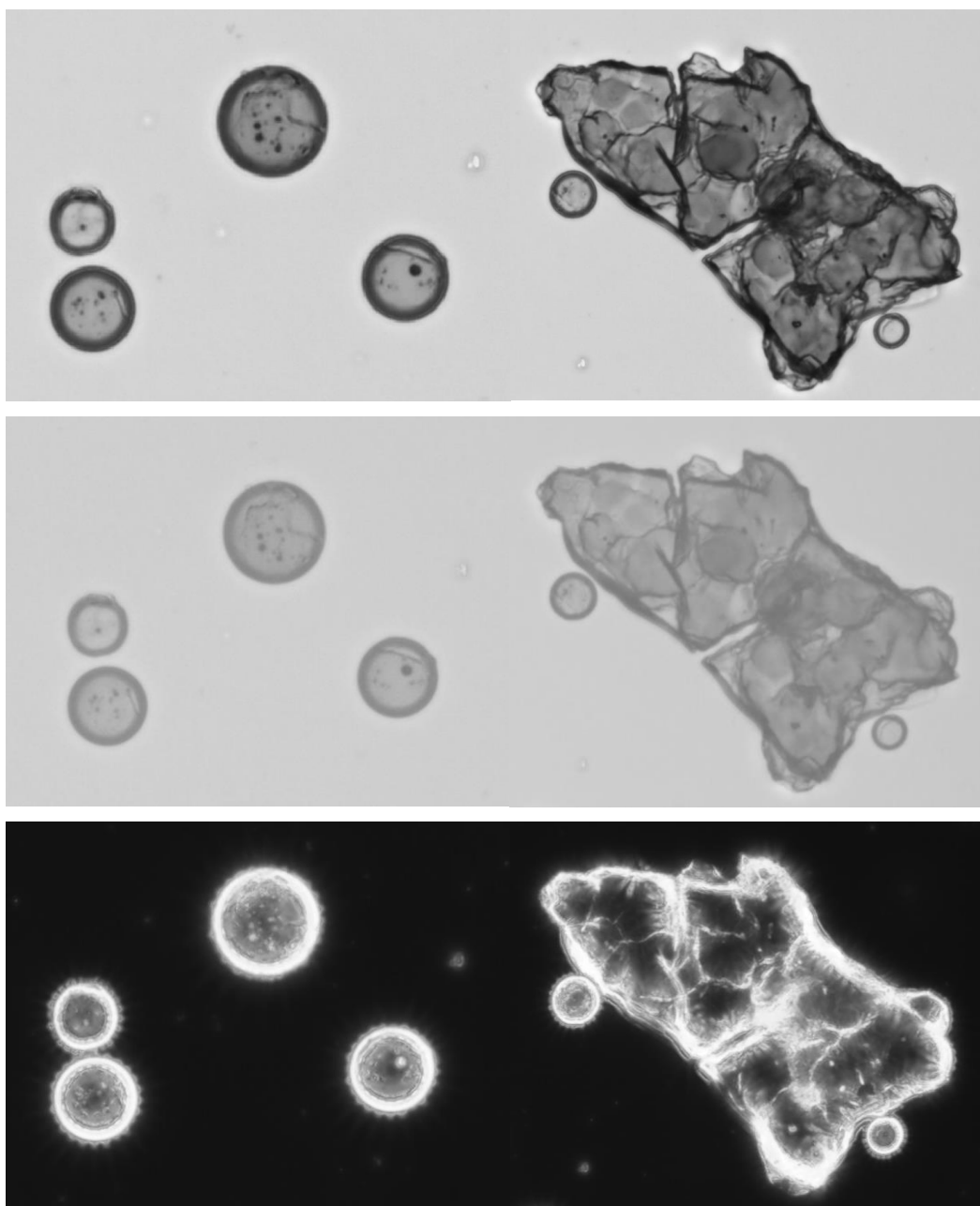


Figure 10 Top row: Pictures taken with the default diascopic illumination; Middle row: Pictures taken with bright field episcopic illumination; Bottom row: Pictures taken with dark field episcopic illumination

4.3.2 Frame overlap

It is important to notice that some particles will be cut by the edge of the measurement frame. If these cut particles are accepted for measurement, they will introduce an error by biasing lower particle sizes. (ISO 13322-1:2004(E)) To remedy this, frames are set to overlap so that particles at the edge of one frame appear in the middle of another frame. This occurs in both horizontal and vertical directions. See Figure 11.

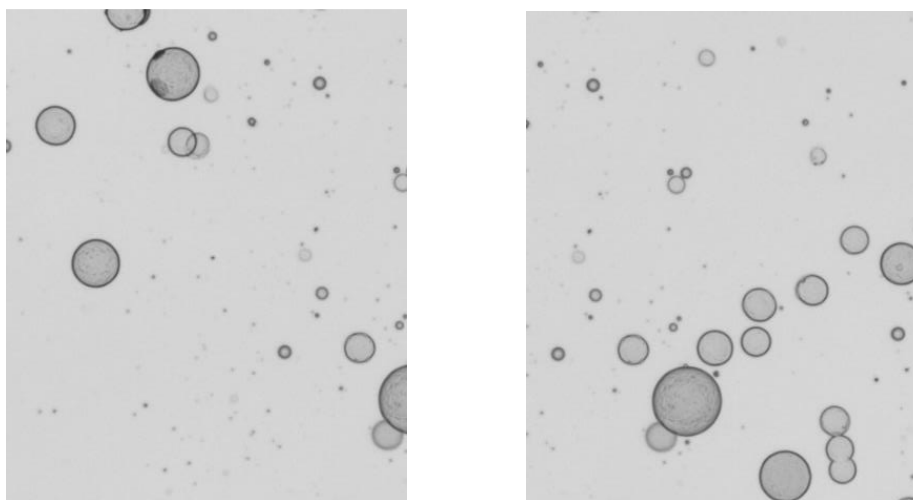


Figure 11 Frame overlap in the horizontal direction. Notice how the particle at the lower right corner is cut by the edge of the measurement frame, but appears intact in the second image

4.3.3 Z-stacking

The depth of field can be widened by a technique called *Z-stacking* (or *focus stacking*), where images are taken at multiple focal distances and then combined into one so that the final picture is as if it had a combined depth of field of all the individual pictures. The trade-off is that the time needed to perform a measurements increases significantly because more images are taken in every one point.

There are two z-stacking algorithms available: *differential*, which is the most recent algorithm, and *legacy*, which is preserved only to allow the reproduction of older measurements that were carried out using the original algorithm. More algorithms may be released in the future.

4.3.4 Merged-objective measurement

Measurement range can be widened by the use of multiple objectives on one sample. If two areas are scanned with different objectives, the results are combined so that the merge point is the smallest recommended diameter of the lower magnification. Particles measured with the higher magnification that are larger than the merge point are not included in the results. If the area for the higher magnification is smaller than the area for the lower magnification, different areas are compensated by multiplying the contribution that particles measured with the higher magnification have to the results by the fraction A/a , where A is the area scanned with the lower magnification and a is the area scanned with the higher magnification. Performing a merged-objective measurement has a significant time penalty. (Malvern Instruments 2009b)

4.3.5 Measurement phases

Each measurement consists of the following phases presented in Figure 12.

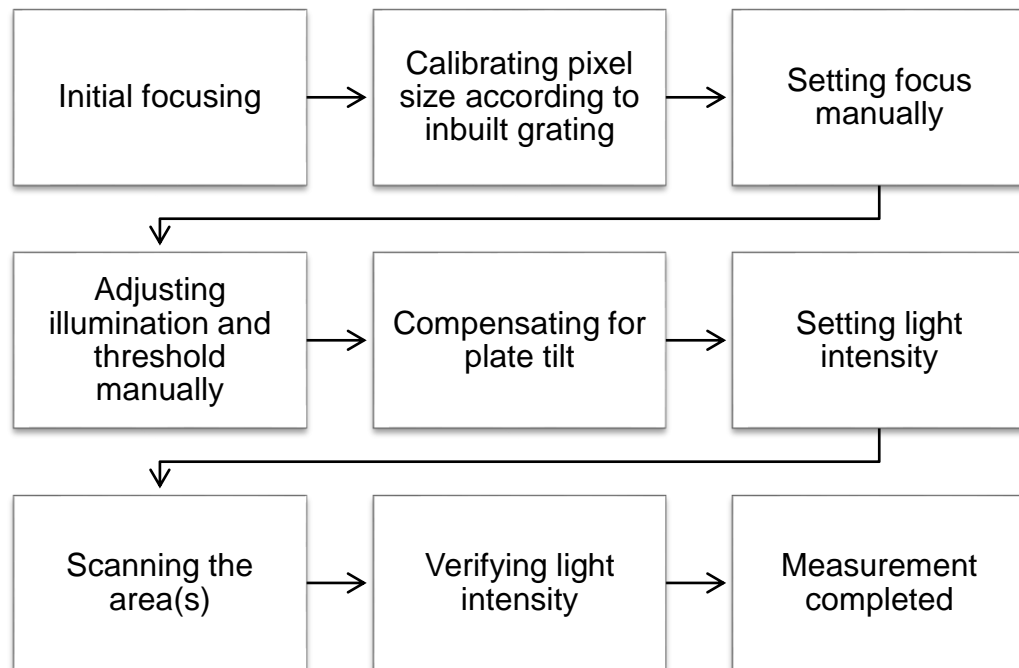


Figure 12 *Morphologi G3* measurement presented as a flow chart

During initial focusing the software finds the focus reference point using the z-level reference point mounted on the sample carrier holder. The pixel size is calibrated using the

grates. The grating surface is found by using the top light and projecting a cross onto the surface. The surface is in focus, when the edges of the cross appear sharp.

Focus, illumination and threshold can be set to a fixed value, thus these steps can be omitted. For the currently-used method, only the focus is set manually, while the others are set automatically to a predetermined level.

During the compensation of plate tilt, the plate surface is checked at a number of defined positions near the corners of the measurement area. This is unnecessary for measurements using low objectives, owing to their deep depths of focus.

4.4 Image segmentation

4.4.1 Segmentation by threshold

Segmentation is the process by which an image is divided into *areas of interest* and into the *background*. The simplest of segmentation method is *greyscale thresholding*, in which every pixel lighter than a fixed threshold level is identified as background; the rest is identified as areas of interest (particles). *Morphologi* captures 8-bit images, meaning that each pixel has a total of 256 possible from 0 to 255, with 0 representing the darkest and 255 the brightest value possible. This method works best if the image histogram is bimodal with a clear distance between the two peaks. See Figure 13 for an example.

A good threshold level should detect the whole particle boundary, but no pixels of the background around it. The software has a hole filing algorithm that can fill in particle images, as long as the perimeter is complete. The complete detection of the perimeter is usually easy because of the so-called *halo*, which is a dark ring appearing around particles. Figure 14 demonstrates the threshold setting.

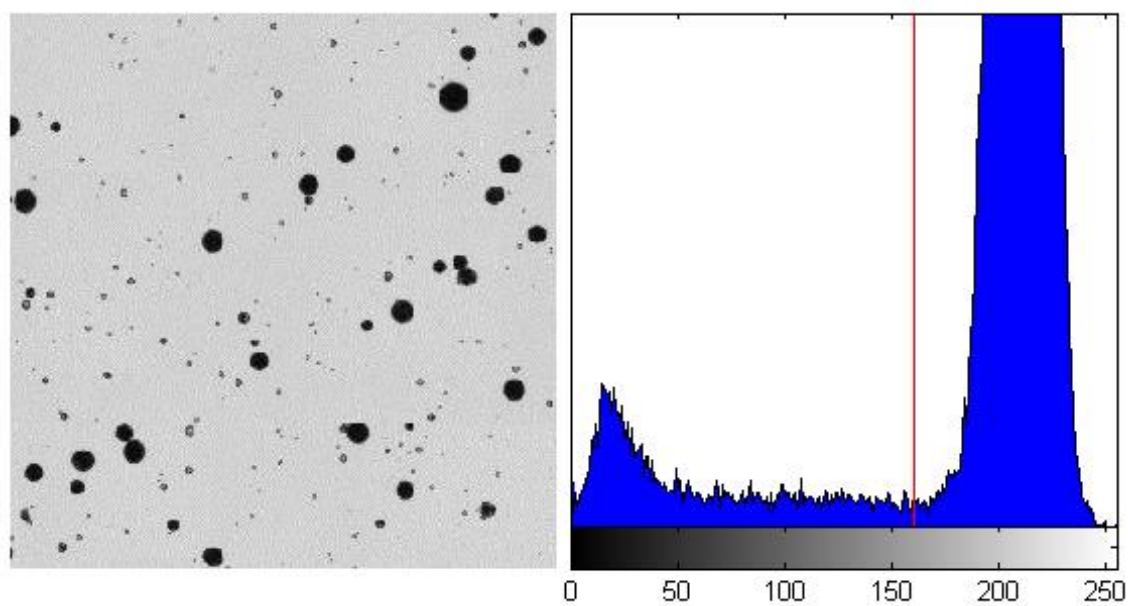


Figure 13 An image taken with *Morphologi G3*, and its histogram representation; the red line marks the threshold value (160) that was used to segment the image

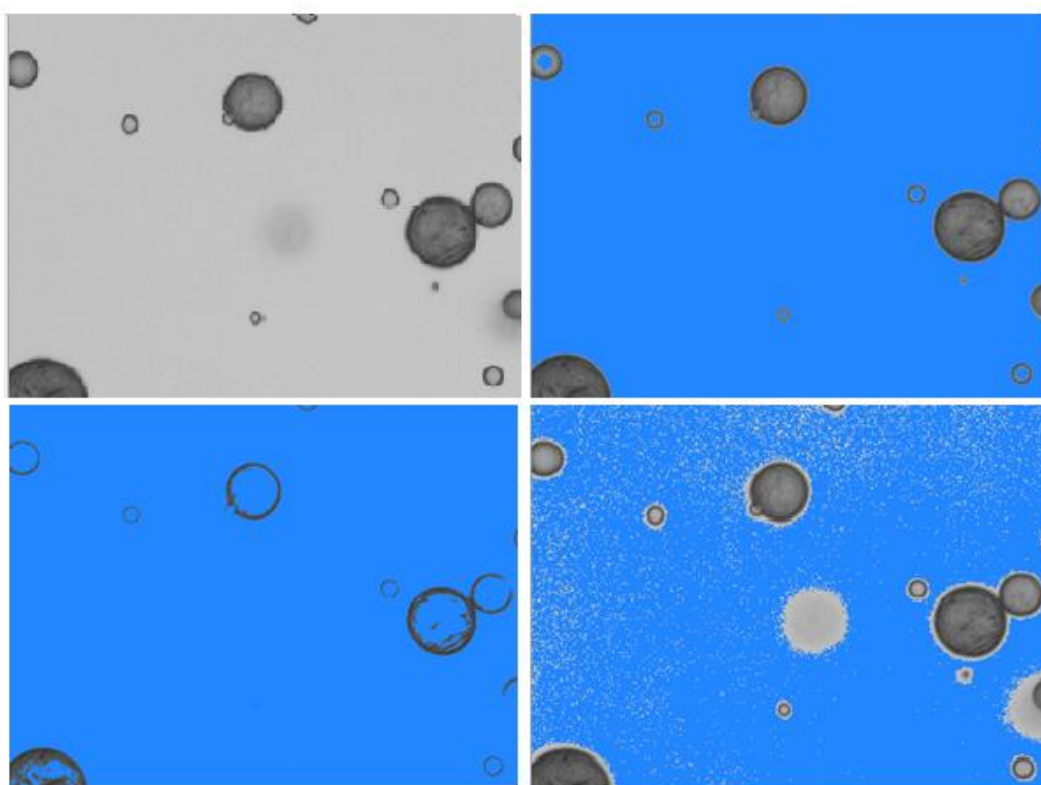


Figure 14 Clockwise from top left: the image to be thresholded; threshold set properly; threshold set too high, background starting to be counted as particles; threshold set too low, particles start to disappear

4.4.2 Segmentation by watershed

Watershed is a segmentation method that can be used to separate touching particles (Figure 15). There are different algorithms for the method, but they are all based on finding the particle edge. This method is applied after segmentation by thresholding, and the algorithm is good only for spherical particles; it is not suitable for needle-like particles – especially if they are crossed. (Malvern Instruments 2013, p. 6-27) The effect of watershed was tested experimentally; the results are presented in Chapter 5.3.

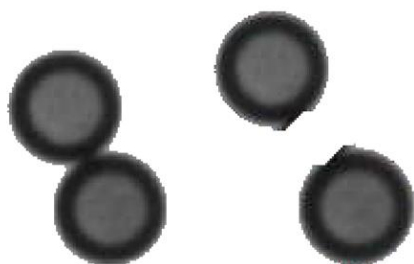


Figure 15 A paired particle cut in two by the watershed algorithm

4.5 Particle image measurements

4.5.1 Pixel size and measurement resolution

The pixel size x_r (also called the *resolution*) is determined by calibrating the instrument over four calibration grids. The grid bars are separated by a fixed and constant space. The grid spacing can be traced to *National Physical Laboratory* in the United Kingdom and *National Institute of Standards and Technology* in the United States. Calibration is carried out before each measurement to ensure the correct correspondence between pixel size and the used physical unit. The grid spacing may change slightly according temperature changes.

The minimum particle size recommended in Table 4 is based on the assumption that images that contain less than 110 pixels cannot provide accurate enough shape information. The area of a 110-pixel image is calculated by $A = 110 \times x_r^2$, and the corresponding minimum CE diameter by $x_{CD} = \sqrt{(4 \times A/\pi)}$. (See Equation (22) in the next section.) The relevance of this recommendation to the results is discussed in Section 6.2.2.

Table 5 Resolution (pixel size) and the minimum pixel size (Malvern Instruments 2013, p. 15-2)

Optics	x_r (μm)	Calc. minimum (μm)	Given minimum (μm)
x2.5	1.12	13	13
x5	0.560	6.6	6.5
x10	0.280	3.6	3.5
x20	0.140	1.7	1.8
x50	0.056	0.7	0.5

4.5.2 Image size and shape descriptors

According to ISO 13322-1:2004, the primary values of image analysis are the area and the maximum and minimum *Feret's* diameters of a particle image. The *Feret's diameter* is the distance between two parallel tangents that are on the opposite sides of a particle. Largest possible *Feret's* diameter x_{Fmax} corresponds to the *length* and the smallest diameter x_{Fmin} to the *width* of the particle. (BS 2955:1993) (ISO 9276-6:1998(E))

In *Morphologi*, length is defined so that all possible lines between two points on the perimeter are projected onto the *major axis*, and width so that the lines are projected onto the *minor axis*. Major axis is the axis that passes through the centre of mass at an orientation corresponding to the minimum rotational energy of the shape; the minor axis passes through the centre of mass as well but is perpendicular to the major axis. (Malvern Instruments 2013, pp. 2-9–2-10) Therefore, width and length are different depending on whether one uses the definitions presented in the standards or the ones that are used by *Malvern*.

The aspect ratio is defined as the ratio of width and length, as shown in the equation

$$\text{Aspect ratio} = \frac{\text{width}}{\text{length}}. \quad (21)$$

Assuming that particles are spherical, particle size is expressed as circular equivalent diameter x_{CD} , defined by the equation

$$x_{CD} = \sqrt{\frac{4A}{\pi}}. \quad (22)$$

The *circularity* expresses to what degree the projected area deviates from that of a perfect circle. The circularity C is defined for the projected area A and the perimeter P in Equation (23). (ISO 9276-6:1998(E))

$$C = \sqrt{\frac{4\pi A}{P^2}} \quad (23)$$

A more sensitive version of circularity is the *high sensitivity (HS) circularity*, which is obtained by squaring the circularity:

$$\text{HS Circularity} = C^2 \quad (24)$$

The *convexity* characterises the *roughness* of the image perimeter and is defined by the equation

$$\text{Convexity} = \frac{P_C}{P}, \quad (25)$$

where the P_C is the length of the perimeter of the *convex hull*. (ISO 9276-6:1998(E)) The convex hull of an object is the smallest perimeter that encompasses the object so that every two points on the perimeter can be joined by a straight line that remains within the convex hull (Figure 16). If areas constrained by the perimeters in Equation (25) are used instead, convexity is replaced by *solidity*.

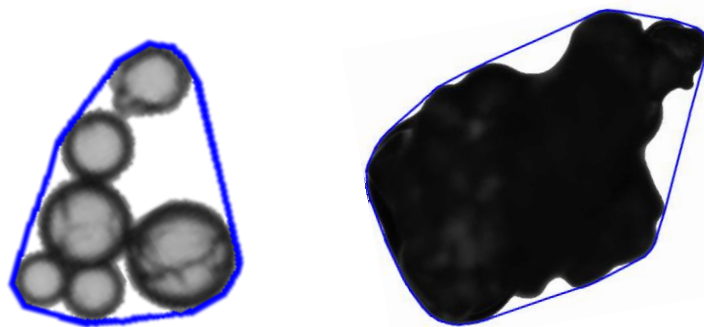


Figure 16 Convex hull of the particle image marked with a blue line

The *elongation* is a measure of the elongation of an image, and it is defined in Equation (26). (Malvern Instruments 2013, p. 2-6) This definition is different from the one in ISO 9276-6:2008.

$$\text{Elongation} = 1 - \frac{\text{width}}{\text{length}} \quad (26)$$

4.6 Post-measurement

4.6.1 Particle image exclusion

Not all particles can be seen as representing of the sample. A common problem is that some particles are touching each other and are therefore interpreted by the software as one large particle. Unless properly filtered out, pairs and collections of particles will bias the results towards larger sizes.

After a measurement particle images are classified into customised classes, based on the descriptors presented in the previous chapter. The classification process will be assessed in Chapter 6.1. Some non-representative images can be excluded from the measurement based on the classification or manual intervention.

Aggregates are assemblies of particles, which are loosely attached to one another, as opposed to *agglomerates*, which are assemblies of rigidly joined particles. (BS 2955:1993) Agglomerates should be measured as one, but aggregates should not. However, the distinction between the assemblies is not always clear from the images. See Figure 17 for examples.

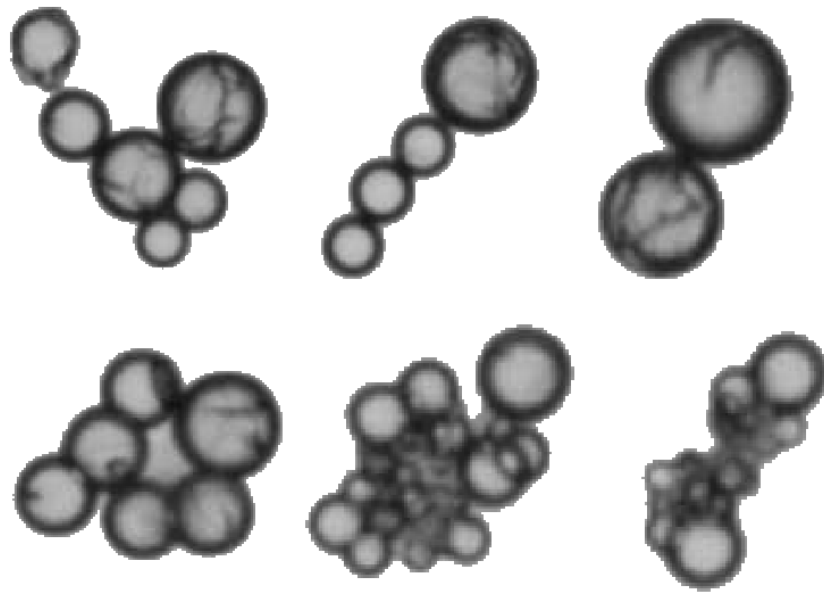


Figure 17 Assemblies of particles; the first row shows touching particles; particles in the second row might be either collections of touching particles or agglomerates

If the threshold level is set too high, some particles may appear as C-shaped, incomplete particles. As the perimeter is not complete, the hole filling algorithm cannot fill in the missing part. Incomplete images are interpreted by the software as being smaller than the true size, and their inclusion in the measurement would bias the results towards smaller sizes.

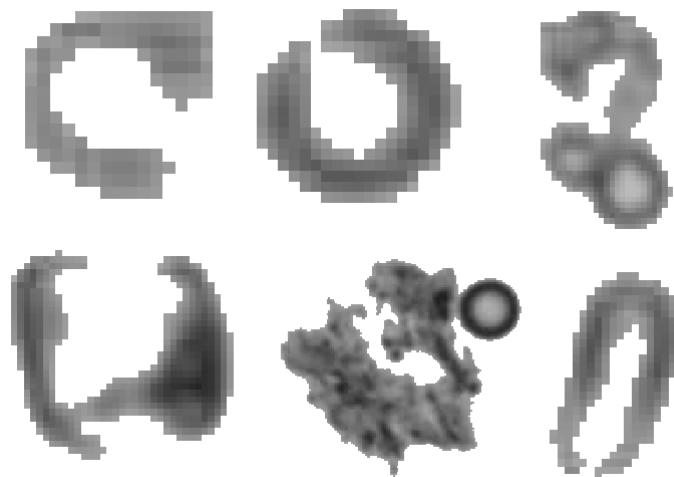


Figure 18 Images with incomplete perimeters, the true size and shape information is lost

Gas bubbles are often easily recognised because of the bright spot they have in the middle, unfortunately however, the software is usually not capable of this.

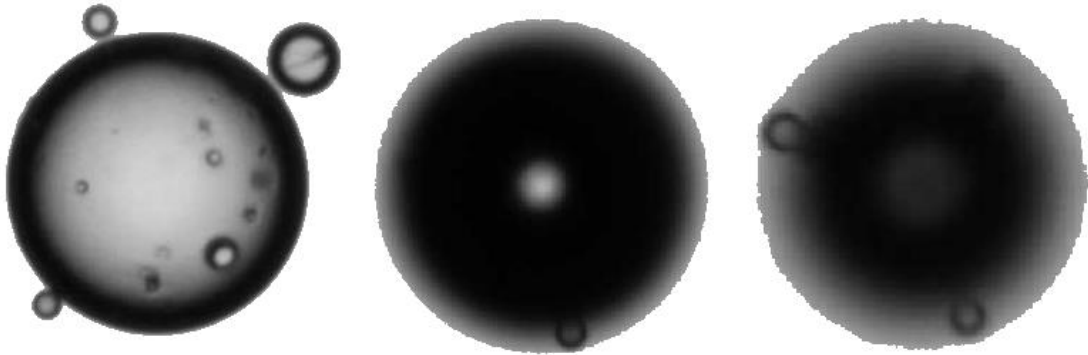


Figure 19 Different appearances of gas bubbles; the first bubble might also be a hollow particle

4.6.2 Results reporting

A report page that lists measurement parameters and statistical values and presents a volume-curve representation of the $q_r^*(x)$ -distribution is created by the software and then communicated to the requestors. The plotted volume graph is smoothed over 11 points – which is the default setting – and the reported mean diameter is the $\bar{D}_{4,3}$ (or $\bar{x}_{1,3}$ using the ISO-notation). Percentiles $x_{10,3}$, $x_{50,3}$, and $x_{90,3}$ are also reported. The dispersion of the distribution is characterised by the range (x_{min} , x_{max}) and the *span*, defined by the equation below.

$$\text{span} = \frac{x_{90,r} - x_{10,r}}{x_{50,r}} \quad (27)$$

For each magnification $\times 2.5$, $\times 5$, and $\times 10$, two pictures are taken, preferably with the aid of z-stacking if need be.

Part II. Examination of the currently-used method

5 Sample preparation and measurement

5.1 Sample concentration

The optimal sample concentration had been determined to be approximately 0.4% by weight. This concentration should provide a large enough sample population yet not have a large number of particles touching. However, as that concentration was determined using a reference sample that had a $\bar{D}_{4,3}$ -mean of 60 μm , the concentration cannot be generalised to apply to samples of different sizes. If the particles are smaller, the concentration ought to be smaller as well, and if the particles are very large, the concentration ought to be larger.

Using a sample from the pilot that was known to consist of smaller particles ($\bar{D}_{4,3}$ of approximately 20 μm) and that had a solid content of 14.5%, four subsamples (Table 6) were prepared.

Table 6 Sample concentrations

Sample no.	Slurry (g)	Oil added (g)	Weight percentage
1.	0.366	12.887	0.41%
2.	0.193	12.971	0.22%
3.	0.106	13.171	0.12%
4.	0.046	12.911	0.05%

Pictures taken using the above-mentioned concentrations are presented in Figure 20.

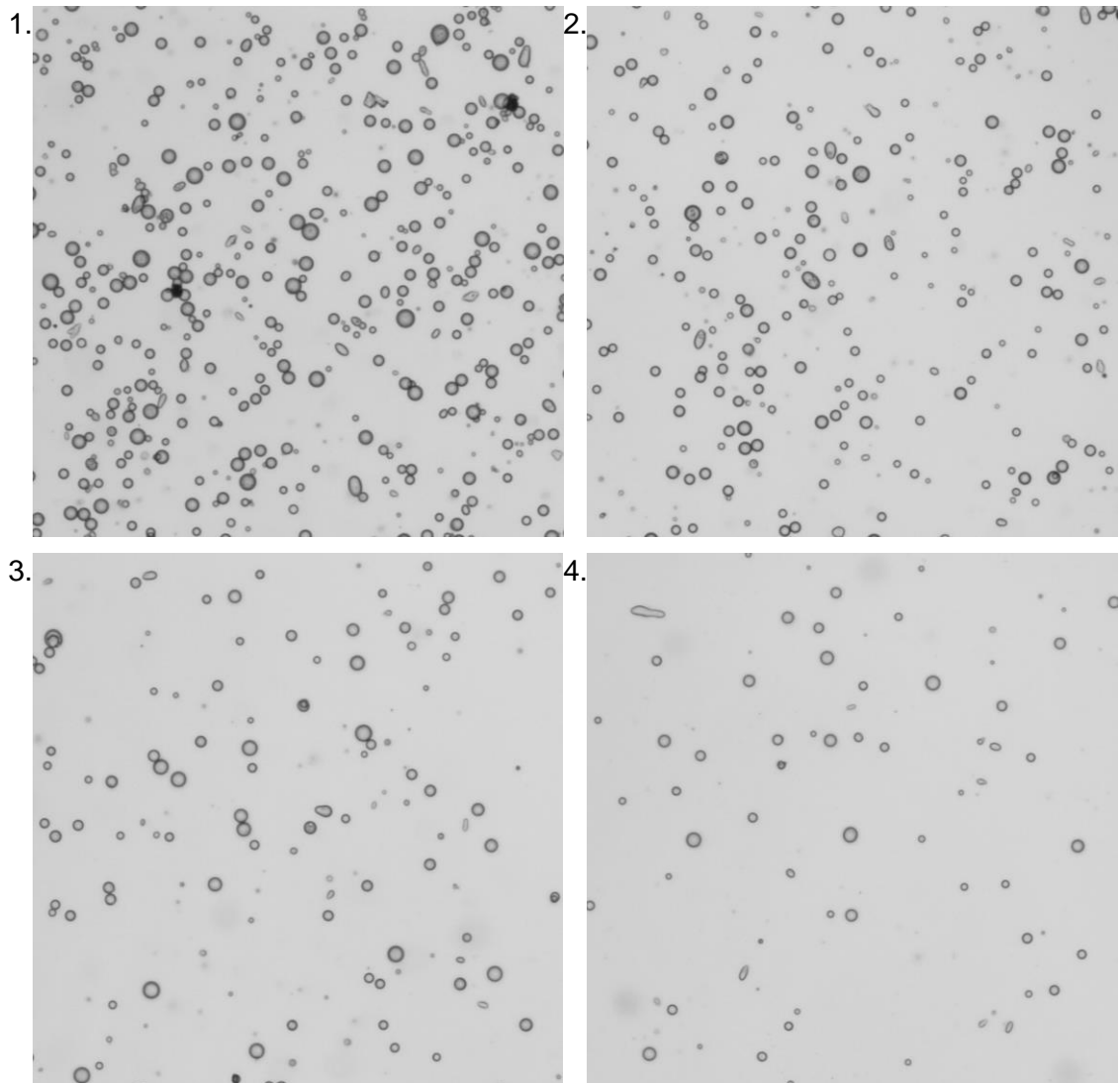


Figure 20 Pictures of samples 1 through 4, taken with the $\times 5$ -objective

The pictures suggest that aiming at about 0.1% would be a suitable choice for pilot samples of a smaller diameter.

Exact determination and documentation of the concentration of each individual sample is most likely unneeded because all measurements are based on the number of individual particles. A discussion regarding the minimum required sample population can be found in Chapter 7.2. The concentration could nevertheless be documented in order to allow the repeatability of measurements.

5.2 Focusing

Particles suspended in oil do not always settle properly. In the wet cell quite often some particles get stuck to the upper sheet of glass while the rest settle to the bottom, leaving little of interest in between. Consequently, a considerable proportion of particles is left out of focus and thus not measured.

Uneven settling is a real problem because it is possible that particles of the same kind will settle to the same level, thus excluding the out-of-focus particles will categorically leave out certain kinds of particles. Fortunately, however, particle settling is usually good; the example in the picture below is an extreme case.

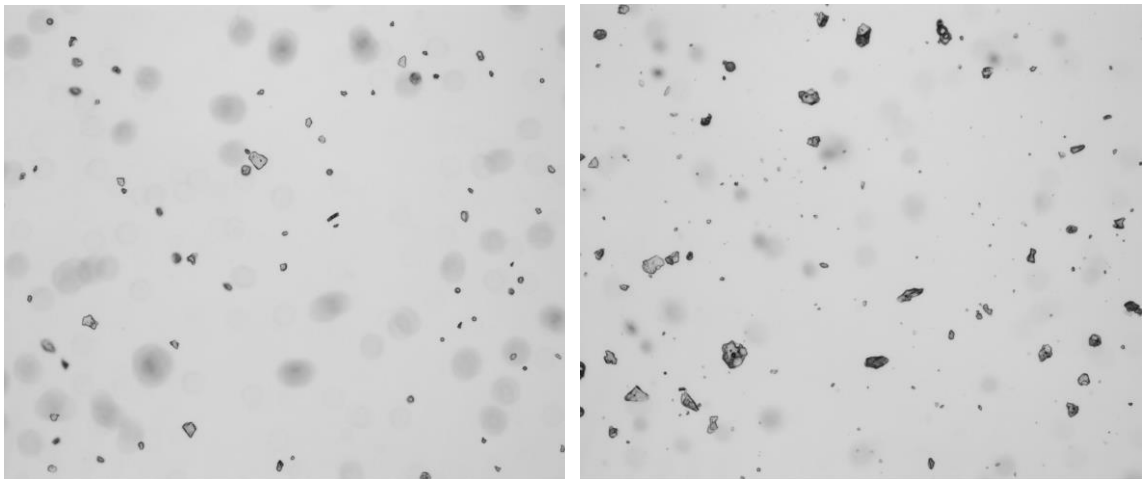


Figure 21 Focus set on particles on the top glass (left) and on the bottom (right) using a magnification of $\times 5$

One solution to uneven settling would be z-stacking, as introduced in Section 4.3.3. The trade-off is that taking more images increases the measurement time. An easy solution would be to set manually two focus points, one for the bottom and the other for the upper sheet of glass. However, this feature is not available with the software; instead, a fixed step size is used to determine the focus distance at which images are taken. Therefore, for the $\times 5$ -objective, a total of 6 layers ($244\ \mu\text{m}$) would be needed to cover the depth of the wet cell; for the $\times 10$ -objective the maximum number of layers is eight, which covers a depth of $85\ \mu\text{m}$.

The depth of field (DOF) is presented in-scale with the total depth of the wet cell as well as some of the minimum and maximum particles from Table 4 in the picture below.

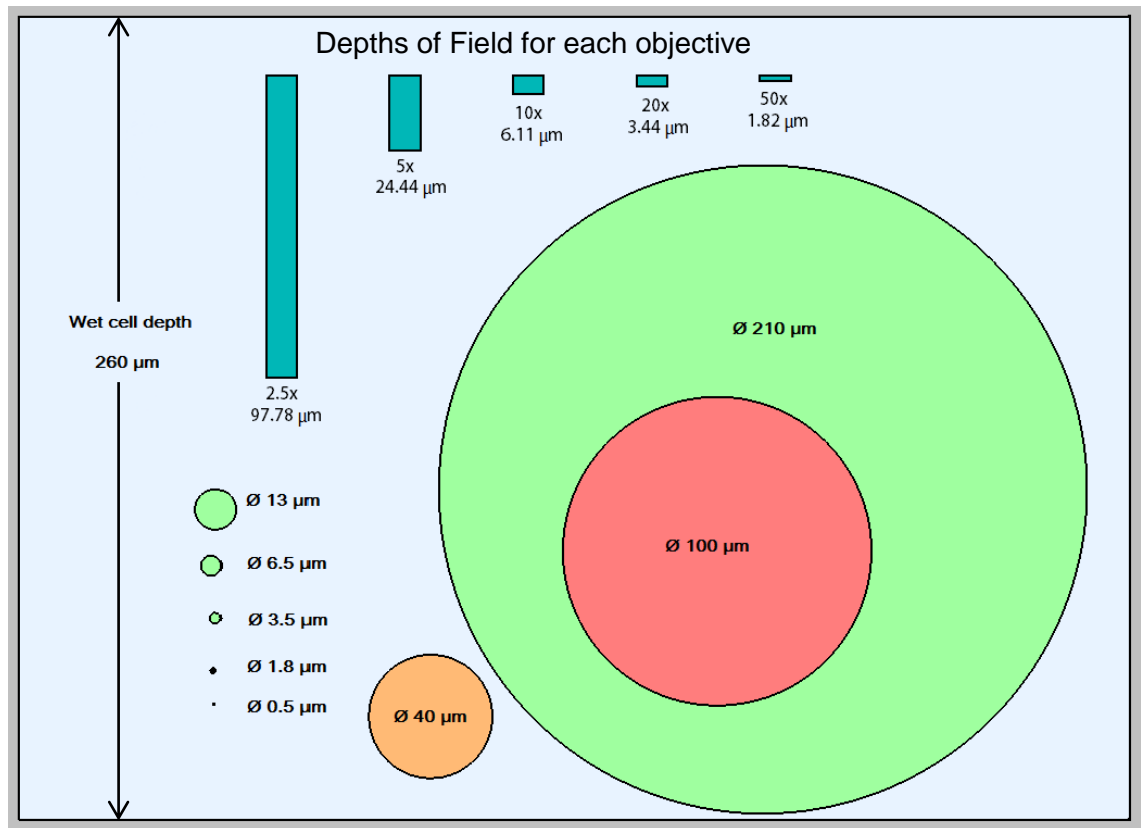


Figure 22 In-scale picture showing the DOFs as bars and some of the minimum and maximum particles sizes as given in Table 4

5.3 Watershed segmentation experiment

5.3.1 Background

As stated before, sample concentration ought not to be too high, lest particles aggregate and be measured as one, biasing the results towards larger size. The problem is best remedied by using a sample that is dilute enough, yet contains a sufficient number of particles. However, more often than not numerous particles can still be found touching, and the categorical exclusion of such a large amount of sample data may bias the results towards smaller size, as larger particles are more likely to be touching. Watershed segmentation, as introduced in Section 4.4.2, may offer an improvement in such cases; currently watershed segmentation has not been used in any of the methods currently in use.

It was assumed that watershed would only have a noticeable effect if there were a considerable number of touching particles in the sample. Watershed would, therefore, be used to improve the quality of measurement of highly-concentrated samples.

5.3.2 The experiment

The effect the use of watershed has on the results was evaluated experimentally. Two samples were prepared, one with a normal concentration of particles and the other with a highly excessive concentration of particles (Figure 23). Both were measured with the currently-used ZN method – albeit with a reduced area to save time and computer space. The obtained images were stored on computer's hard drive and then measured with and without watershed.

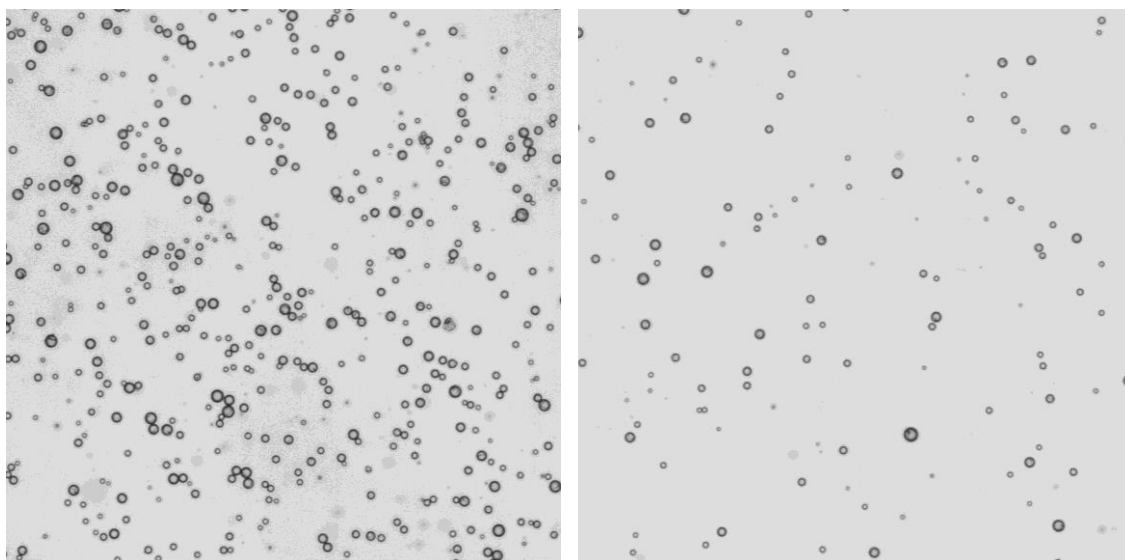


Figure 23 Highly-concentrated sample (left) with many aggregated particles, and a sample with a proper concentration (right) with only a small number of touching particles

5.3.3 Results and conclusions

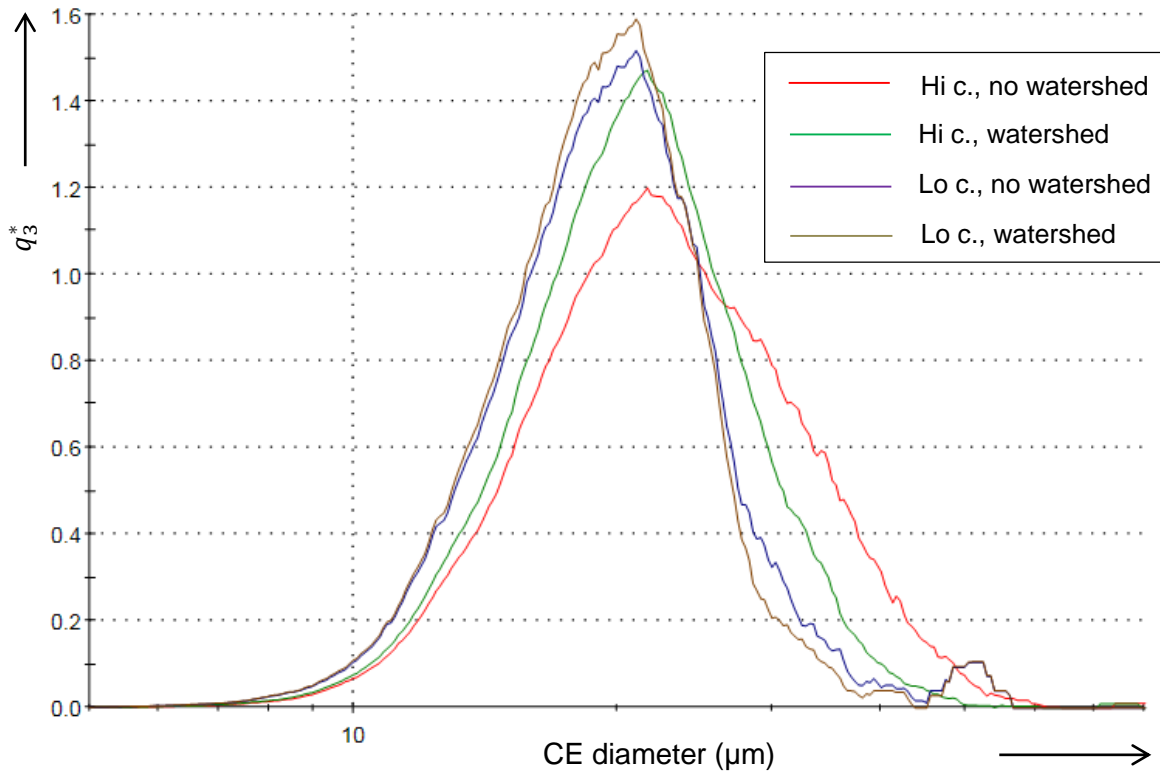


Figure 24 The effect of watershed segmentation on the highly-concentrated sample (Hi c.) and the sample with a lower concentration (Lo c.)

The results presented in Figure 24 above suggest that if the sample is prepared properly with only a small number of touching particles, the use of watershed has little effect. However, should sample concentration turn out to be too high, the use of watershed can have a noticeable effect. As the separation algorithm is quite weak and fails to separate even some clear cases of touching particles, there ought to be no danger of it separating agglomerates, which are of interest. Overall, the use of watershed segmentation can save a considerable number of particles from exclusion and therefore improve the sample data.

5.4 Fines detection experiment

5.4.1 Background and experiment

Fines are small particles. Whilst there is no fixed size, below which particles are to be considered fines, in this discussion particles beneath the size of 10 μm are defined as

fines. The number of detectable fines depends mainly on the choice of objective. A poly-disperse sample was measured using the first four objective in order to study fines detection.

The sample was prepared normally in the wet cell and then measured using modified versions of the currently-used ZN method. In order to make results comparable, exactly the same area was measured of the same wet cell; therefore, the results are based on the same particles. The threshold level was also set automatically for each magnification in order to minimise the potential differences in thresholding. Particle images below 10 px were excluded.

5.4.2 Results and discussion

The results are presented in Table 7 and illustrated in Figure 25 and Figure 26.

Table 7 Statistics for different magnifications (Mag.)

Mag.	N	$\bar{D}_{1,0}$ (μm)	$\bar{D}_{4,3}$ (μm)	$x_{10,0}$ (μm)	$x_{10,3}$ (μm)
×2.5	58,529	16.1	48.4	5.4	22.3
×5	80,538	12.9	46.9	3.5	20.3
×10	131,651	9.2	45.9	2.1	19.0
×20	221,135	6.5	45.6	1.4	18.7

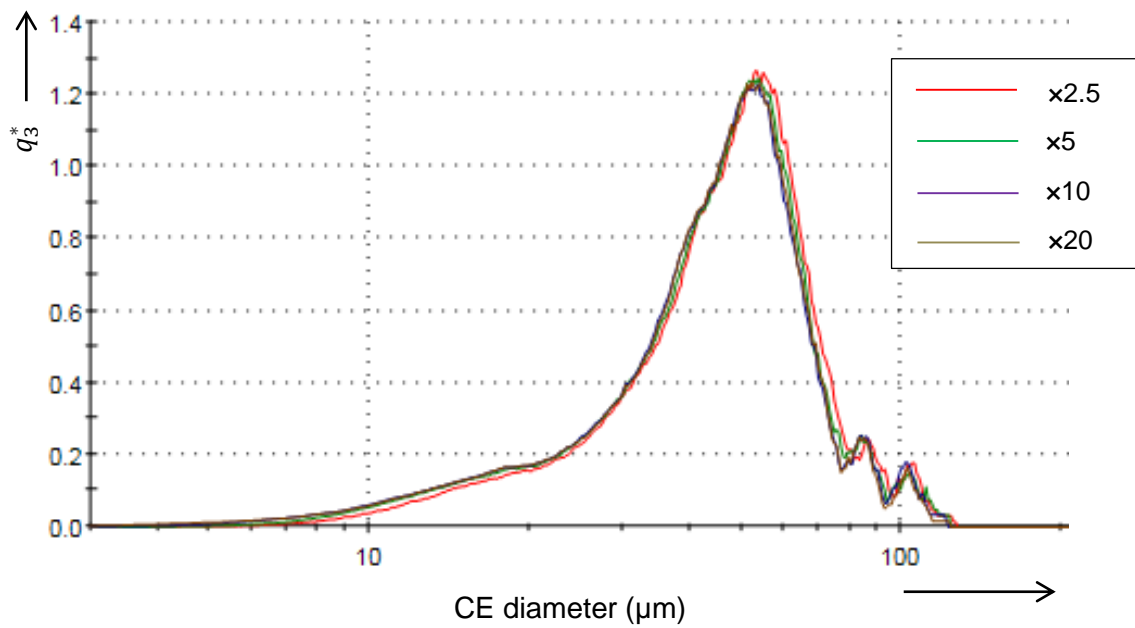


Figure 25 Graphical representation of the volume-weighted distribution; it remains virtually unchanged by the detection of fines

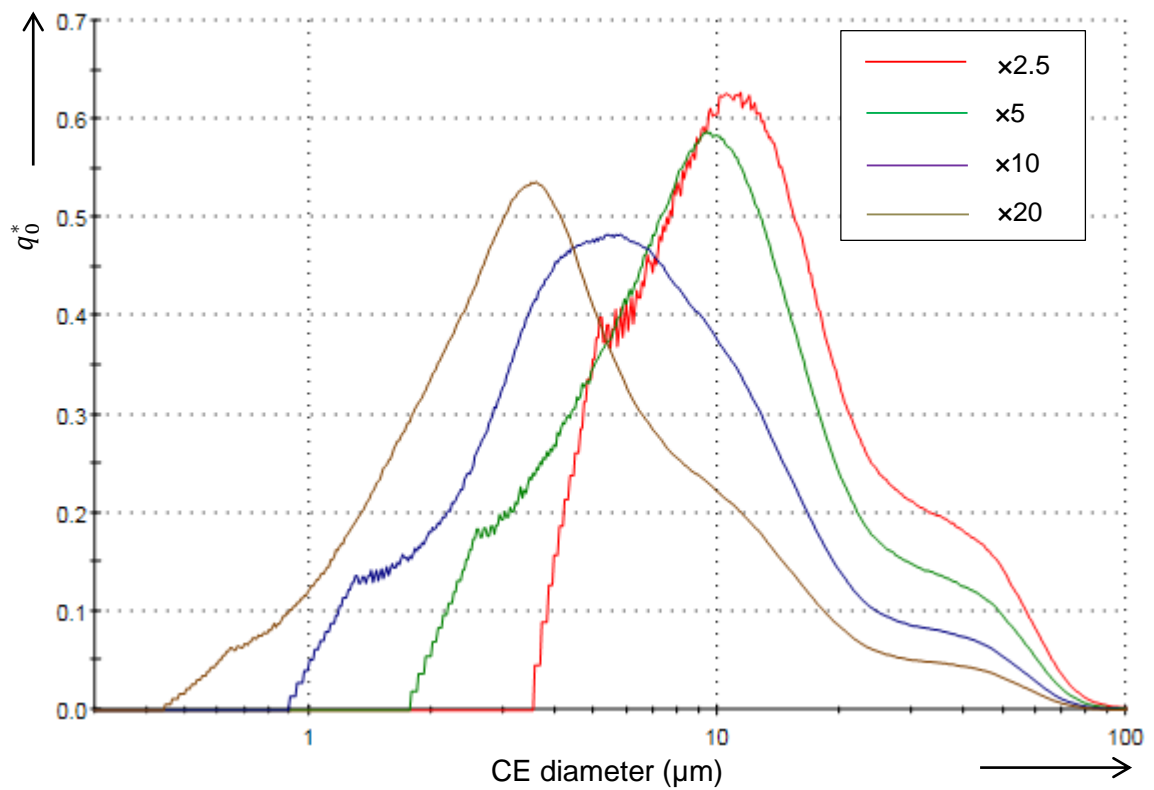


Figure 26 Graphical representation of the number distribution; only the distribution obtained by the x20-objective looks somewhat untruncated

The curve obtained using the $\times 20$ -objective suggests that the mode of the number-based distribution lies at about $3.5\ \mu\text{m}$. This may of course be an overestimation, and had an even higher magnification been used, more fines might have been detected. The mode seems to be roughly at the point where the curve for the $\times 5$ -objective starts to become truncated, thus leaving most of the particles outside of the capability of the $\times 5$ -objective. Nevertheless, from the practical point of view particles around the size of $10\ \mu\text{m}$ are considered as fines, and statistical information of the *distribution* of the sizes of particles lower than that size is most likely unneeded.

Although the number of particles detected was greatly increased by using a higher objective, the contribution the fines make to the volume-weighted distribution was very minimal. As only the volume-weighted results are of interest for most of time, there is no need to be too concerned about detecting fines.

6 Data handling

6.1 Particle classification

6.1.1 Spherical

If the sample constitutes mostly of spherical particles, the descriptors circularity and HS circularity can be used to separate the bulk of particles into the class *spherical*. This can further be divided into smaller classes according to particle size, such as *spherical, small* and *spherical, large*. This classification works for most pilots samples, but is not very good for laboratory samples, because of their varying morphologies.

6.1.2 Particle aggregates

If the sample is prepared correctly, the number of particle aggregates should be small. This number can be further reduced by the use of watershed, as was demonstrated in Section 5.3. However, some amount of manual particle exclusion is still necessary, and classifying images into classes such as *touching, pairs*; *touching, chains*; and *touching, groups* is useful.

The table below presents typical particle aggregates compared to real, non-spherical particles and their shape descriptors. It is shown that aggregates with more than two particles are easily classified using elongation, but paired particles are almost impossible to separate from non-spherical particles. It is also difficult to distinguish between aggregates and agglomerates.

6.1.3 Incomplete images

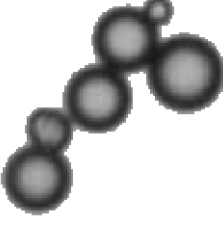
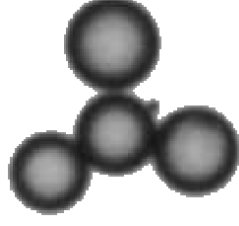
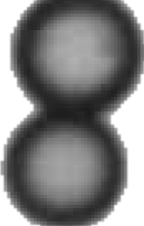

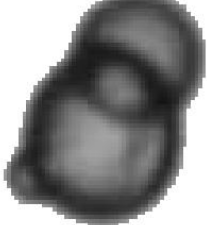
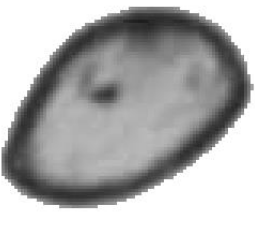
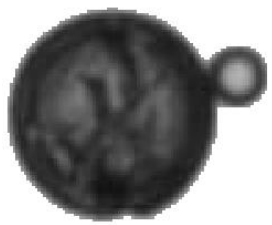
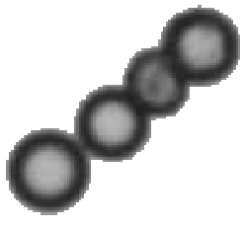
Incomplete images as presented in Figure 18 are characterised by their low solidity and convexity, and they are therefore easily classified. However, it should be noted that incomplete particles cannot be separated from curled fibres.

6.1.4 Bubbles

Bubbles appear spherical and solid, and they are difficult to separate from particles. The used approach is based on the fact that bubbles often appear darker than particles; hence, they have lower pixel intensity mean. Bubbles are usually uniformly dark, compared to particles that are darker on the edges and lighter in the middle; thus, they also

have low pixel intensity standard deviation. Unfortunately, however, this classification does not work automatically even for most catalysts. If the catalyst particles appear dark as well, bubbles cannot be distinguished from particles, except for when bubbles are much larger in size than the largest of particles; see Figure 13 for an example of a dark catalyst. Table 8 shows a number of particle images and their shape descriptors.

Table 8 Particle aggregates and non-spherical particles with their shape descriptors (Elong. = Elongation; HS Circ. = HS Circularity)

							
Elong.	0.560	Elong.	0.028	Elong.	0.465	Elong.	0.313
Solidity	0.716	Solidity	0.735	Solidity	0.929	Solidity	0.951
Circularity	0.573	Circularity	0.622	Circularity	0.852	Circularity	0.902
HS Circ.	0.328	HS Circ.	0.387	HS Circ.	0.725	HS Circ.	0.813
							
Elong.	0.330	Elong.	0.339	Elong.	0.191	Elong.	0.696
Solidity	0.978	Solidity	0.999	Solidity	0.954	Solidity	0.852
Circularity	0.930	Circularity	0.956	Circularity	0.895	Circularity	0.664
HS Circ.	0.865	HS Circ.	0.915	HS Circ.	0.801	HS Circ.	0.441

6.2 Histogram construction

In each *Morphologi* measurement, the data is represented as a histogram, constructed as described in Section 3.4.1. This chapter will discuss some issues related to the histogram construction.

6.2.1 Linear and logarithmical bin size

By default, logarithmically evenly-spaced bins are used so that the range from 0.1 μm to 2,000 μm is divided into 1,000 bins. This is also the case for all the methods currently in use. Bin settings are user-adjustable, and linearly evenly-spaced bins can also be selected.

As already discussed in Section 3.4.1, ISO 9276-1 recommends that, if a non-linear abscissa is used, the transformed distribution $q_r^*(x)$ be used instead of the $q_r(x)$ -distribution. The way *Malvern* seems to apply this is that when a logarithmic series of bins is used, the $q_r^*(x)$ -distribution is applied regardless of the abscissa used, and when a linear series of bins is used, the $q_r(x)$ -distribution is applied regardless of the scaling of the abscissa. However, as both bin size and abscissa are logarithmic in all of the methods used, the software plots histograms in accordance with the standard. Most importantly, results should be comparable; therefore, the histogram type will not be changed.

6.2.2 Number-based resolution

Two aspects are to be considered when investigating the number-based resolution: bin width and distribution truncation. See also Section 5.4 for an experiment regarding the detection of fines.

Because of limited resolution (pixel size), particles are measured discretely, smaller particles having fewer possible values. A problem arises when the default logarithmic bin size is used, as the width of some bins is actually smaller than the difference between possible particles sizes that can be measured. This leads into many empty bins at low particle sizes, as no particles can ever be measured with this size.

Consider the example in Table 9 below. The three lowest particle sizes are presented in the column *CE diameter*, and their respective counts in the adjacent column. No particle sizes were measured between these three sizes.

Table 9 CE diameter of particles and their bin counts. Note how the particle size can have only certain values owing to limited measurement resolution and how several bins are left empty.

CE diameter (μm)	Particle count	Bin number	Bin upper limit (μm)	Bin count
2.17	129	311	2.1610	0
2.26	98	312	2.1825	129
2.35	105	313	2.2043	0
		314	2.2262	0
		315	2.2484	0
		316	2.2708	98
		317	2.2934	0
		318	2.3163	0
		319	2.3394	0
		320	2.3627	105

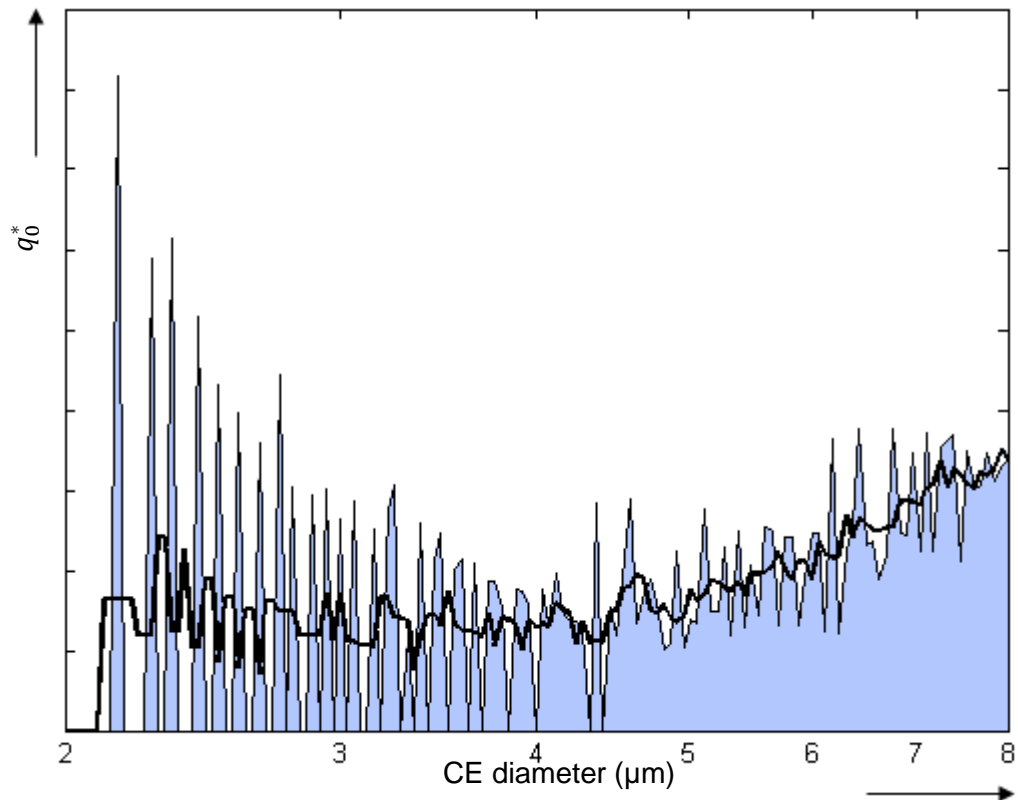


Figure 27 Left tail of a number-based distribution showing empty bins as gaps; the black line represents a frequency curve that has been smoothed over eleven points

This problem could be averted by making the bin size either larger or linear. The latter option would be a drastic change, since changing the bin size linear would mean the change from the $q_r^*(x)$ -distribution to the $q_r(x)$ -distribution. However, as can be seen in Figure 27, smoothing quite effectively removes the spikes.

Choosing a narrower bin width would smooth the otherwise spiky histogram in much the same way as smoothing by running average, as is demonstrated in Figure 28.

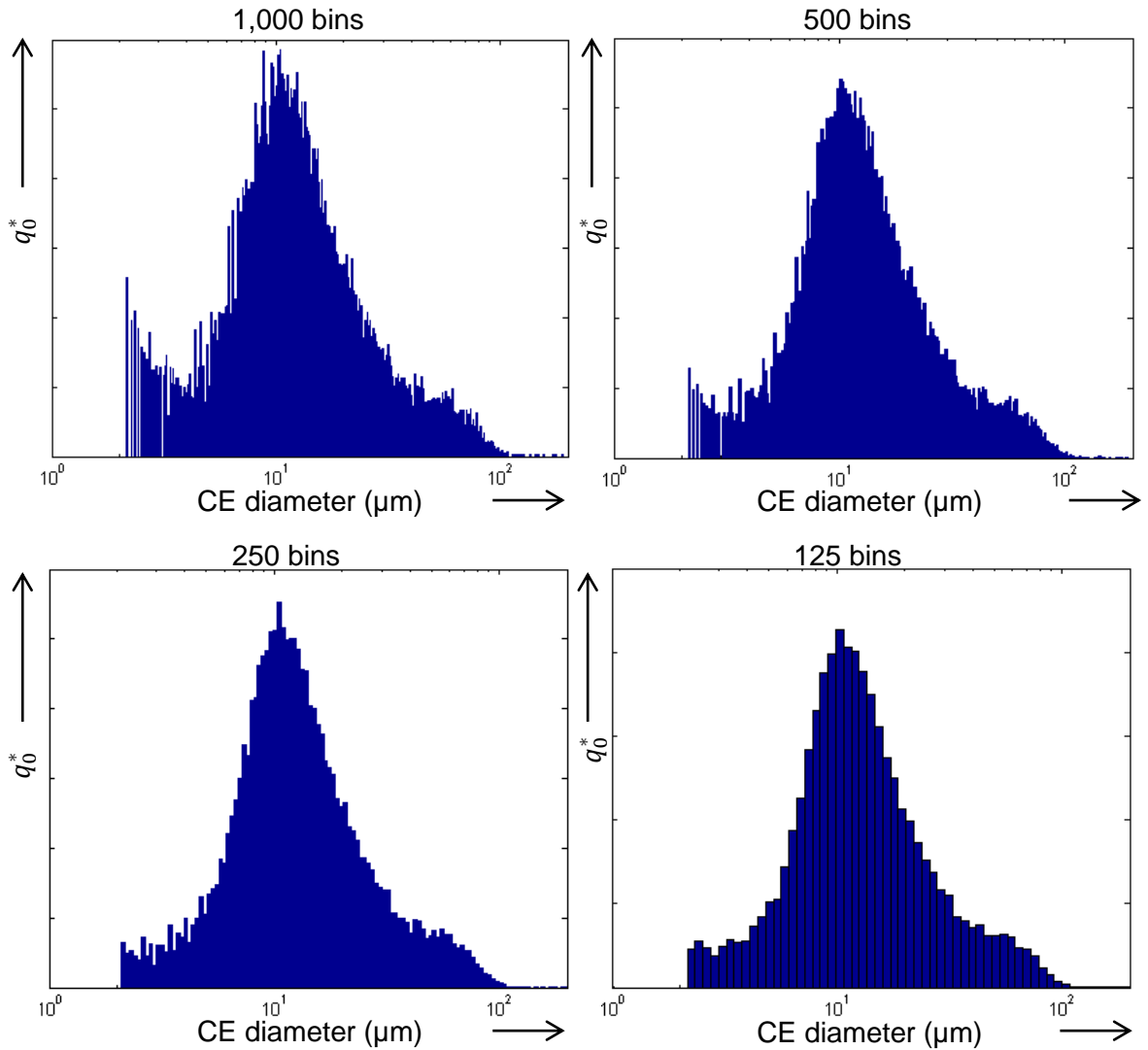


Figure 28 Histograms plotted with different bin sizes; the use of a wider bin width smooths the distribution in much the same way as taking the running average; in the pictures, the range from 0.1 to 2,000 was divided into 1,000, 500, 250, and 125 logarithmic bins respectively

Using the $\times 5$ -magnification, the smallest diameter to be measured accurately according to Table 4 is $6.5\ \mu\text{m}$, which represents 110 pixels. Particles smaller than this size do not provide shape information, because the images are too pixelated for the accurate calculation of CE diameter. However, they do still provide size information, and excluding them causes the number distribution $q_0^*(x)$ to be truncated. This can be seen in Figure 29.

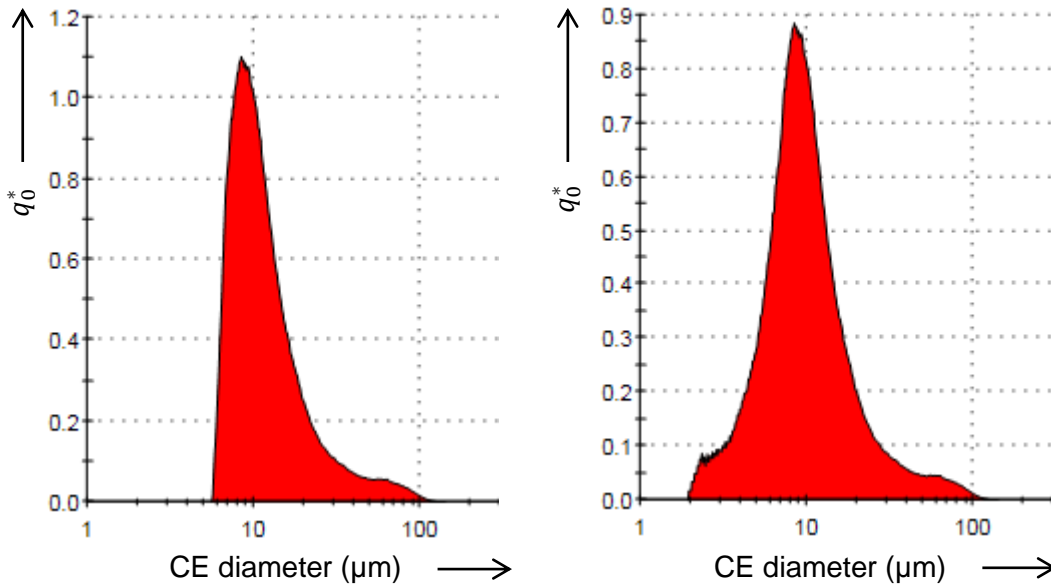


Figure 29 Number-based distribution truncated according to the lower limit of $6.5\ \mu\text{m}$ (left), and distribution left uncut (right).

If only the volume-weighted distribution is of interest, the inclusion or exclusion of fines makes little difference, but if number-based resolution is required, particles below $6.5\ \mu\text{m}$ ought not to be excluded.

6.2.3 Large particles

The presence of large particles – such as agglomerates – is problematic for the volume-weighted distribution. There are two main reasons for that.

Firstly, image analysis is reliable only for spherical particles, and when the CE diameter of a large non-spherical particle is measured according to its projected area and volume-weighted, the volume of the corresponding sphere can be distinctly larger than the true volume of the particle. Figure 30 below illustrates the issue.

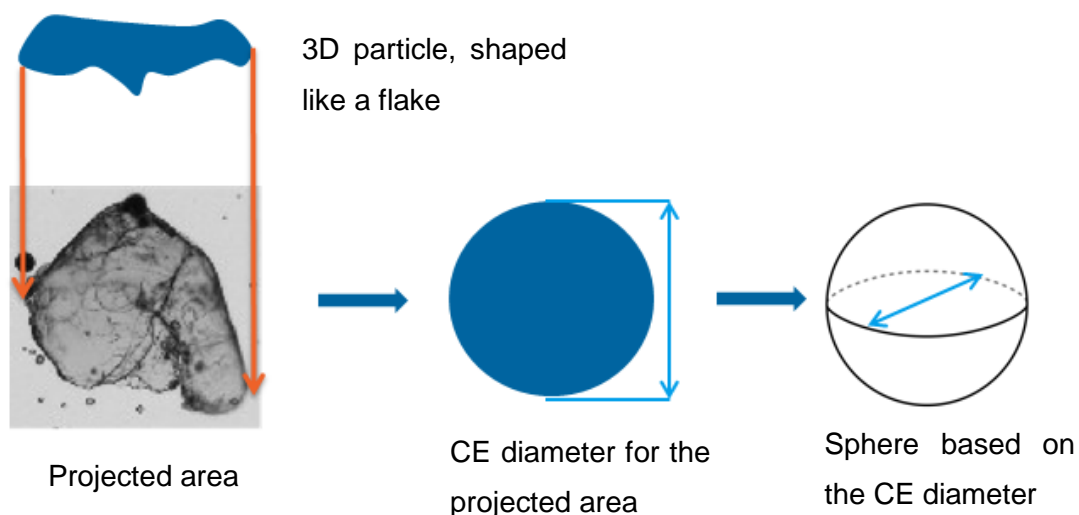


Figure 30 Volume-weighting causes a noticeable overestimation of particle size for non-spherical particles

As it has been observed that most large particles are non-spherical, it can be generalised that the contribution of large particles to the volume-weighted distribution is overemphasised. Furthermore, as the width of the wet cell is approximately 260 μm , it can be stated with certainty that any particles larger than that cannot be spherical.

Another problem is related to the way the histograms are constructed. Large particles appear as spikes separate from the main distribution (Figure 31). From the theoretical point of view, this would mean that all the large particles are concentrated at the peaks and that there would be no large particles between the peaks. It is clear that such conclusions cannot be made on the basis of only a few particles.

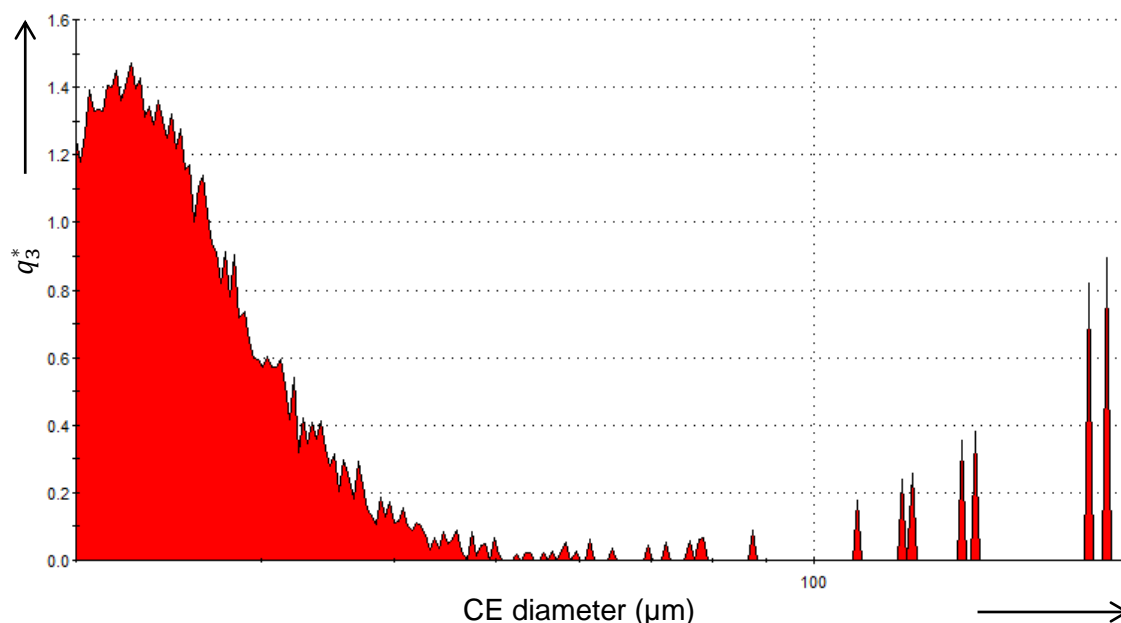


Figure 31 Large particles appearing as spikes separate from the main distribution; in this case, only seven particles out of over 130,000 were larger than 100 μm

Furthermore, large particles have a profound effect on all volume-weighted statistical values, rendering them completely useless. Even the mode value may change, as it is obtained by taking the highest peak of unsmoothed distribution; thus, one of the separate peaks might be higher than the mode of the main distribution.

These things considered, large particles should be excluded from the measurement. It is best accomplished manually because adjusting a fixed exclusion point would be unsuitable for several kinds of distributions.

At best image analysis can provide *qualitative* information of large particles. As this qualitative information reveals whether large particles are agglomerates or impurities, it is probably more useful than *quantitative* information. If quantitative information is needed, one potential method would be sieving.

6.3 Documentation of results

Measurement results are documented as described in Chapter 4.6.2. The standard ISO 13322-1 provides a comprehensive list of aspects that ought to be included in a particle size measurement report. However, for in-house measurements the standard need not be followed to the letter, and only useful values and files are communicated to the requestors. This chapter presents some points worth noticing when using the reported values.

6.3.1 The mode

The mode was not available by default in the *Morphologi* software, and *Malvern* was asked to provide a custom calculation for the mode. This calculation was implemented to the report page. However, the algorithm only finds the highest value on the *unsmoothed* distribution, that is the bin with the highest relative quantity. This values does not always represent the mode of the *smoothed* distribution, which is demonstrated in the picture below.

Unless Malvern introduces an algorithm for finding the mode of a smoothed distribution, the reported mode value has to be verified manually and requestors should be wary of mode values that appear to be out of place.

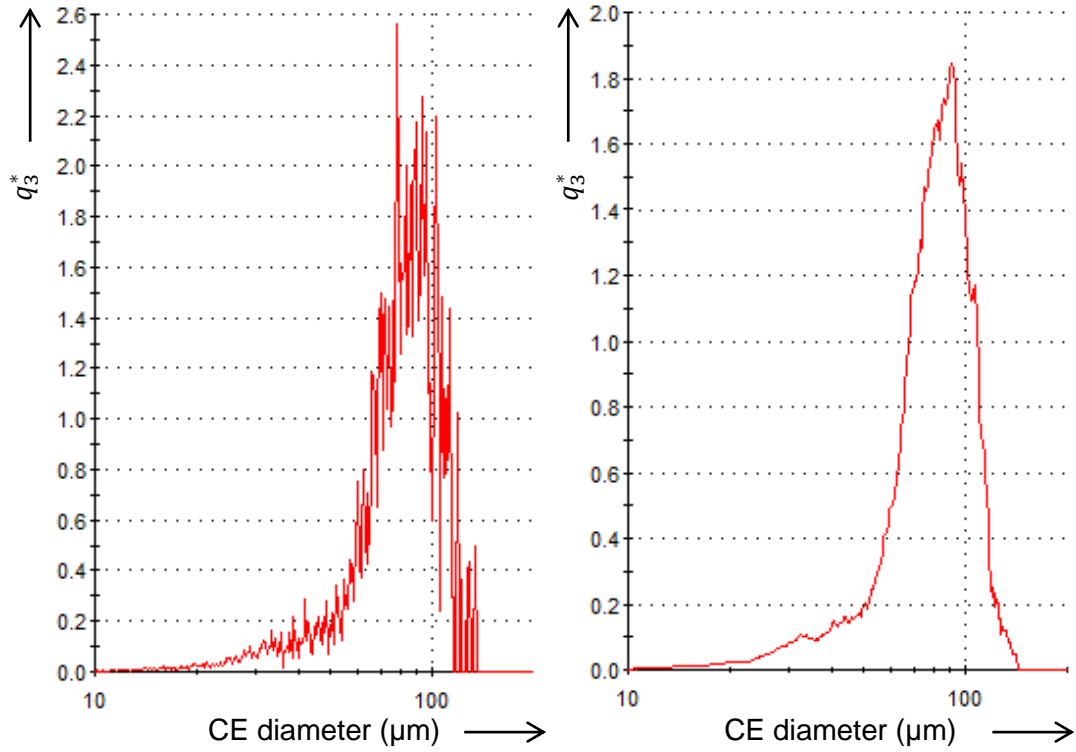


Figure 32 A distribution before and after smoothing over the default eleven points. The mode on the unsmoothed curve is 78 μm ; on the smoothed curve it is 91 μm .

6.3.2 The span

Distribution width has been characterised by the span, as defined in Equation (27). However, this quantity cannot be used as a reliable measure of distribution width, because it is not independent of the location of the distribution. If a distribution is moved any distance a along the abscissa, the span is changed thus:

$$\frac{x_{90,r} - x_{10,r}}{x_{50,r}} \rightarrow \frac{(x_{90,r} + a) - (x_{10,r} + a)}{x_{50,r} + a} = \frac{x_{90,r} - x_{10,r}}{x_{50,r} + a}$$

Therefore, it is the case that span can be different for size distributions of identical width. Furthermore, there are no references for the span in any of the sources used in this thesis and only a few references were found online. Thus, it can be concluded that the span is neither a well-established concept nor a reliable measure of distribution width.

One potential use for the span would be in quality control, if it is expected that the product has an unvarying size distribution. Should any characteristics of the distribution change,

the span would be altered accordingly. The span therefore reveals only whether or not distributions differ from each other, but it does not specify what the difference is. Similarly, the quantity is also usable for screening purposes and for comparing distributions.

In order to be a usable measure of distribution width alone, the span should be independent of any transference along the abscissa. The easiest way to accomplish this is to use only the numerator $x_{90} - x_{10}$ as a measure of width, or if the relationship with the median is required, then $(x_{90} - x_{10})/(x_{50} - x_{10})$ would be a solution.

A more statistically rigorous quantity would be the standard deviation. The *Morphologi* software provides standard deviation only for number-based distribution $q_0(x)$; thus, it has not been incorporated into reports of the volume-weighted distribution $q_3(x)$. However, the formulae for the estimator of standard deviation of any $q_r(x)$ -distribution that were presented in Section 3.3.3 are relatively simple. *Malvern* was requested to deliver a custom calculation based on the formula given in Equation (13).

6.3.3 The mean diameters and the percentiles

The mean diameters $\bar{D}_{1,0}$ and $\bar{D}_{4,3}$ represent the mean diameters of the $q_0(x)$ - and $q_3(x)$ -distributions respectively. As the transformed distributions $q_0^*(x)$ and $q_3^*(x)$ are plotted instead, the reported values do not correspond directly to the plotted graphs. Although this has little practical significance, it might be a potential source of confusion, if the difference is not acknowledged.

For the volume-weighted distribution, the percentiles are usually representative. For the number-based distribution, however, the percentiles are often out of place because they are based on a truncated distribution; see the discussion in Section 6.2.2.

7 ISO and BS standards-based assessment

7.1 Estimation of statistical error

7.1.1 Theoretical background

The standard ISO 14488 presents the total error as a sum of two parts: the *fundamental error* and the *segregation error*.

The fundamental error is a result of the discrete nature of particles. As particles are subject to random variations of sizes and other properties, samples exhibit randomness as well. Fundamental error depends on sample amount; the larger the sample, the smaller the error because of random variations. (ISO 14488:2007(E))

The segregation error is related to the segregation of particles in any of the sampling steps. It cannot be predicted theoretically, but has to be determined experimentally by taking multiple subsamples at different points of the sampling process. (ISO 14488:2007(E))

The fundamental error can be estimated by the *standard error* of the relative quantity of a histogram bin. Assuming that particles have been dispersed at random (see Section 7.3 for further information) and that there are no experimental errors, every particle has an equal probability of being sampled and the sampling probability of any one particle is independent of other particles. Under such assumptions, the mathematics of *Poisson* distribution can be applied to estimate the standard error. Using the ISO-notation for histograms presented in Section 3.4.1, the standard error for the size proportion $\Delta Q_{r,i}$ is given by the equation below. (BS 3406-4:1993)

$$S(\Delta Q_{r,i}) = \sqrt{\frac{\Delta Q_{r,i}^2}{n_i} \left(1 - 2\Delta Q_{r,i} + n_i \sum_i \frac{\Delta Q_{r,i}^2}{n_i} \right)} \quad (28)$$

The approximate 95% confidence interval is then obtained from the equation

$$\Delta Q_{r,i} \pm 2S(\Delta Q_{r,i}). \quad (29)$$

For the estimation of segregation error the whole sampling process presented in Figure 9 ought to be evaluated, each sampling step separately. However, the sampling is performed according to a sampling plan, and for the purposes of this thesis, the segregation error is assumed to be negligible.

7.1.2 Assessment and conclusions

A typical pilot sample containing 40,000 particles was chosen as the basis for the estimation of standard error. Using the default bin width of 1,000 bins from 0.1 μm to 2,000 μm , both number-based and volume-weighted histograms were made. The 95% confidence interval was determined using Equations (28) and (29), and plotted with curve representation of the histogram. All plots were smoothed over eleven points to reduce spikiness and to ease comparison. The results are presented in Figure 33 and Figure 34.

The effect of fundamental error on the number-based distribution is barely noticeable. This was to be expected, as measured population sizes are quite large. For the volume-weighted distribution, however, the effect becomes more noticeable owing to the increasing contribution and decreasing number of particles. Samples that are heavily skewed toward larger size are more susceptible to large standard error – especially if the tail is thin, as then there will be less particles to be measured. The effect of distribution width on the required sample size is discussed in further detail in the next chapter.

The fundamental error can be assumed insignificant – provided a large enough sample population. Therefore, the main source of error is non-uniform sample dispersion at any of the sampling steps during sample preparation. While the whole sampling process has not been evaluated, the effect of sample dispersion during a measurement is discussed further in Chapter 7.3.

This discussion is based entirely on the number of particles measured and makes no assumptions about the underlying distribution; thus, every bin is considered independently. An alternative, and perhaps a more useful way of estimating required sample size and determining confidence level is based on the assumption of log-normality. This way is presented in the next chapter.

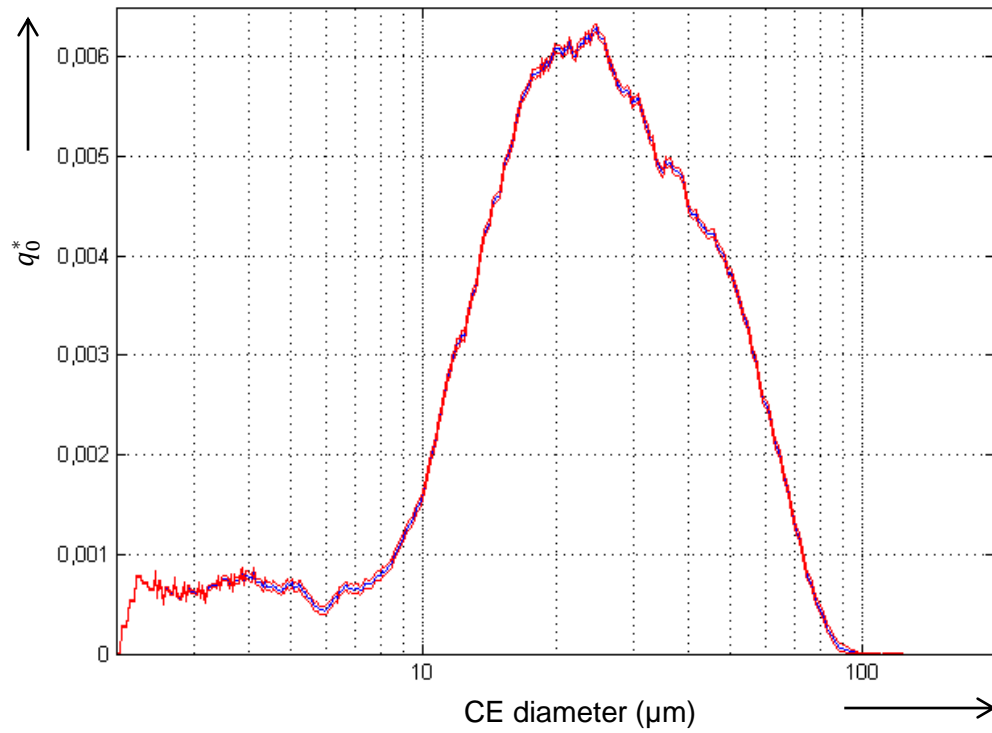


Figure 33 The number-based distribution, with 95% confidence interval marked in red, assuming a standard error according to *Poisson* distribution; the confidence interval is very narrow and of constant width

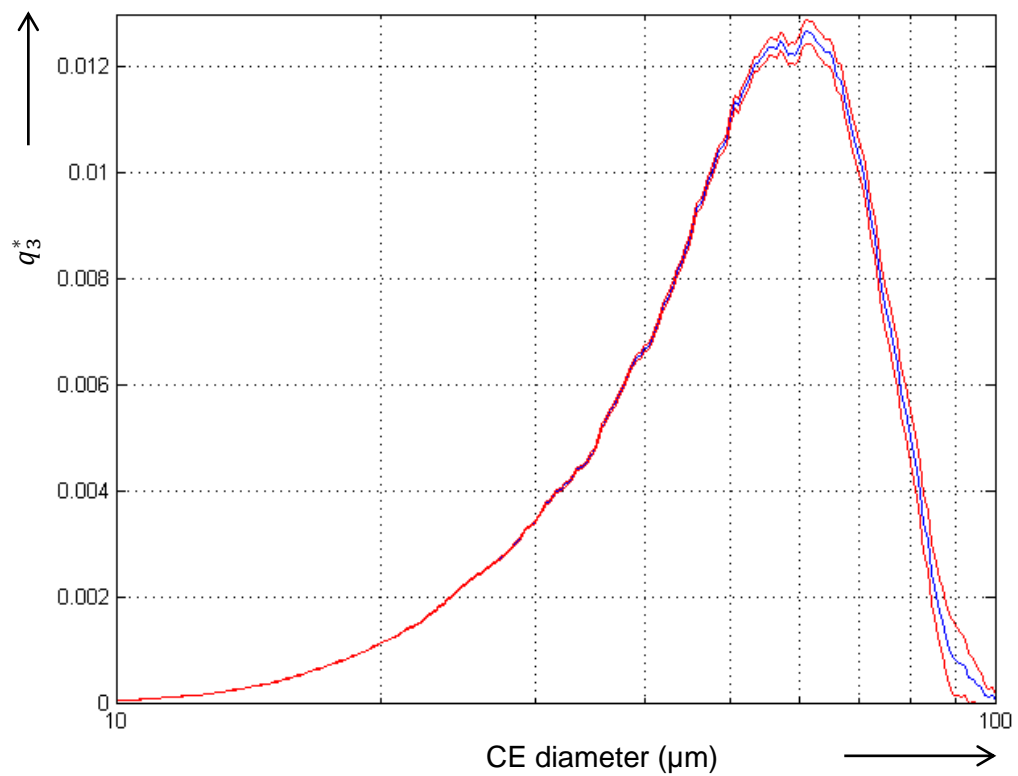


Figure 34 The volume-weighted distribution, with 95% confidence interval marked in red, assuming a standard error according to *Poisson* distribution; the confidence level is very narrow at first, but increases towards larger size

7.2 Estimation of minimum sample size

7.2.1 Theoretical background

The effect of sample size on the relative error of mean diameters was studied by *Masuda* and *Iinoya* in 1971. They proposed a theoretical model that can be used to estimate the minimum number of particles required for a certain confidence level. The validity of the theoretical formula was further tested experimentally for the publication of the standard ISO 13322-1 in 2004. The experiments confirmed that the minimum number of particles required can indeed be estimated by theoretical calculations. The theory and the experiments can be found in more detail in the standard. (ISO 13322-1:2004(E))

Assuming a log-normal distribution, the required number of particles N^* for a given confidence level can be calculated using the equation

$$\lg(N^*) = -2 \lg(\delta) + \lg(\omega), \quad (30)$$

where δ is the *admissible error*, i.e. the highest error that can be tolerated, and ω is a parameter that depends on the mean diameter examined. For the volume-weighted mean diameter $\bar{D}_{4,3}$ it is given by the equation

$$\omega = 36u^2\sigma^2(18\sigma^2 + 1), \quad (31)$$

where $\sigma = \ln(\sigma_g)$, and σ_g is the geometric standard deviation as defined in Equation (14). (ISO 13322-1:2004(E))

The parameter u is related to the confidence level P by the equation below.

$$\Phi(-|u|) \approx \frac{1 - P}{2} \quad (32)$$

If one desires to find out the confidence level for a given combination of sample population, admissible error and geometric standard deviation, it can be accomplished by rearranging Equation (32) to equation

$$P \approx 1 - 2\Phi(-|u|), \quad (33)$$

where $u = (\delta\sqrt{N})/(\alpha\sigma\sqrt{2c^2\sigma^2 + 1})$, where $\alpha = 6$, and $c = 3$ for the $\bar{D}_{4,3}$. (ISO 13322-1:2004(E))

7.2.2 Assessment and conclusions

In order to assess the minimum population of 10,000 particles specified in the currently-used method, seven pilot samples and two laboratory catalysts were selected. They are presented in Table 10 with their respective minimum populations according to above formulae; the minimum population is represented graphically as a function of geometric standard deviation in Figure 35.

Table 10 Number of particles required for various catalysts, for $\delta = 0.05$, and $P = 0.95$ ($u = 1.65$)

Sample	σ_g	σ	ω	N^*
Pilot 1	2.059	0.722	750	300,000
Pilot 2	2.121	0.752	870	349,000
Pilot 3	1.303	0.265	21	9,000
Pilot 4	1.411	0.344	51	21,000
Pilot 5	1.445	0.368	64	26,000
Pilot 6	1.541	0.433	110	45,000
Pilot 7	1.311	0.271	24	9,000
Lab 1	2.034	0.710	700	281,000
Lab 2	1.282	0.249	18	7,000

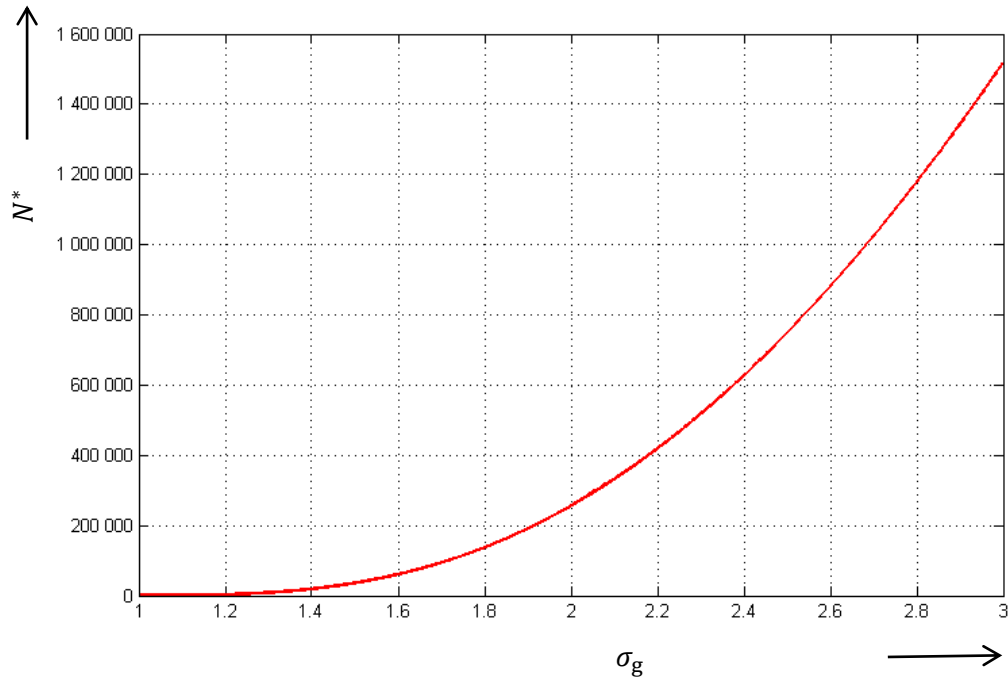


Figure 35 Graphical representation of the required sample size N^* as a function of geometric standard deviation σ_g , for $\delta = 0.05$, and $P = 0.95$ ($u = 1.65$)

The measured populations and confidence levels for the examined samples are presented in Table 11.

Table 11 Number of particles measured and their confidence levels when $\delta = 0.05$

Sample	N	P (%)
Pilot 1	47,883	57
Pilot 2	12,806	29
Pilot 3	35,463	100
Pilot 4	126,536	100
Pilot 5	205,640	100
Pilot 6	115,386	100
Pilot 7	103,862	100
Lab 1	36,747	52
Lab 2	125,772	100

The results imply that because of the huge variations in the geometric standard deviations, all samples cannot be measured with equal precision, if the sample populations are assumed to be approximately equal. On the basis of the values in Table 10, the minimum population of 10,000 may not be sufficient with most samples.

The number of particles present in a scanned area depends on the concentration of the oil slurry as well as the size of the area itself. If the sample population were to be increased, it would be better to increase the area rather than the concentration, since too highly concentrated slurries may have particles touching each other. Nevertheless, the measured populations in Table 11 have been considerably larger than 10,000 and with a few exceptions a confidence level of 100% has been obtained, and it can be concluded that the area and targeted weight percent are sufficient.

The assumption of log-normality may not hold true for most samples; compare the plots in Figure 36 and Figure 37. In reality smaller particles are often more numerous than larger particles, resulting in a thick tail or even a second rise at lower particle sizes of the distribution curve. However, a great number of small particles can be identified as noise or they fall beneath the 6.5 μm limit, and they will eventually be excluded from the data. Furthermore, the purpose of the theoretical calculations is not to quantify the error of each measurement, but to give a serviceable approximation of the required number of particles, which can be used as a basis in method development.

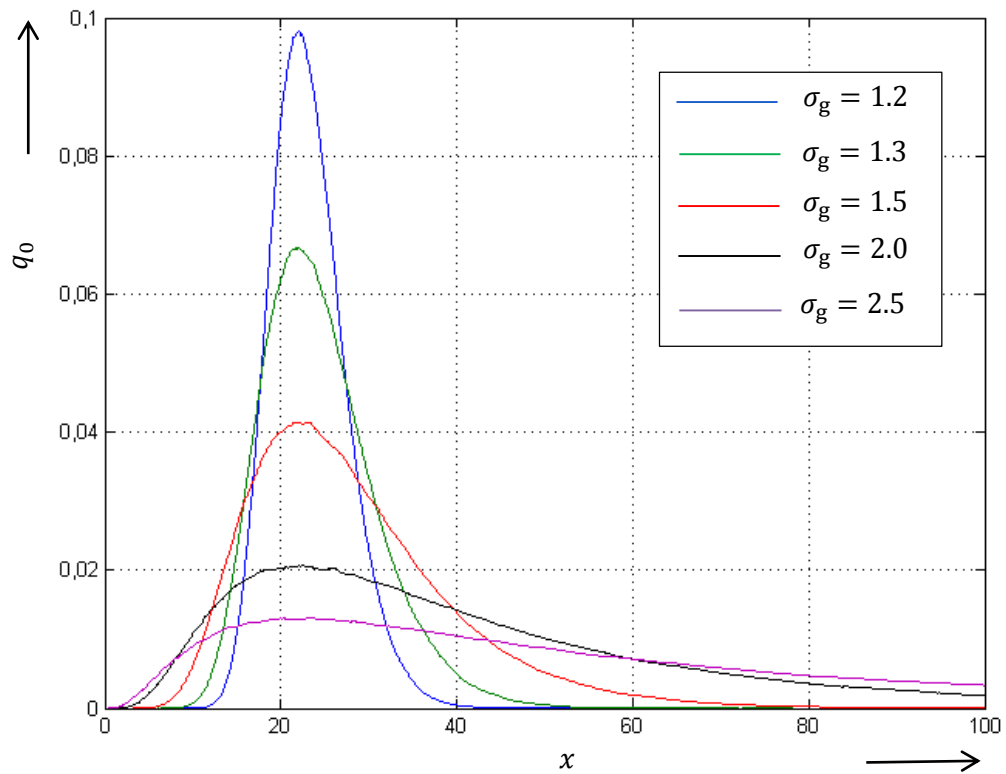


Figure 36 The log-normal distribution with different spreads characterised by the geometric standard deviation

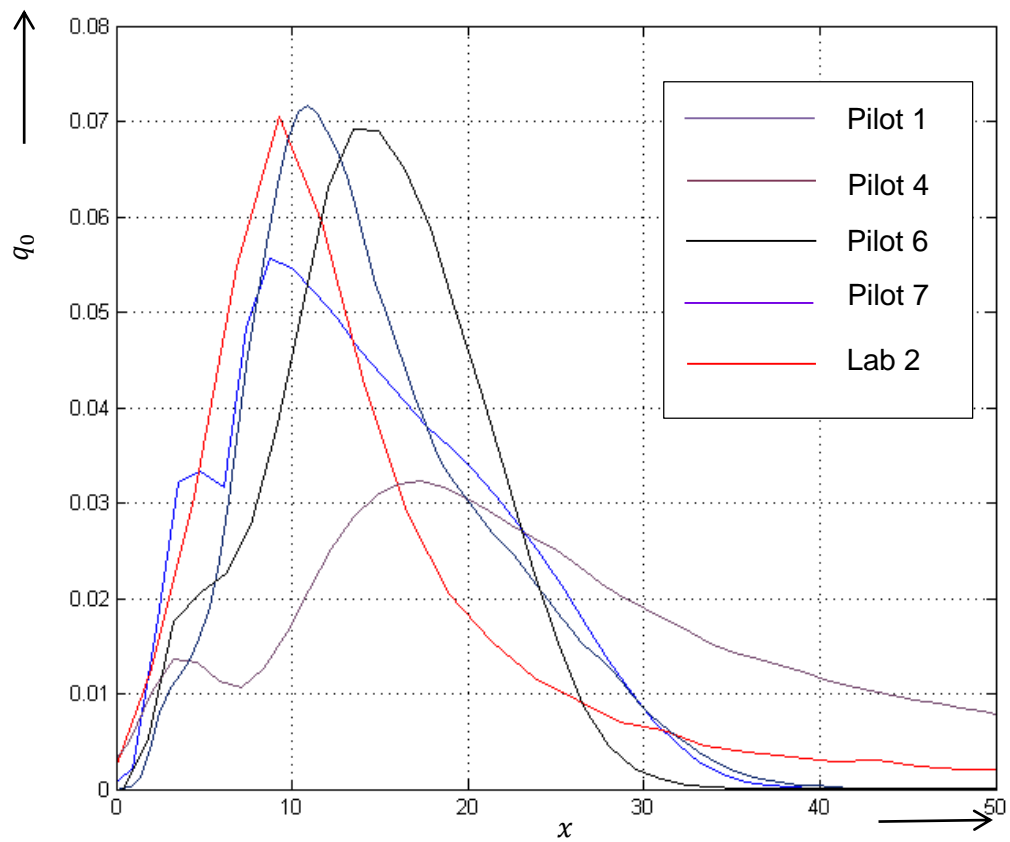


Figure 37 Plotted distributions of some of the samples used in sample size evaluation; the assumption of log-normality is rough at best

7.3 Homogeneity of frame counts

One essential quality criterion presented in the standard ISO 13322-1:2004(E) is the requirement that particles ought to be uniformly distributed among all frames. As only a portion of the sample plate is measured, a non-uniform distribution might lead into an area bias.

7.3.1 Standard's recommendations

If particles are uniformly distributed among all frames, the variances of each and every frame should not differ from each other too much. This can be tested by performing the *F*-test on a set of two frames and the Bartlett's χ^2 -test on a set of more than two frames under the null hypothesis that the variances are equal. The acquired *p*-value should not exceed the chosen significance level. (ISO 13322-1:2004(E)) Both tests are easily available in many statistics software as a built-in feature.

ISO 13322-1 also suggests that Student's *t*-tests be carried out for every combination of two frames and frames that have a *p*-value higher than the desired admissible error under the null hypothesis that the variances are uniform should be rejected. (ISO 13322-1:2004(E)) However, since the number of frames is as high as 1,000, circa 500,000 tests would have to be carried out, which is not realistic. Thus, the standard is not applicable for routine use in this case. In addition, the *Morphologi* software does not come with the built-in algorithm for testing and rejecting frame counts.

7.3.2 Assessment and conclusions

The set of samples used in previous chapter was also used to assess the homogeneity of frame counts. The scanned area of 599 mm² is divided into a total of 1064 frames in 38 rows and 28 columns. Because the number of frames is very high, contiguous frames were compiled into 4 larger rectangular frames and the tests required by the standard were performed on them.

Three pilot samples Pilot 8, Pilot 9, and Pilot 10 were selected for Bartlett's test. The results are presented in Table 12. The first two samples yielded a *p*-value close to zero,

but the last one yielded a p -value of 0.98. Thus, under the null hypothesis that the variances are equal, only the last sample passes the test. However, although there are *statistically* significant differences between the frames in the first two samples, a visual comparison of number-based density distributions $q_0(x)$ and box plots of the groups reveals that there is most likely no *practically* significant difference. See Figure 38 for the plots.

In conclusion, it can be stated that the standard is not very practical for estimating sample homogeneity. As automatic tests for homogeneity are not available, visual evaluation by the operator remains the best measure of particle dispersion in the sample. A new sub-sample is to be prepared and measured, should non-uniform sample dispersion be suspected.

Table 12 The results of statistical tests of homogeneity, the pooled group is the combination of the four groups

Pilot 9				Pilot 11			
Group	Count	Mean	Std Dev	Group	Count	Mean	Std Dev
1	24,879	2.603	0.477	1	4,785	2.287	0.685
2	25,229	2.601	0.482	2	4,536	2.308	0.688
3	25,205	2.605	0.478	3	5,840	2.300	0.684
4	25,043	2.597	0.483	4	4,802	2.358	0.684
Pooled	100,346	2.602	0.480	Pooled	19,963	2.312	0.686
Bartlett's test p -value		0.1		Bartlett's test p -value		0.98	

Pilot 10			
Group	Count	Mean	Std Dev
1	46,022	2.381	0.554
2	44,876	2.392	0.546
3	44,891	2.387	0.544
4	43,768	2.386	0.551
Pooled	179,557	2.386	0.549
Bartlett's test p -value		0.0	

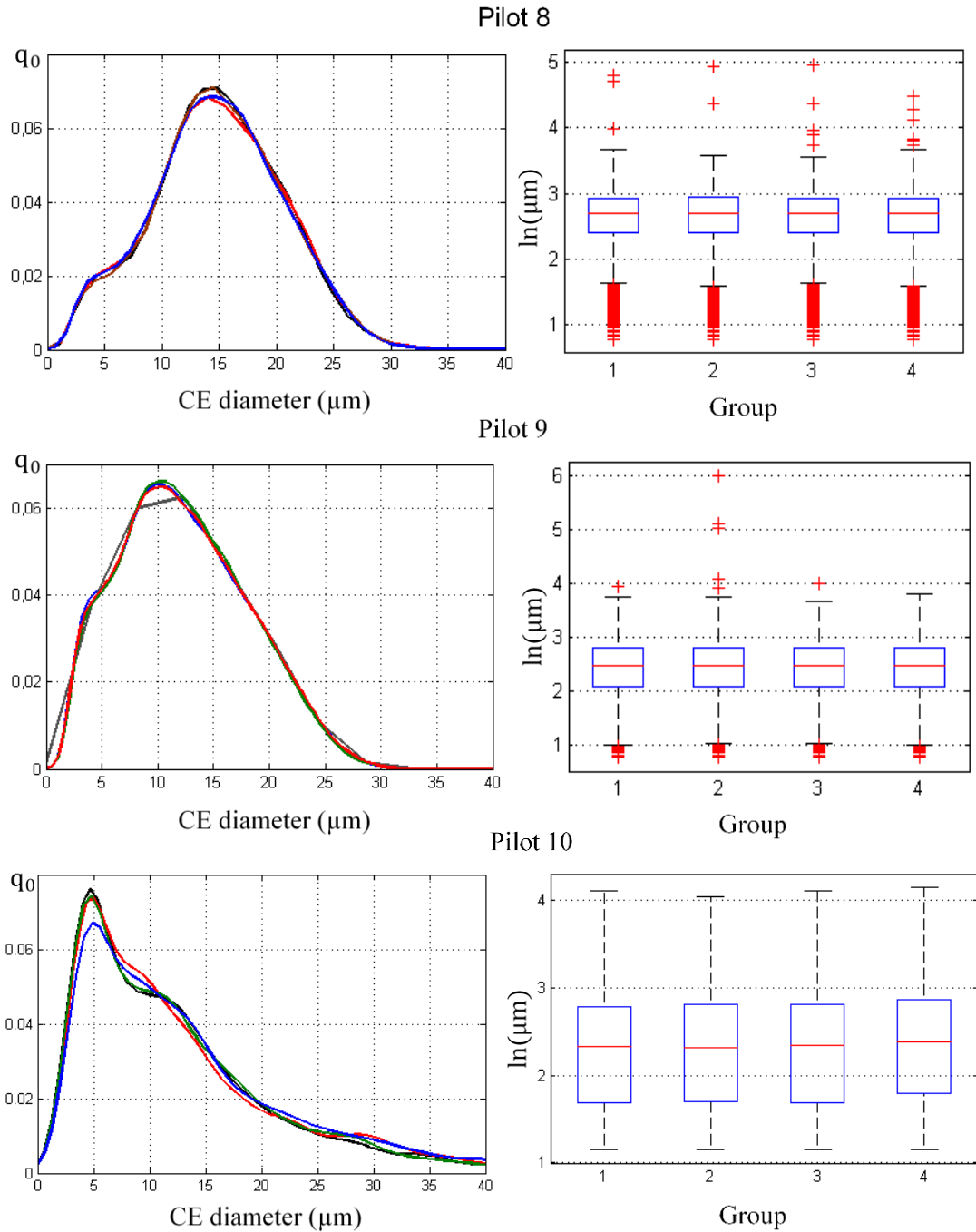


Figure 38 Comparative plots of the $q_0(x)$ -distributions and box plots for each group. Notice that the box plots are based on the natural logarithms of the diameters, hence the unit $\ln(\mu\text{m})$. The edges of the boxes are at 25th and 75th percentiles, and the whiskers extend from $p_1 - 1.5(p_1 - p_2)$ to $p_2 + 1.5(p_2 - p_1)$, where p_1 and p_2 are the 25th and 75th percentiles respectively; the outliers are plotted individually.

Part III. Development of two new methods

8 The High-throughput Method

Catalyst design requires systematic and frequent experimentation, which gives rise to the need for a method that is quick but nevertheless reliable. This chapter documents the development of a high-throughput method for ZN catalysts, hereinafter referred to as the *quick method* in this chapter.

8.1 Method development

8.1.1 Measurement parameters

Speed was selected as the primary factor for development. Because the wet cell used in the currently-used method needs to be washed – a step that takes up a surprisingly large amount of time – the disposable microscope slides were selected instead. Furthermore, the slide carrier can hold up to four slides, and thus multiple samples can be measured in one run.

Another choice that significantly affects measurement time is the choice of objective. The fastest is the $\times 2.5$ because one measurement frame covers such a large area; the trade-off, however, is decreased image quality and reduced sensitivity to fines. (See Table 4) As the primary interest lies in the volume-weighted size distribution and there is no need to obtain a large collection of high-quality images, the $\times 2.5$ -magnification was selected for further testing. The selected measurement area on the slide is shown in Figure 42.

8.1.2 Threshold optimisation

A set of images were collected and stored on the computer's hard drive. Using the software's threshold estimation, an initial threshold level of 156 was obtained for the images. The same images were analysed using the threshold level 156, as well as the following levels: 135, 140, 145, 150, and 160. The results are presented in Table 13 and Figure 39.

Table 13 Number of particles detected, and number-based and volume-weighted mean diameters for each threshold level examined

Threshold	N	$\bar{D}_{1,0}$ (μm)	$\bar{D}_{4,3}$ (μm)
135	780	17.9	47.1
140	913	17.1	46.8
145	1,097	15.8	46.6
150	1,273	15.0	46.5
156	1,458	14.4	46.6
160	1,605	14.1	46.3

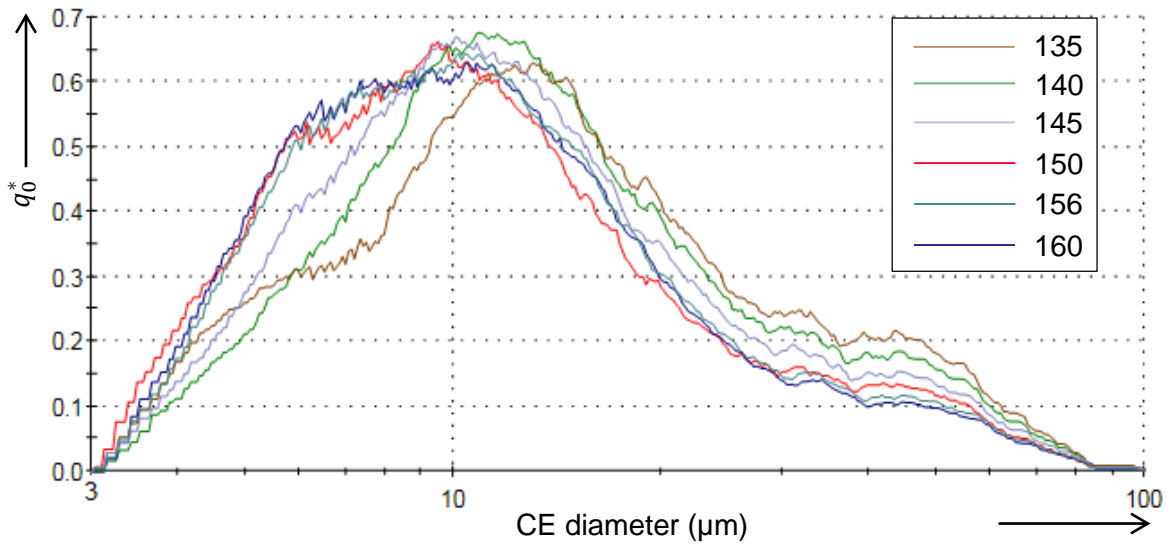


Figure 39 The effect of threshold level on the number-based distribution

The results are as one might expect based on the discussion in Section 4.4.1. Increasing the threshold level also increases the total number of smaller particles detected, and decreasing the values suppresses the distribution at lower particle sizes, hence emphasising the tail at larger sizes.

Images were also viewed individually to see how particle boundaries were detected, and save for the most extreme threshold values, no particular difference was noticed. The level 150 was, therefore, selected for the method. Should the measurement parameters be changed, the threshold level should be re-evaluated.

8.1.3 Classification

Yet another time-consuming task is data handling. In the ideal world all data handling would be automated and thus user-independent and fast. If all particles are spherical, circularity (see Equation (23)) or HS circularity (see Equation (24)) can be used as a basis for exclusion of touching and incomplete particles. Unfortunately there is no reliable way of distinguishing between large particles and bubbles.

For quick classification and data handling, particles are classified into the following four classes; particles that are not in any of the classes are to be excluded (Table 14).

Table 14 Image classes for the quick method

Spherical	CE Diameter < 60 μm HS Circularity > 0.85
Spherical, large	CE Diameter \geq 60 μm HS Circularity > 0.80
Non-spherical, solid	HS Circularity < 0.85 Solidity > 0.95 Aspect ratio > 0.80

The difference in HS Circularity for the two spherical classes is due to the fact that large particles are more likely to have smaller particles adjacent to the perimeter, thus reducing the circularity value.

8.2 Comparison with the currently-used method

Three lab samples were selected as the basis of comparative examination of the quick method. The samples were selected so that they represent samples with small, normal and large particle size, as can be seen in Figure 40. It was expected that the measurement with a low magnification would perform poorly with the sample 1 that had mostly small particles, but have less effect on samples 2 and 3.

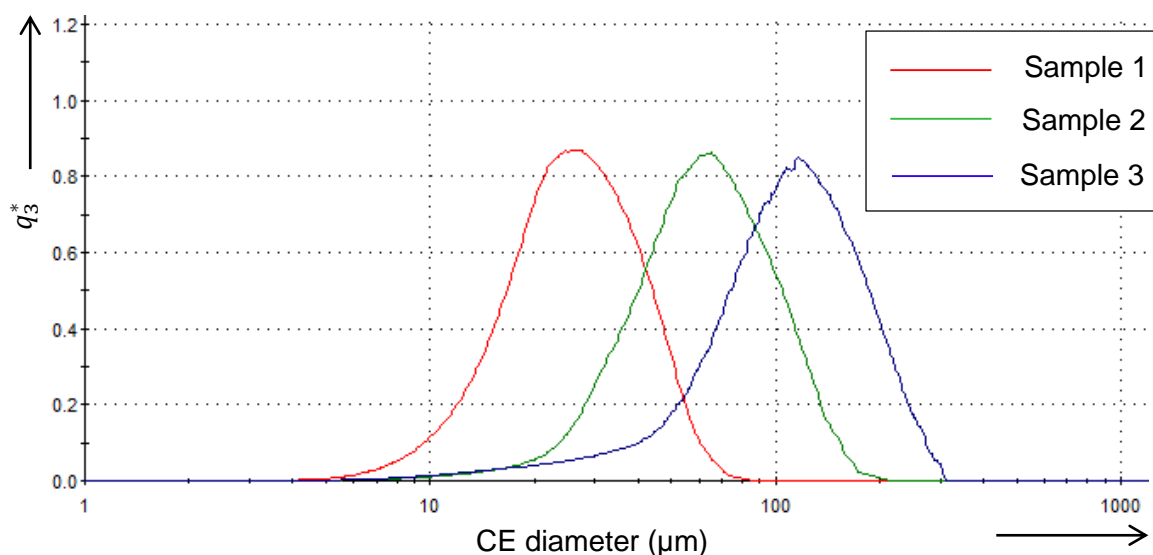


Figure 40 Volume-weighted distributions of the test samples; the test samples were selected so that there would be one with small particles, one with average-sized particles and one with relatively large particles

8.2.1 Comparison using standard microscopy slides

The samples were measured using the currently-used method and with the microscope slides using the $\times 2.5$ -magnification; bubbles were excluded manually. The results are presented in Figure 43 on page 69.

For Sample 1, the results were very much alike, but for samples 2 and 3, the distributions obtained by the microscopy slides were noticeably broader. The reason for this is that the coverslip squeezed and broke the large particles; Sample 2 had less large particles than Sample 3, and therefore the effect was less noticeable. It became clear that normal microscope slides are unsuitable as sample plates, as shown in Figure 41.

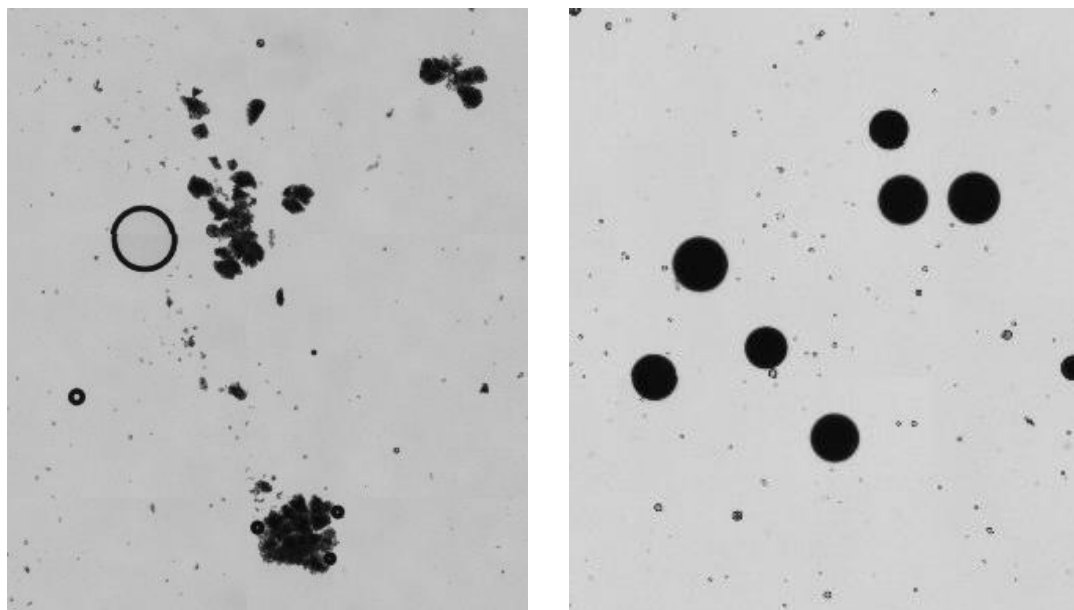


Figure 41 Large particles in the sample three broken apart and squeezed by the coverslip, as well as an air bubble on the microscope slide (left); all particles are intact in the wet cell (right)

Measurement without the coverslip was tested, but owing to the slurry spreading poorly on the slide, it would not be a feasible solution. They would also be an increased risk of slurry dropping down over the edge of the slide.

8.2.2 Comparison using concave microscope slides

Consequently, concave microscope slides that have a shallow depression in the center of the slide for retaining the sample were tested. As there is enough space in the depression, large particles remain intact.

As the depression is circular, the measured area was also set circular, as opposed to the rectangle area on the normal slide. The measured areas on both the normal and concave slides are presented in Figure 42. As the slurry is held stationary in the depression, the use of coverslip was deemed unnecessary. Furthermore, abandoning the coverslip reduces bubble formation noticeably, and the few bubbles that do form are, nevertheless, easily removed with the tip of the needle.

Comparison of results obtained by the wet cell, normal slide and the concave slide are presented in Figure 43 based on the volume-weighted distribution.

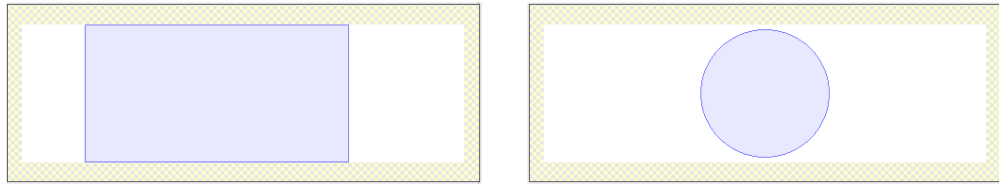


Figure 42 Scanned areas marked in blue on the normal slide with a coverslip (left) and on the concave slide without a coverslip (right)

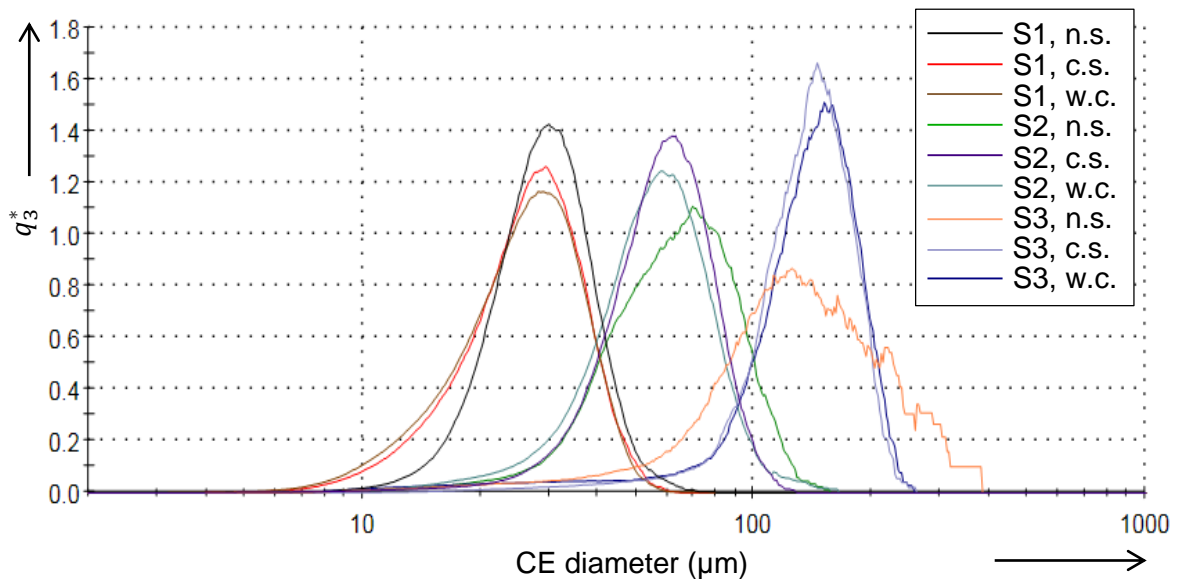


Figure 43 The $q_3^*(x)$ -distributions obtained by different methods. (S1 = Sample 1, S2 = Sample 2, S3 = Sample 3, n.s. = normal slide, c.s. = concave slide, w.c. = wet cell)

8.2.3 Sample dispersion on the concave slide

A concern was that larger particles would slide down the depression, while smaller ones would be carried farther away from the centre of the concavity by the spreading oil phase. This would result in a bias towards larger particles. Furthermore, particles at the centre would be likely to be touching.

The composite image of the whole measurement area below suggests that – although larger particles seem to have a tendency to concentrate at the centre – the degree of aggregation at the centre is not very big (Figure 44).

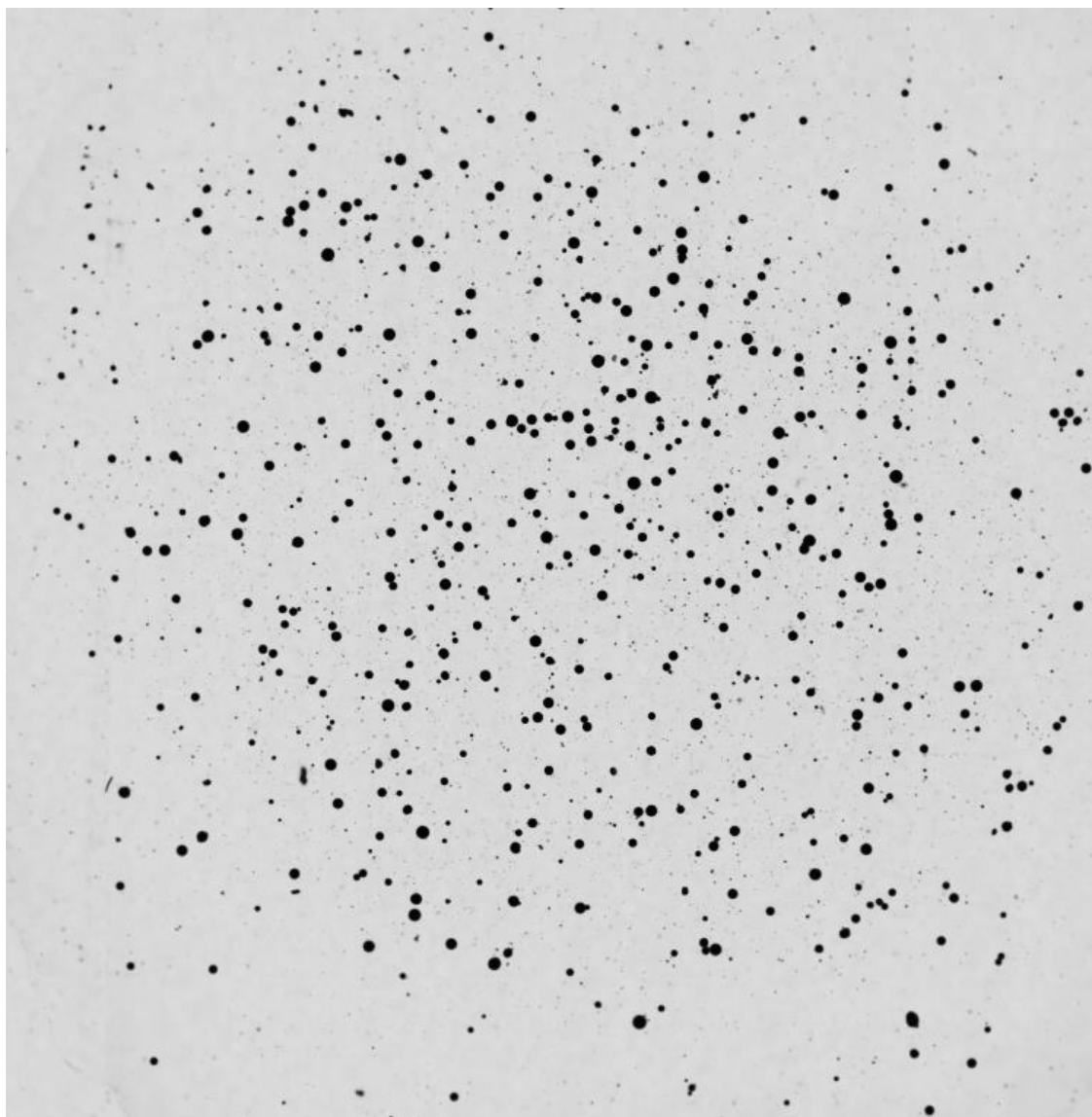


Figure 44 Combined image of the frames of the concave slide measurement

8.3 Discussion and conclusions

The original version with normal microscope slides was found unsuitable because it causes large particles to squeeze and it is very prone to bubble formation. Concave microscope slides turned out to be suitable, and the results were similar to those obtained by the wet cell.

There is a noticeable trade-off when increasing the measurement speed. However, the initial tests suggest that the accuracy is fairly good, and the method is suitable for screening purposes. Quite surprisingly, measurement accuracy was fairly good even with Sample 1, which had mostly small particles.

From the practical point of view, the use of the microscope slide holder has the benefit that four samples can be measured in one run. This saves a considerable amount of time needed in sample preparation. In fact, if none of the microscope slides had been found suitable, the whole concept of high-throuput method might have been found impractical, as the benefit of speeding up the wet cell measurement would hardly be justified, as it is not the measurement time itself that makes measurements take a long time to finish. Concave slides are more expensive than normal slides, so it is probably a good idea to wash them for reuse.

9 The Detailed Method

9.1 Background

The second new method to be developed, the *detailed method* is intended to collect a large number of high-quality images of SS particles, as well as to determine their size distribution. It should be available for both non-prepolymerised and prepolymerised catalysts, the former of which is smaller in size and more challenging to handle because of its pyrophoricity and high reactivity. As SS particles have a partially transparent shell, the use of an optical instrument can reveal the internal morphology, which is of great interest in catalyst development. Pictures taken with an electron microscope only show the outer layer. See Figure 45 below.

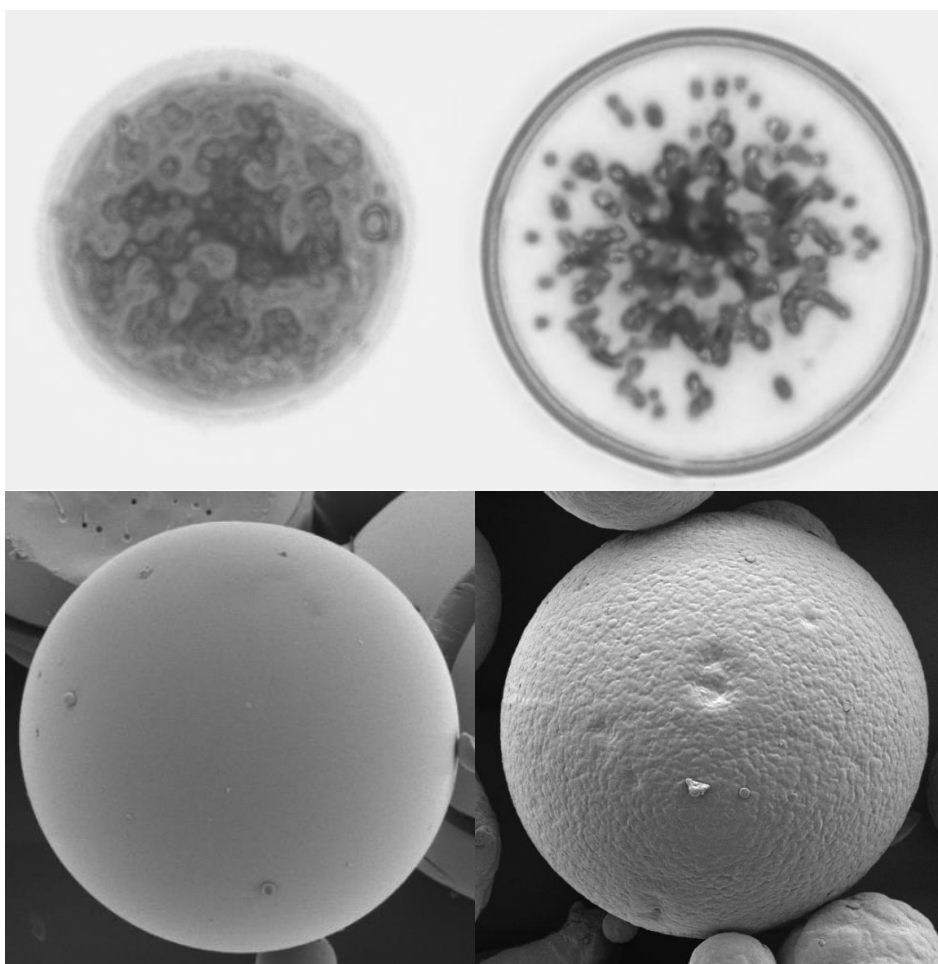


Figure 45 Top row: *Morphology G3* images of non-prepolymerised and prepolymerised SS catalyst particles showing internal morphology; Bottom row: SEM images of the same catalysts show only the outer layer

9.2 Method development

9.2.1 Designs for the detailed measurement

Three different designs were considered for the basis of the detailed method:

- (i) Merged-objective measurement for PSD and imagery
- (ii) Single-objective measurement for PSD and imagery
- (iii) Small-area measurement for imagery only

The design (i) was considered first. However, as the merge point is the minimum CE diameter of the lowest objective, only the smallest particles are photographed with the higher objective, and the images obtained of larger particles are no better in quality than they would have been if the normal method had been used. Thus, this design was abandoned, but may be reconsidered in the future, if *Malvern* changes the software to allow merge point adjusting.

Design (ii) is the scanning of a reasonably-sized area for a statistically sufficient sample population using a high objective. Small frame sizes and narrowed depths of field would lead into significantly increased measurements times; thus, the possibility to run the measurement overnight was examined.

Design (iii) is otherwise similar to design (ii) except that it scans a considerably smaller area to save time, and the acquired images cannot therefore be used for the determination of particle size distribution, but are, however, sufficient for a morphological study. The PSD data would be gathered using the currently-used method; thus, two measurements would be needed for one sample.

9.2.2 Sample carrier

The wet cell had been used for all prepolymerised samples and the slides for all non-prepolymerised samples due their higher reactivity. However, the wet cell is better for samples in a suspension because it prevents more efficiently the suspension from moving. Furthermore, the use of coverslip can squeeze or break particles apart, as was shown in Section 8.2.1.

A risk assessment was carried out in regard of the use of the wet cell for non-prepolymerised samples, and the risks associated thereof were regarded small owing to the low concentration of the suspension. Therefore, the wet cell was selected to be used for both catalyst types.

9.2.3 Acquisition of high-resolution imagery

As the currently-used method uses the $\times 10$ -objective, the two higher objectives $\times 50$ and $\times 20$ were tested for the collection of detailed images; the $\times 10$ -objective was used as a reference. A medium area was scanned using the $\times 20$ -objective for both non-prepolymerised and prepolymerised particles. As measurement time was very long, the measurements were performed overnight. For the $\times 50$ -objective, only a small test area was scanned. In order to remedy the very shallow depth of field, z-stacking was used, as presented in the Table 15 below.

Table 15 Used layers of z-stacking and the corresponding depths of field

Magnification	Number of layers	DOF (μm)
$\times 10$	3	24.4
$\times 20$	4	20.6
$\times 50$	6	15.3

Captured images are presented from Table 16 through Table 21. Four representative images were selected at the 10th, 50th, and 90th percentiles of the volume-weighted distribution to allow the comparison of images of different size. Note, however, that the images themselves have the same size in the tables.

Table 16 Images of prepolymerised particles at three percentile points, obtained by the $\times 10$ -objective; the smallest particles are not very sharp

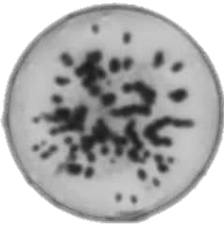
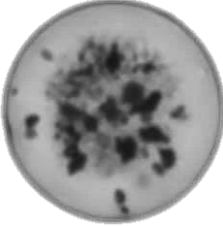
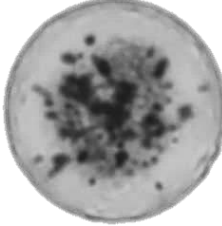
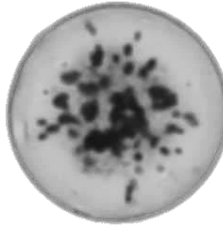
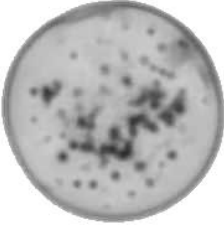
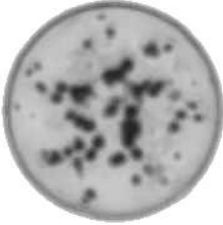






$x_{90,3}$				
$x_{50,3}$				
$x_{10,3}$				

Table 17 Images of non-prepolymerised particles at three percentile points, obtained by the $\times 10$ -objective; the smallest particles are not very sharp

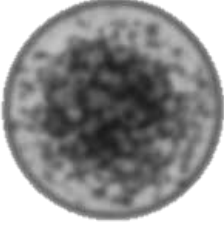
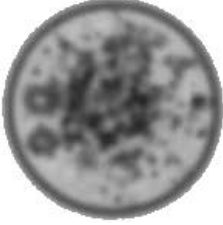
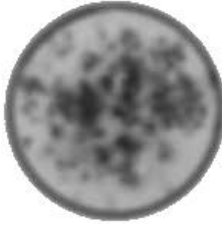
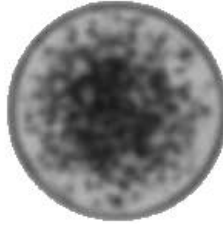

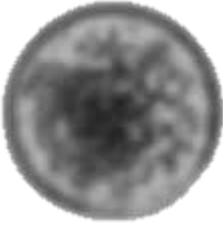
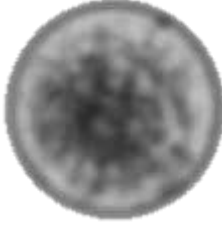





$x_{90,3}$				
$x_{50,3}$				
$x_{10,3}$				

Table 18 Images of prepolymerised particles obtained by the x20-objective; image

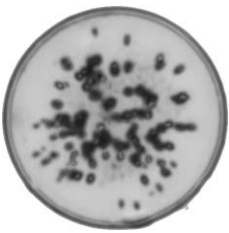
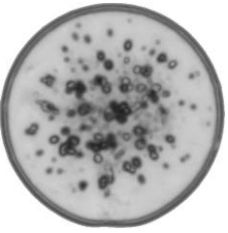
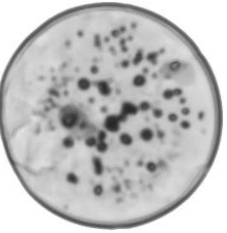
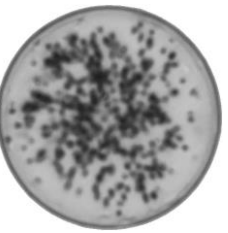
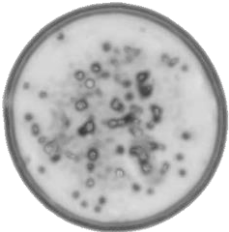
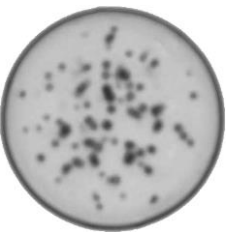
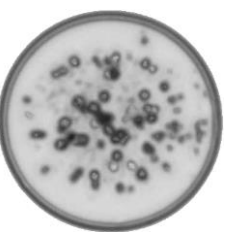
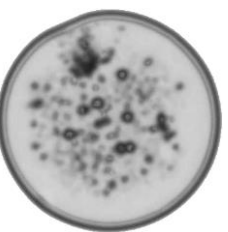
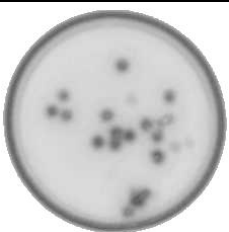

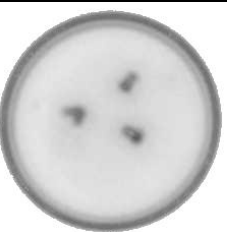
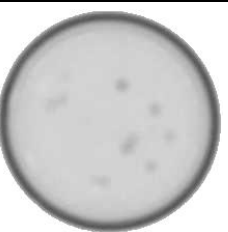
$x_{90,3}$				
$x_{50,3}$				
$x_{10,3}$				

Table 19 Images of non-prepolymerised particles obtained by the x20-objective

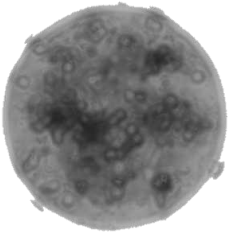
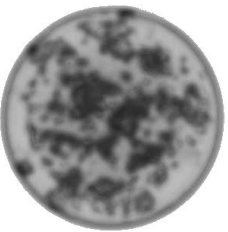
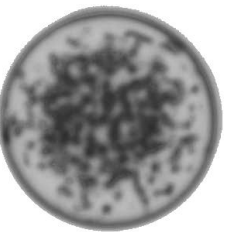
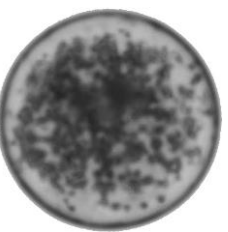
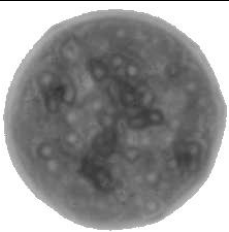
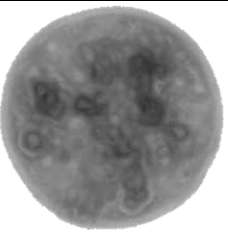
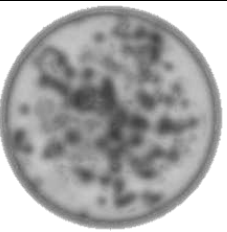
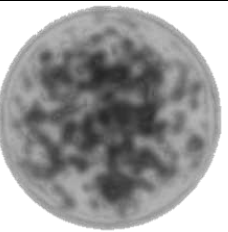




$x_{90,3}$				
$x_{50,3}$				
$x_{10,3}$				

Table 20 Images of prepolymerised particles obtained by the x50-objective; there is no substantial improvement in image quality compared to the previous magnification

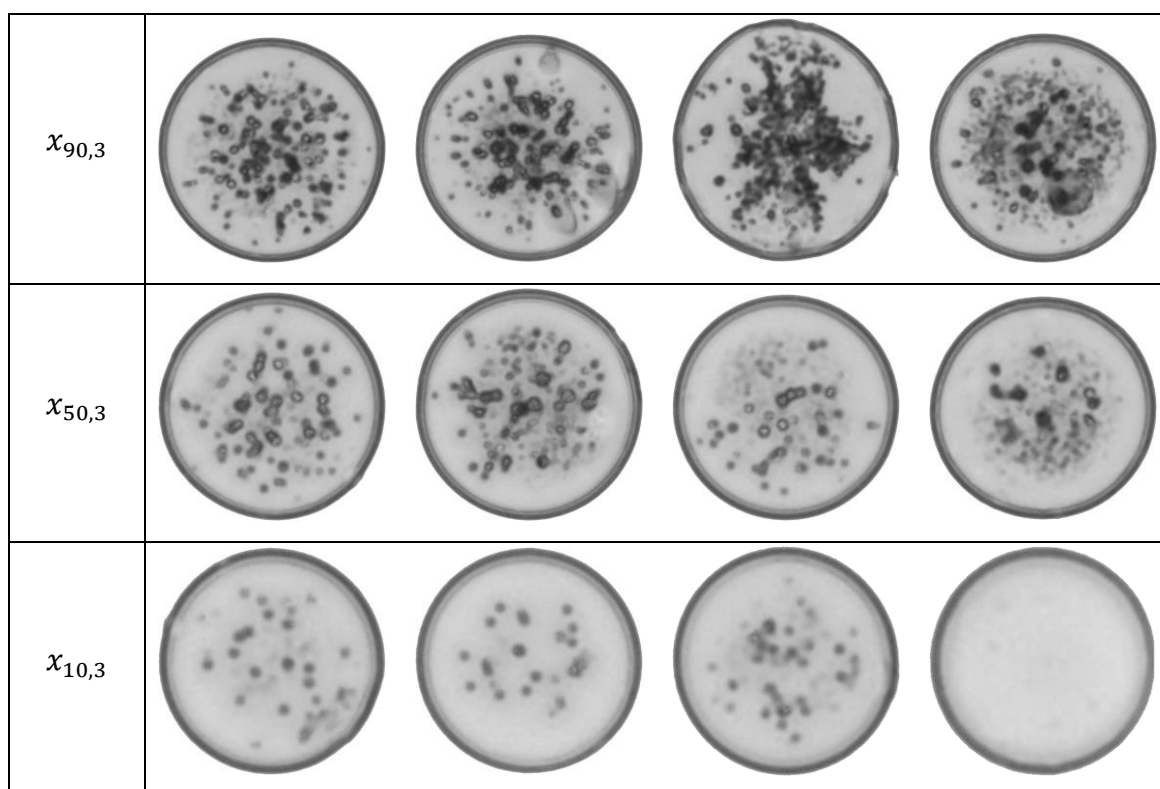
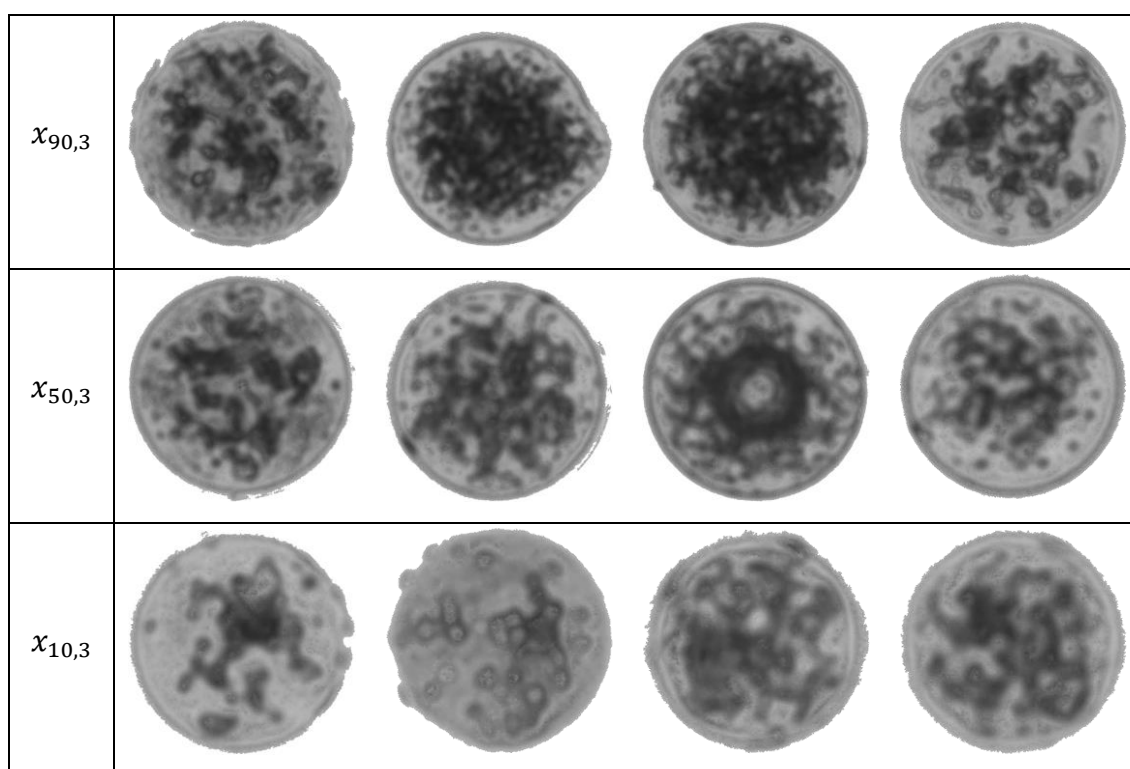


Table 21 Images of non-prepolymerised particles obtained by the x50-objective



9.3 Comparison of size distributions

The $q_0(x)$ - and $q_3(x)$ -distributions based on the data collected by the overnight $\times 20$ objective measurements were compared with corresponding distributions obtained using the currently-used wet cell $\times 10$ -measurement. The comparative plots are presented in Figure 46 for non-prepolymerised particles and in Figure 47 for prepolymerised particles. The same filters were used to remove bubbles and particle aggregates.

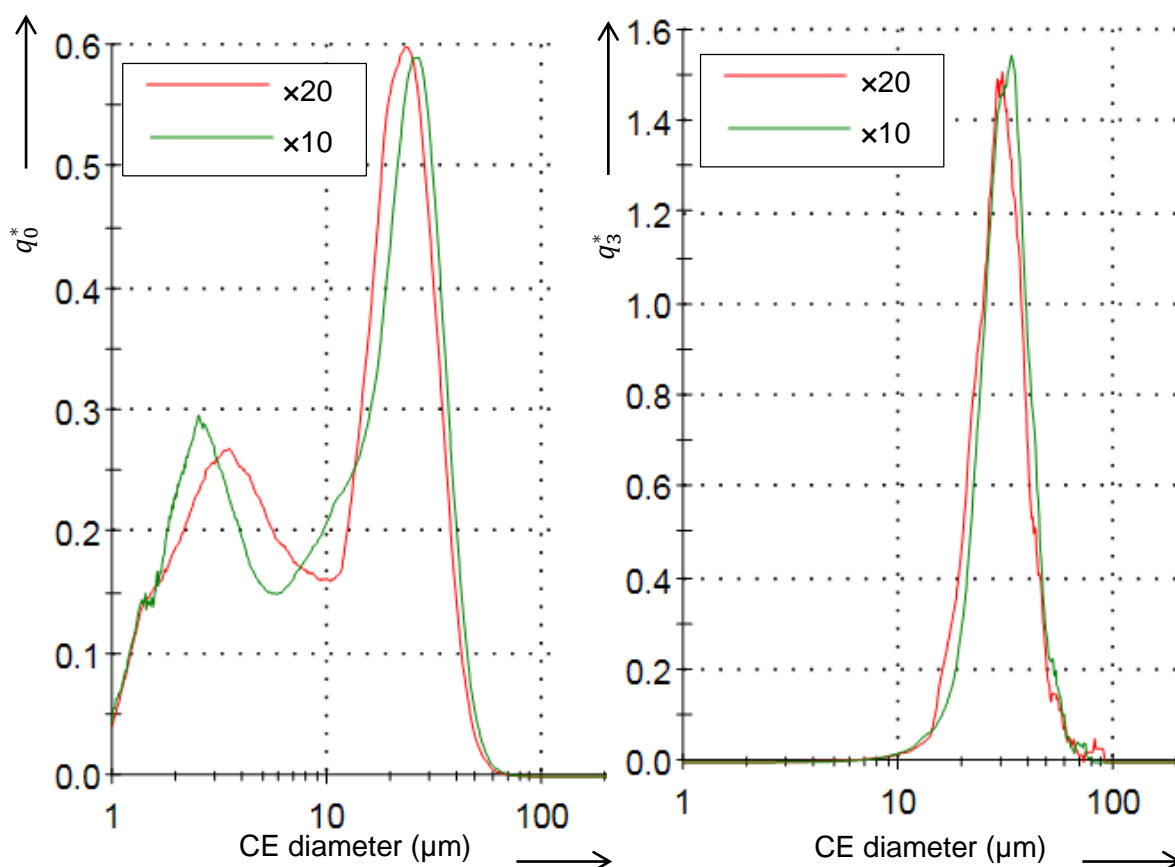


Figure 46 The number-based (left) and the volume-weighted (right) distributions of the catalyst before prepolymerisation, truncated at $1.0\ \mu\text{m}$

For the non-polymerised catalyst the results are somewhat inconclusive. The plots are clearly different, but it is hard to determine the cause for the difference. The difference may be due to the lower magnification's poorer thresholding.

For the prepolymerised catalyst, however, the results are as expected. The higher magnification enables more fines to be measured. Nevertheless, the increase in number-

based resolution has little practical significance, and thus may not justify the excessively long measurement time in itself.

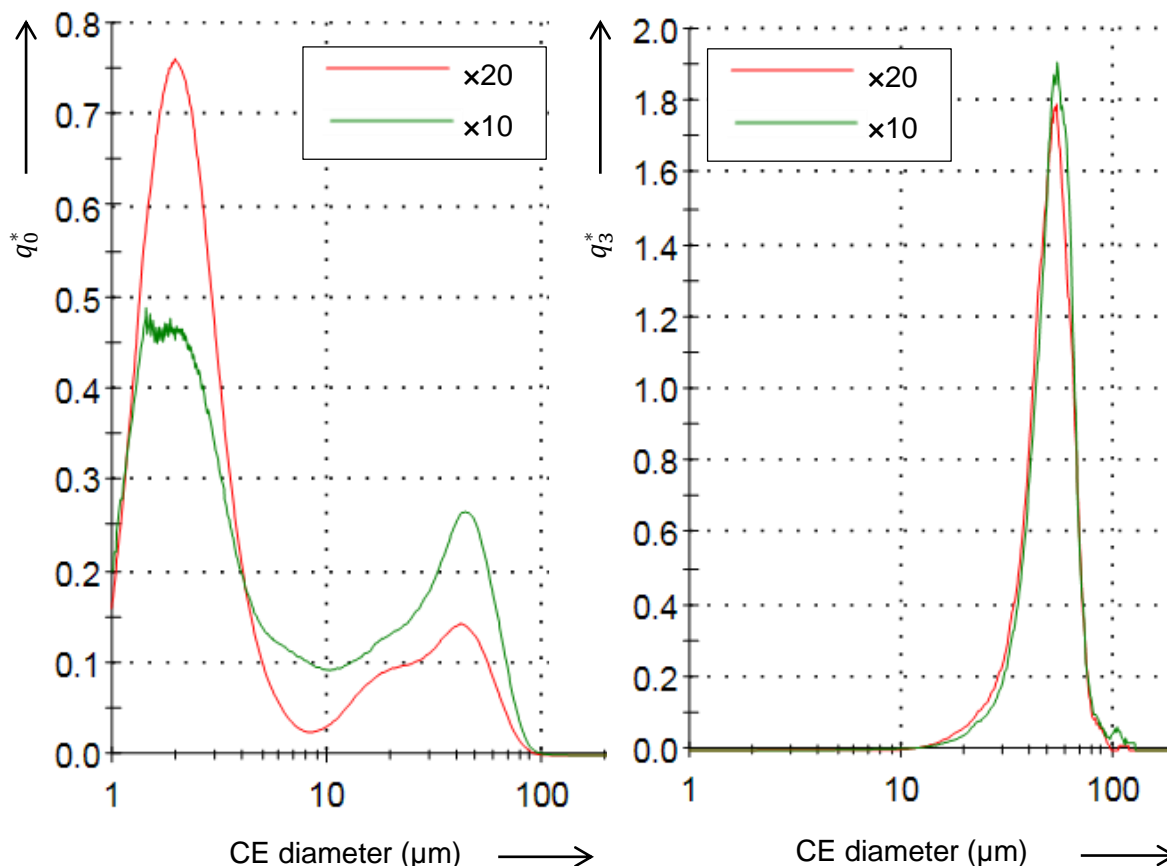


Figure 47 The number-based (left) and the volume-weighted (right) distributions of the catalyst after prepolymerisation, truncated at 1.0 μm

Although unrelated to method development, it is interesting to see how prepolymerisation spreads the number-based distribution towards larger sizes, lowering the higher peak of the non-prepolymerised distribution and accentuating the portion of smaller particles. The volume-weighted distribution, however, clearly shows that the distribution is moved towards larger size. This is good example of how looking at the number-based results may lead into seemingly counter-intuitive conclusions.

9.4 Discussion and conclusions

The difference in image quality between magnifications ×10 and ×20 was noticeable. From the images taken with the ×10-magnification, it was not perfectly clear whether small particles were compact or whether their pores were simply not showing, but the

images taken with the $\times 20$ -objective clearly indicate that smaller particles are indeed more compact.

Furthermore, the higher resolution makes it easier to use image analysis techniques to quantify the porosity of the catalyst, which is among the most important topics of internal morphology. The *Morphologi* software is not capable of this, and the images should be exported into another program for any such analysis. The software is, however, capable of presenting distributions based on pixel intensity mean and standard deviation. See Figure 48 below.

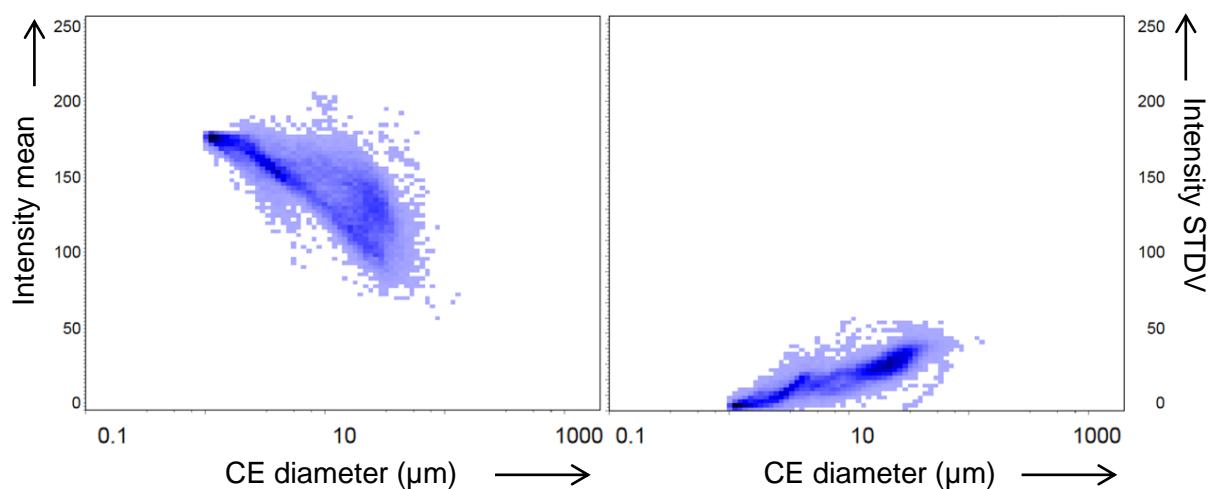


Figure 48 The number-based distributions of the prepolymerised sample based on diameters and intensity mean (right) and standard deviation (right)

If small prepolymerised particles are more compact, their intensity mean should be higher and intensity standard deviation lower than that of larger particles, owing to a smaller number of pores appearing as dark spots. The scattergrams above seem to comply with the expectation. However, intensity mean and standard deviations are not very good measures of porosity, and the figure above should only be taken as an example of what *could* be done, if the images were imported into some other software for the quantification of porosity.

The choice between designs (ii) and (iii) depends on how many images are required for the image analysis; it has little practical effect on the volume-weighted size distribution. In the end, the detailed method is sort of an *ad hoc* method, and the parameters can be adjusted according to the requirements of the sample and project.

10 Conclusions

The currently-used method is a serviceably good method, but care should be taken when samples contain non-spherical particles or large outliers. The inclusion of even one such large outlier may render the volume-weighted results unusable. Whilst samples from the pilot are usually of good quality, lab samples can be very different, ranging from large flakes and other non-spherical particles to small and perfectly spherical particles with a narrow size-distribution. The method is, therefore, more suitable for quality control than research, but this is the case with routine analyses in general. The key to reliable results is consistent data handling, even between different operators.

The classification of particles into classes according to their shape descriptors is anything but fool-proof. For example, bubbles are often inseparable from dark spherical particles of the same size, and elongated particles are difficult to separate from chains of adjacent particles. Certain segmentation algorithms, such as the watershed currently offered by the software, could be used to improve particle detection.

Standards such as the ISO standard ISO 13322-1 and the British standard BS 3406-4:1993 present detailed mathematical theories and requirements for the assessment of particle size analysis using image analysis tools. However, these theories were found to be somewhat impractical, but may give serviceable estimates for the basis of method development.

Of the two new methods, the quick method provides a quick assessment for ZN catalysts, but the trade-off has to be acknowledged. It works best, when particles are spherical and the distribution is relatively narrow with a mean size close to at least 60 μm . The method is ideal for screening purposes; should more detailed information be required, the currently-used wet cell method for ZN is to be used. Only time and experience will show the true usefulness of the quick method.

The detailed method that was intended for collection of high-quality images for studies of internal morphology was shown to be suitable and applicable for *prepolymerised* catalysts. First measurements have already suggested that smaller particles are more compact than larger ones. Because of the darker colour of *non-prepolymerised* catalysts, it remains to be seen if any useful information can be obtained from the images thereof.

11 Summary

The literature review presented in Chapter 3 *Particle Size Analysis* summarises the main concepts in the data handling of particle size analysis, such as the DIN/ISO and M-R-notations and logarithmically transformed histograms $\bar{q}_{r,i}^*$. The chapter gives enough information to enable one to apply the concepts, and will therefore be useful for anyone working with particle size data. It is not, however, intended to give any detailed information about the derivation of the equations; such information can be found in the cited references. Chapter 4 *Image Analysis using Morphologi G3* serves as an introduction to the instrument, but not to image analysis in general.

The second part *Examination of the currently-used method* gives valuable information about the currently-used method, which is also the most important of the available methods. It discusses several issues and potential improvements. Perhaps the single most important conclusion of the part is the unreliability of volume-weighting, when it is based on large and non-spherical particles. It will also serve as a basis in future method development.

Two new methods were developed in the third part *Development of two new methods*. Both developments resulted in a usable method that could be applied to the specific cases they were designed for. The high-throughput method will be used for screening purposes, and it is quick and easy to use. The detailed method is used for collecting high-resolution images of certain SS catalysts. The images will make it possible to quantify porosity and other features of internal morphology. The detailed method was more of an *ad hoc* -method, but is easily modifiable for different purposes.

Finally, all the method discussed in this thesis can be summarised for different catalyst types as follow

$$\begin{array}{l} \text{ZN} \left\{ \begin{array}{l} \text{currently-used} \\ \text{high-throughput} \end{array} \right. \\ \\ \text{SS} \left\{ \begin{array}{l} \text{prepolymerised} \left\{ \begin{array}{l} \text{currently-used} \\ \text{detailed} \end{array} \right. \\ \text{non-prepolymerised} \left\{ \begin{array}{l} \text{currently-used} \\ \text{detailed} \end{array} \right. \end{array} \right. \end{array}$$

12 References

- Alderliesten, M. 1990a. Mean Particle Diameters. Part I: Evaluation of Definition Systems. *Particle & Particle Systems Characterization* 7 pp. 33–241.
- Alderliesten, M. 1990b. Mean Particle Diameters. Part II: Standardization of Nomenclature. *Particle & Particle Systems Characterization* 8 pp. 237–241.
- Alderliesten, M. 2011. Mean Particle Diameters. Part VI: Fundamental Distinction between Statistics Based (ISO/DIN) and Physics Based (Moment-Ratio) Definition Systems. *Particle & Particle Systems Characterization* 27 pp. 7–20.
- BS 2955:1993. Glossary of terms relating to particle technology. London: British Standards Institution.
- BS 3406-4:1993. Part 4: Guide to microscope and image analysis methods. London: British Standards Institution.
- Carlton, R. 2011. *Pharmaceutical Microscopy*. King of Prussia: Springer.
- Dodge, Y. 2008. *The Concise Encyclopedia of Statistics*. Neuchâtel: Springer.
- ISO 13322-1:2004(E). *Particle size analysis – Image analysis methods – Part 1: Static image analysis methods*. Geneva: International Organization for Standardization.
- ISO 14488:2007(E). *Particulate materials – Sampling and sample splitting for the determination of particulate properties*. Geneva: International Organization for Standardization.
- ISO 9276-1:1998(E). *Representation of results of particle size analysis – Part 1: Graphical representation*. Geneva: International Organization for Standardization.
- ISO 9276-2:1998(E). *Representation of results of particle size analysis – Part 2: Calculation of average particle sizes/diameters and moments from particle size distributions*. Geneva: International Organization for Standardization.
- ISO 9276-3:1998(E). *Representation of results of particle size analysis – Part 3: Adjustment of an experimental curve to a reference model*. Geneva: International Organization for Standardization.

- ISO 9276-6:1998(E). *Representation of results of particle size analysis – Part 6: Descriptive and quantitative representation of particle shape and morphology*. Geneva: International Organization for Standardization.
- Leschonski, K. 1984. Representation and Evaluation of Particle Size Analysis Data. *Particle & Particle Systems Characterization* 1 pp. 89–95.
- Malkusch, W. 2002. Quantitative Image Analysis Methods And Limitations. *Tools & Techniques For Life Science Researchers* 27 (2).
- Malvern Instruments. 2009a. Method Development to Measure Polydisperse Samples on the Morphologi G3S. Technical report. Available at: www.malvern.com. [Accessed 2014]
- Malvern Instruments. 2009b. *Performing a merged objective measurement on a Morphologi® instrument*. Technical report, Malvern Instruments. Available at: www.malvern.com. [Accessed 2014]
- Malvern Instruments. 2013. *Morphologi G3 User Manual, Man0410 Issue 5.0*. Malvern: Malvern Instruments.
- Malvern Instruments. 2014. *Software Update Notification Morphologi Software v.812: PSS0025-27*. Software update notification, Malvern Instruments. Available at: www.malvern.com. [Accessed 2014]
- Rawle, A. [no date] *Basic Principles Of Particle Size Analysis*. Technical Paper, Malvern Instruments. Accessed 2014. Available at: www.malvern.com.